



**TECHNICAL LIBRARY**

***REPRINT:***

**VIBRATORY STRESS RELIEF  
OF  
MILD STEEL WELDMENTS**

**S. Shankar**

**A dissertation submitted to the faculty  
of the Oregon Graduate Center in partial fulfillment of the  
requirements for the degree of Doctor of Philosophy**

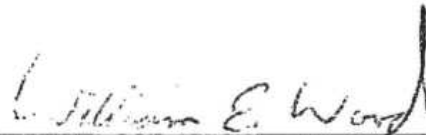
**January 1982**

S. Shankar  
B.S., Bangalore University, India, 1971  
B.E., Indian Institute of Science, India, 1974

A dissertation submitted to the faculty  
of the Oregon Graduate Center  
in partial fulfillment of the  
requirements for the degree  
Doctor of Philosophy  
in  
Materials Science

January, 1982

The dissertation "Vibratory Stress Relief of Mild Steel Weldments" by S. Shankar has been examined and approved by the following Examination Committee:



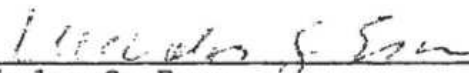
---

William E. Wood, Thesis Advisor  
Professor



---

Jack H. Devletian  
Associate Professor



---

Nicholas G. Eror  
Associate Professor



---

M. A. K. Khalil  
Assistant Professor

ACKNOWLEDGEMENTS

I wish to express my sincere thanks to Bob Turpin for assisting in the fabrication of experimental set-up; to Nancy Christie and Nancy Fick for typing; and to Barbara Ryall for her beautiful art works.

Above all, I am very grateful to my research advisor, Professor William E. Wood, for his support and guidance during the course of this work.

ಹಂಚಿಗಾಗಿ

ಅಮ್ಮ , ಅಪ್ಪಯ್ಯರಿಗೆ

- ಶಂಕನಿಂದ

## TABLE OF CONTENTS

	<u>Page</u>
ABSTRACT.....	1
OBJECTIVE.....	2
CHAPTER 1—INTRODUCTION.....	4
CHAPTER 2—BACKGROUND .....	7
2.1. Vibratory Stress Relief .....	7
2.2. Mechanism of Stress Relief by VSR.....	9
2.3. Residual Stress Measurement Techniques.....	10
2.3.1. Sectioning Method .....	11
2.3.2. X-Ray Diffraction Method .....	12
2.3.3. Blind-Hole-Drilling Method .....	13
2.4. Residual Stresses in Butt Welds.....	17
CHAPTER 3—EXPERIMENTAL.....	19
3.1. Material Selection.....	19
3.2. Weldment Preparation.....	19
3.3. Vibration Table Analysis.....	22
3.4. VSR Treatment of Welded Specimens.....	25
3.5. Residual Stress Measurement.....	27
3.5.1. Sectioning .....	11
3.5.2. X-Ray .....	29
3.5.3. Blind-Hole-Drilling .....	29
3.6. Electron Microscopy.....	31
3.7. Mechanical Testing.....	32
3.7.1. Tensile Testing .....	32
3.7.2. Fatigue Testing .....	32

	<u>Page</u>
CHAPTER 4--RESULTS AND DISCUSSION.....	35
4.1. Vibration Analysis.....	35
4.2. Residual Stress Analysis.....	40
4.2.1. Verification of Longitudinal Residual Stress Pattern Developed in a Butt Weldment.....	43
4.2.2. The Effect of Resonant Vibratory Treatment on the Longitudinal Residual Stress Distribution .	45
4.2.3. Effectiveness of the Vibratory Treatment on the Location of Weldments .....	65
4.2.4. The Effect of Frequency of Vibration on the Longitudinal Residual Stress Distribution .....	66
4.2.5. Effect on Macrostressess .....	72
4.3. Microstructural Analysis.....	76
4.4. Effect on Mechanical Properties.....	80
CHAPTER 5--CONCLUSIONS.....	85
REFERENCES.....	87
APPENDIX--Corrections for Blind-Hole-Drilling Analysis.....	90
Theoretical Analysis.....	91
Practical Considerations.....	95
Experimental.....	97
Discussion.....	100
Machining Effect.....	100
Localized Plastic Flow Effect.....	107
Recommendations .....	112

## LIST OF FIGURES

	<u>Page</u>
1. Variation of resolved stresses $S_r$ and $S_\theta$ as a function of the distance $r$ , from the hole edge, in a direction (a) parallel to the applied stress $S_{app}$ , $\theta = 0^\circ$ and (b) at right angles to the applied stress, $\theta = 90^\circ$ .....	16
2. A schematic plot of longitudinal residual stress vs. distance from the weld center line. $S_y$ is the yield stress of the base material .....	18
3. Schematic of weld-joint preparation .....	21
4. Schematic of the tension plate weldment .....	23
5. Schematic showing the end view of the vibration table .....	24
6. Schematic of the setup used for the vibrational analysis of table top .....	26
7. Schematic of strain gauge layout in a SAE 1018 butt welded specimen used to verify the pattern of longitudinal residual stress distribution. Sectioning was done along the dotted lines .....	28
8. Schematic of the weldment used for sectioning .....	30
9. Geometry of constant amplitude axial fatigue test specimen ..	33
10. Schematic showing (a) the position of vibrator on the table, (b) iso-amplitude lines at 10 Hz, and (c) iso-amplitude lines at 30 Hz. The numbers are amplitudes of vibration in millimeters .....	36
11. Iso-amplitude lines at (b) 10 Hz, (c) 20 Hz, and (d) 30 Hz, when (a) the vibrator is clamped to a corner of the table .....	37
12. Motions of the table when vibrator was clamped to the center of the table and vibrated at (a) 10 Hz, (b) 30 Hz, and (c) 40 Hz .....	38
13. Strain gauge rosette arrangement and the blind-hole geometry for determining residual stresses .....	41
14. Longitudinal residual stress distribution in a SAE 1018 butt weldment .....	44



	<u>Page</u>
15. Longitudinal residual stress distributions as determined by the uncorrected hole-drilling method .....	52
16. Residual stress distribution in a weldment vibrated at 40 Hz	63
17. The redistribution of longitudinal residual stresses as a result of the resonant vibratory treatment at 40 Hz .....	64
18. The effect of frequency of vibration on the longitudinal residual stress distribution .....	71
19. Residual stress distribution in the unvibrated weldments showing excellent agreement between sectioning and corrected hole-drilling techniques .....	73
20. Residual stress distribution in the weldments vibrated at 40Hz .....	74
21. Transmission electron micrographs of the annealed A-36 mild steel samples .....	78
22. Transmission electron micrographs of samples obtained from the resonance vibration treated A-36 mild steel plate .....	79
23. S-N curve of fatigue samples from the unvibrated A-36 steel weldment .....	81
24. S-N curve obtained from the fatigue samples of weldment treated at 30 Hz .....	82
25. S-N curve obtained from the fatigue samples of resonant vibrated weldment .....	83

#### APPENDIX

A1. Strain gauge rosette arrangement and the blind-hole geometry for determining residual stresses .....	93
A2. Variation of the resolved stresses as a function of the distance from the hole edge .....	96
A3. Overestimation of the applied stress $S_{app}$ , due to localized yielding near the hole .....	98
A4. Schematic of the strain gauge layout on the test specimen ...	99
A5. Plot of average strain vs. applied stress for the parallel gauge .....	103

	<u>Page</u>
A6. Plot of average strain vs. applied stress for the transverse gauge .....	104
A7. Variation of $\epsilon_M$ with the drilling clearance for the parallel gauge .....	105
A8. Variation of $\epsilon_M$ with the drilling clearance for the transverse group .....	106
A9. Plot of average strain vs. applied stress for parallel gauge .....	110
A10. Plot of average strain vs. applied stress for transverse gauge .....	111
A11. Percentage error in strain as a function of applied stress for a parallel gauge at various hole sizes .....	113
A12. Percentage error in strain as a function of applied stress for a transverse gauge at various hole sizes .....	114

LIST OF TABLES

	<u>Page</u>
I. CHEMICAL COMPOSITION (IN WT. PCT.) AND MECHANICAL PROPERTIES OF A-36 MILD STEEL .....	20
II. BLIND-HOLE-DRILLING STRESS ANALYSIS OF AS WELDED, UNVIBRATED WELDMENTS (WITHOUT CORRECTION FACTORS) .....	
Weldment #1.....	46
Weldment #2.....	47
Weldment #3.....	48
III. BLIND-HOLE-DRILLING STRESS ANALYSIS OF THE VIBRATED WELDMENTS (WITHOUT CORRECTION FACTORS) .....	
Weldment #1.....	49
Weldment #2.....	50
Weldment #3.....	51
IV. LONGITUDINAL RESIDUAL STRESSES IN THE VIBRATED SAMPLES AS DETERMINED BY THE SECTIONING TECHNIQUE .....	
Weldment #1.....	53
Weldment #2.....	54
Weldment #3.....	55
V. BLIND-HOLE-DRILLING STRESS ANALYSIS OF AS WELDED, UNVIBRATED WELDMENTS (WITH CORRECTION FACTORS) .....	
Weldment #1.....	57
Weldment #2.....	58
Weldment #3.....	59
VI. BLIND-HOLE-DRILLING STRESS ANALYSIS OF THE VIBRATED WELDMENTS (WITH CORRECTION FACTORS) .....	
Weldment #1.....	60
Weldment #2.....	61
Weldment #3.....	62

VII.	RESIDUAL STRESS ANALYSIS BY THE SECTIONING TECHNIQUE (GAUGE FACTOR = 2.04 FOR ALL THE STRAIN GAUGES) .....	
	As welded, control weldment .....	68
	Weldment vibrated at 30 Hz .....	69
	Weldment vibrated at 40 Hz .....	70
VIII.	RESIDUAL STRESSES IN THE TENSION WELDMENT AS DETERMINED FROM THE CORRECTED HOLE-DRILLING TECHNIQUE .....	75
IX.	EFFECT OF THE FREQUENCY OF VIBRATION ON THE MECHANICAL PROPERTIES OF A-36 STEEL BUTT WELDS .....	84

APPENDIX

A-I.	VARIATION OF AVERAGE STRAIN WITH APPLIED STRESS FOR GAUGE #1, WHICH IS PARALLEL TO THE APPLIED STRESS, $\theta = 0^\circ$ . SPECIMEN #1 .....	101
A-II.	VARIATION OF AVERAGE STRAIN WITH APPLIED STRESS FOR GAUGE #3, WHICH IS TRANSVERSE TO THE DIRECTION OF APPLIED STRESS, $\theta = 90^\circ$ , SPECIMEN #1 .....	102
A-III.	VARIATION OF AVERAGE STRAINS RECORDED FROM GAUGE #1 AS A FUNCTION OF APPLIED STRESS FOR VARIOUS HOLE SIZES. SPECIMEN #2 .....	108
A-IV.	VARIATION OF AVERAGE STRAINS RECORDED FROM GAUGE #3 AS A FUNCTION OF APPLIED STRESS FOR VARIOUS HOLE SIZES. SPECIMEN #3 .....	109
A-V.	MODIFICATION OF RELAXED STRAINS OF ROSETTE #1, WELDMENT #1, TO ACCOUNT FOR THE DRILLING ERROR AND THE ERROR DUE TO LOCAL YIELDING .....	116

## ABSTRACT

### Vibratory Stress Relief in Mild Steel Weldments

S. Shankar, Ph.D.  
Oregon Graduate Center, 1982

Supervising Professor: William E. Wood

The influence of resonant and sub-resonant frequency vibration on the longitudinal residual stresses, in A-36 mild steel weldments has been studied. Residual stress analysis was carried out using sectioning, x-ray and blind-hole-drilling techniques. The hole-drilling method was modified to take into account the effect of local plastic yielding due to stress concentration and the machining stresses, with a resultant accuracy comparable to that obtained by the sectioning method. As a result of the vibratory treatments, residual stress redistribution occurred near the weld; the peak stresses were decreased by up to 30%. The resonant frequency vibration had a more pronounced stress redistribution as compared to the sub-resonant frequency vibration. Transmission electron microscopy studies indicated local plastic deformation as the mechanism by which this stress reduction occurred. Constant amplitude axial fatigue experiments on samples machined from regions adjacent to the weld showed that both the vibratory techniques did not induce any fatigue damage.

## OBJECTIVE

Vibratory methods have been used for the last several decades to modify internal stresses in castings, forgings and welded structures. In recent years, a process called vibratory stress relief (VSR) has been applied with increasing success to attain shape stabilization and to control distortion. Attempts to use VSR methods for stress relief or stress redistribution to guard against service failures such as fatigue and stress corrosion cracking have met with limited success. Although to date several studies have shown that vibrations do change residual stresses, there have been few fundamental studies undertaken to establish the mechanism(s) by which vibratory methods alter the residual stresses during welding. The lack of fundamental analysis combined with suggested operating practices that were contradictory in nature has increased the skepticism about the success of the technique in reducing residual stresses. A better understanding of the process in terms of its mechanism(s) together with the attendant effects is essential if VSR is to be used as a viable technique for altering residual stresses.

The objectives of this investigation were to study:

1. The conditions under which VSR works;
2. The effect of VSR on residual stresses and the extent of stress relief;

3. The mechanism(s) by which VSR brings about the stress relief; and finally,

4. Whether or not VSR causes fatigue damage.

## CHAPTER 1

### INTRODUCTION

Residual stresses are of concern to producers and users of all types of machinery and structures and may cause dimensional instability during machining, contribute to low-stress brittle fracture and reduce fatigue strength. Those who make and use welded fabrications must be particularly concerned with the effects of residual stresses because of the relatively high residual stress levels inherently produced with most common welding processes.

When it is desired to reduce residual stresses in a fabrication to as low a level as possible, the most widely used and successful method is thermal stress relief. Specifying temperature, time and heating and cooling rates are all that is usually necessary to guarantee reduction of residual stresses to reliably low levels throughout a fabrication.

Thermal stress relief, however, can have certain adverse effects such as scaling, discoloration, loss of finish, distortion, metallurgical changes in the microstructure, etc. It is also, in some instances, time consuming and, with increasing energy costs, very expensive. Since residual stresses are developed to some degree in virtually every machining operation, there are many situations where it would be advantageous to stabilize the part at several stages of fabrication. Thermal cycling would be impractical in these cases.



Also, large components like gas storage tanks, bridge structures, and rail car panels are impossible or impractical to stress relieve by thermal treatments. In this background, an alternative technique of stress relief <sup>1,2</sup> that employs mechanical vibration, has emerged. This process is called vibratory stress relief (VSR) or vibratory metal stabilization (VMS). Over the last fifteen years, this method of stress relief has evolved from a little-known art into a basic process, and one which for some industries is now well tried and established as an alternative to thermal treatment for stabilizing castings, fabrications, and bar components. <sup>3-5</sup>

The major interest in vibrational stress relief has been its relative simplicity compared with thermal stress relief. For instance, compared with thermal stress relief equipment commercially available, vibratory stress relief equipment is far less expensive, requires considerably less time for the stress relief treatment, is more portable, generally occupies less floor space, and causes no oxide scale formation. However, there is little experience in predicting the effectiveness of the treatment and there is little quantitative information on the effectiveness, use, or magnitude of any effects and the mechanism involved. In the absence of such quantitative information, it is difficult to determine when and where vibratory stress relief may be effectively applied, particularly in massive complex fabrications.

The present study was undertaken to provide some quantitative data on the vibratory stress relief process applied to A-36 mild steel butt welds. The various phases of this study focused on the

analysis of vibration, residual stress analysis using sectioning, x-ray and blind-hole-drilling techniques, and the effect of vibration on the microstructure and the mechanical properties of the weldments. This comprehensive study is unique in that it combines vibration methodology, residual stress analysis, microstructural analysis, and mechanical testing.

## CHAPTER 2

### BACKGROUND

#### 2.1. Vibratory Stress Relief

Vibration, in its various forms, has been used to stabilize parts for many years. For example, in the ancient art of "hammer annealing," a high amplitude, gradually decaying vibration was induced by repeated hammer blows. Large castings, at one time, were stabilized by dropping them from a considerable height into a pile of sand. In the "natural aging" process, the workpieces were stored outdoors for a considerable period of time. The metal expanded and contracted with changes in ambient temperature at a very low frequency of one cycle per day. The nature of the vibrations produced in these methods made them uncontrollable, unpredictable, and too slow. Gradual experimentation to make the process more repeatable by the control and monitoring of vibrations used has paved the way to the state-of-the-art vibratory stress relief techniques.

The actual process of vibratory stress relief is simple and consists of inducing a metal structure to be stabilized into one or more resonant or sub-resonant vibratory states using high force exciters. Vibrational stress relief equipment commercially available generally consists of a variable-speed motor driving eccentric weights (also known as the vibrator) and its associated power supply and control equipment.

The vibrations can be imparted to the workpiece in two ways.

If the structure is sufficiently large, the vibrator can be clamped directly to it and the motor energized to vibrate the workpiece. The workpiece is isolated from the ground by supporting on rubber or foam pads, so that the vibrations are not lost or taken up by the supporting structure. Another way of imparting vibrations utilizes a special vibration table. Here the vibrator is attached to the table top which is freely suspended on inflatable rubber pads. The workpiece is clamped to the top of the table and the motor energized to vibrate the table and, hence, the workpiece. Small parts, whose natural frequencies lie outside the range of the vibrator, can be effectively treated using the vibration table. By combining the small workpiece with the table, the natural frequencies of the entire combination can be brought down to be successfully vibrated. An accelerometer clamped to the structure or the table is used to find the natural frequencies. The frequency of vibration depends upon the material of the workpiece, its size and shape. In general, the frequencies encountered are less than 100 Hz. The vibratory treatment itself is short, usually less than 30 minutes.

Currently, there are two types of vibratory treatment in practice. In the first type, the unit is attached to the structure and is energized and scanned very slowly from zero to its maximum frequency (e.g., 0-100 Hz in about 8 minutes). The response of the structure is monitored and the resonant frequencies noted. Usually two or three such frequencies exist. The vibrator is then turned off

and returned to a speed that corresponds to the first low resonant frequency of the structure. The vibration is allowed to continue for a given length of time (usually about 10 minutes), at the end of which the frequency is slowly ramped out of the resonant condition until the next higher resonant frequency is found and the process is repeated.

In the second type of vibratory technique, after the initial scanning to determine the resonant frequencies, the vibration is held at frequencies just below each resonant frequency. Usually, the work-piece is vibrated at a frequency 10 Hz below the resonant frequency. One aspect of this study deals with the effectiveness of these two practices.

## 2.2. Mechanism of Stress Relief by VSR

During a thermal stress relief treatment, the yield point of the material is substantially lowered, allowing the stresses (which may now well exceed the new, high temperature yield point) to cause plastic flow and reduce the level of residual stresses. However, the mechanism of stress relief by vibration is not fully understood. Currently, there are two major hypotheses proposed to explain the mechanism of stress relief by vibration. One hypothesis draws an analogy between stress relief by vibration and by heat treatment by relating it to the displacements of the atoms that build up the crystal lattice. <sup>1,31-33</sup> The low-frequency vibrations are supposed to impart sufficient energy to the atoms to enable them to take up new

positions. This theory based on internal friction can presumably be applied to materials that display a pronounced tendency towards natural aging. However, there seems to be no experimental evidence to support this conjecture.

The other hypothesis attributes the stress relief due to the process of plastic deformation.<sup>34, 35</sup> Unlike the previous supposition, a number of experimental investigations<sup>36-40</sup> have shown that during vibrational treatments, the combined residual and cyclic stresses exceed the yield point of the material, resulting in residual stress reduction by plastic deformation. However, none of these investigations presented direct observations of plastic deformation.

In the present investigation, an attempt is made to document the occurrence of plastic deformation in the vibrational treatments.

### 2.3. Residual Stress Measurement Techniques

An accurate assessment of the efficiency of any stress relief treatment involves measurement of residual stresses before and after the treatment, and virtually every conceivable method of monitoring displacements has been employed. For ease of reference these can be classified into the following groups:

1. Mechanical
2. Moiré and associated techniques
3. X-ray
4. Ultrasonic
5. Magneto-elastic
6. Analytical

A complete summary of all the published literature on this subject has been adequately covered in reviews.<sup>6-8</sup>

By far the most practical, well-developed, and hence widely used techniques are sectioning, blind-hole-drilling (both mechanical types), and x-ray. In the present study, the first two methods were widely used, together with x-rays (to a limited extent), for residual stress analysis. Since accurate residual stress analysis is a key part of this investigation, and a shortcoming of many previous studies, a brief description of the methodology, merits, and shortcomings of these three techniques are outlined in the following sections.

### 2.3.1. Sectioning Method

All mechanical techniques involve some degree of destruction. In particular, the sectioning technique is completely destructive and herein lies its major disadvantage. This method has been successfully applied to accurately measure uniaxial and biaxial states of stress and to a limited extent triaxial residual stress. The method consists in carefully sectioning the workpiece in which residual stresses are to be determined into smaller strips and measuring the change in strain in each individual strip. The series of strains thus measured gives the stress distribution in the entire workpiece, using the formula  $\sigma = E\varepsilon$ . The actual geometry of slicing and the formulae to be used depend on specific situations.<sup>9,10</sup> The method, apart from being destructive, is very time consuming since the cutting

process should be done slowly, cooling the specimen with a jet of coolant to ensure that cutting in itself does not produce any strains.

In the present investigation the accuracy of the sectioning technique used was about  $\pm 3.5$  MPa in mild steel samples. Due to this high accuracy of stress measurement, the sectioning technique was used as a standard against which the other stress measurement techniques were compared.

### 2.3.2. X-Ray Diffraction Method

The x-ray diffraction procedure for determining the surface residual stresses is well established.<sup>10-12</sup> The fundamental theory of stress measurement by means of x-rays is based on the fact that the interplanar spacing of the atomic planes within a specimen is changed when subjected to stress. A change  $\Delta d_{hkl}$ , in the interplanar spacing  $d_{hkl}$  will cause a corresponding change,  $\Delta\theta$ , in the Bragg angle of diffraction by the family of planes. The strain  $\Delta d/d$  can be measured by the change in the diffraction angle and the stress can be obtained from the strain with formulae derived from linear isotropic elastic theory.

In practice the angle of diffraction of x-rays is measured either by a back reflection camera or by a suitable diffractometer, with a maximum accuracy of the order of  $\pm 0.02$  degree.<sup>13</sup> This means that the value of the lattice spacing can be determined to an accuracy of the order of  $\pm 0.0002 \text{ \AA}$ , which in turn allows the calculation of the residual stresses to  $\pm 14$  MPa. Thus the x-ray technique has less



accuracy than the sectioning method. Further, additional errors due to instrument misalignment and uncertainty in the elastic constants can bring the total error to  $\pm 34.5$  MPa which is about 12% in mild steels. The x-ray technique is designed for the measurement of macrostresses, but microresidual stresses (due to inhomogeneities in the microstructure) can also be detected by x-rays and these can interfere with the accuracy of the data. Thus, in some materials, including plastically deformed steel, interpretation of the results may be difficult.

However, it is completely non-destructive and determines the total elastic stress present in the sample for a given location and direction independent of the sample geometry without relaxing the stress being measured. Another advantage of this technique is that the area over which the stress is averaged can be varied by limiting the size of the x-ray beam. Using a small beam size (typically of the order of 2 x 2 mm), localized stresses adjacent to welds or fasteners can be measured.

### 2.3.3. Blind-Hole-Drilling Method

It is possible to determine residual stresses by drilling a hole in a specimen and measuring the resulting change of strain in the vicinity of the hole.<sup>14-17</sup> This method, also known as hole-relaxation or hole-drilling method, is the least destructive of the mechanical methods. A hole of only a few millimeters in diameter and

depth may suffice for the stress measurement. Since this amount of destruction can sometimes be tolerated, the method is semidestructive in nature. It is a very simple and economical method and can be used to measure stresses over a very small area in a very short period of time.

In actual practice, a strain gauge rosette which is commercially available is bonded to the specimen with the center of the rosette coinciding with the point where stresses are to be measured. A hole is then drilled at the center of the rosette. From the strain readings taken before and after the drilling of the hole, the principal stresses in the plate before the hole was drilled is computed. Both uniaxial and biaxial stresses can be measured with this technique.<sup>18</sup> The principle of this technique is based on the work of Kirsch<sup>19</sup> on the stress distribution around a circular hole in a plate subjected to unidirectional tension. By superposition, the same principle can be extended to biaxial stress fields.<sup>15 17</sup>

The relaxed strains measured by the gauges on the surface of the structure are dependent on the depth of hole until this exceeds a dimension where strain changes do not affect the surface. It has been very clearly shown<sup>17,18,21,22</sup> that full relaxation is obtained at the surface for a depth equal to the hole diameter. Thus, in practice, where the components of interest are usually thick compared with the hole diameter, blind holes are formed; hence the name blind-hole-drilling.

It is imperative that the method employed to form the hole should not introduce any stresses. The rotating cutters or end mills commonly

employed to drill the hole can introduce appreciable stresses.<sup>21-23</sup>

An alternate technique of hole formation, viz., airbrasive<sup>24</sup> or abrasive jet<sup>21</sup> machining seems to be very effective and the machining strains measured are well within the accuracy of the strain recording equipment. However, not only is the equipment used in this method very expensive but the method itself is more time consuming to drill a hole of given size and in part to handle the ancillary equipment.<sup>23, 24</sup>

Further, drilling the hole in a stress system introduces a localized discontinuity or stress raiser. For instance, as shown in Figure 1, in a uniaxial stress field, the stresses ( $S_{\theta}$ ) at right angles to the direction of the applied stress, reach 3 times the value of the yield stress, near the edge of the hole. In the direction of applied stress, the stress ( $S_r$ ) must always relax to zero at the edge of the hole. In an equal biaxial field, the stresses reach twice the value of yield stress. Thus, if the stress to be measured exceeds 1/3 yield stress for the material in the uniaxial case, and 1/2 yield stress in the equal biaxial case, there will be some plasticity at the edge of the hole. This will affect the Poisson ratio, locally, and errors will be introduced.

However, if an accurate assessment of the machining errors and errors due to local yielding is made, blind-hole-drilling technique can be employed in its current form to accurately measure stresses close to the yield stress for the material.

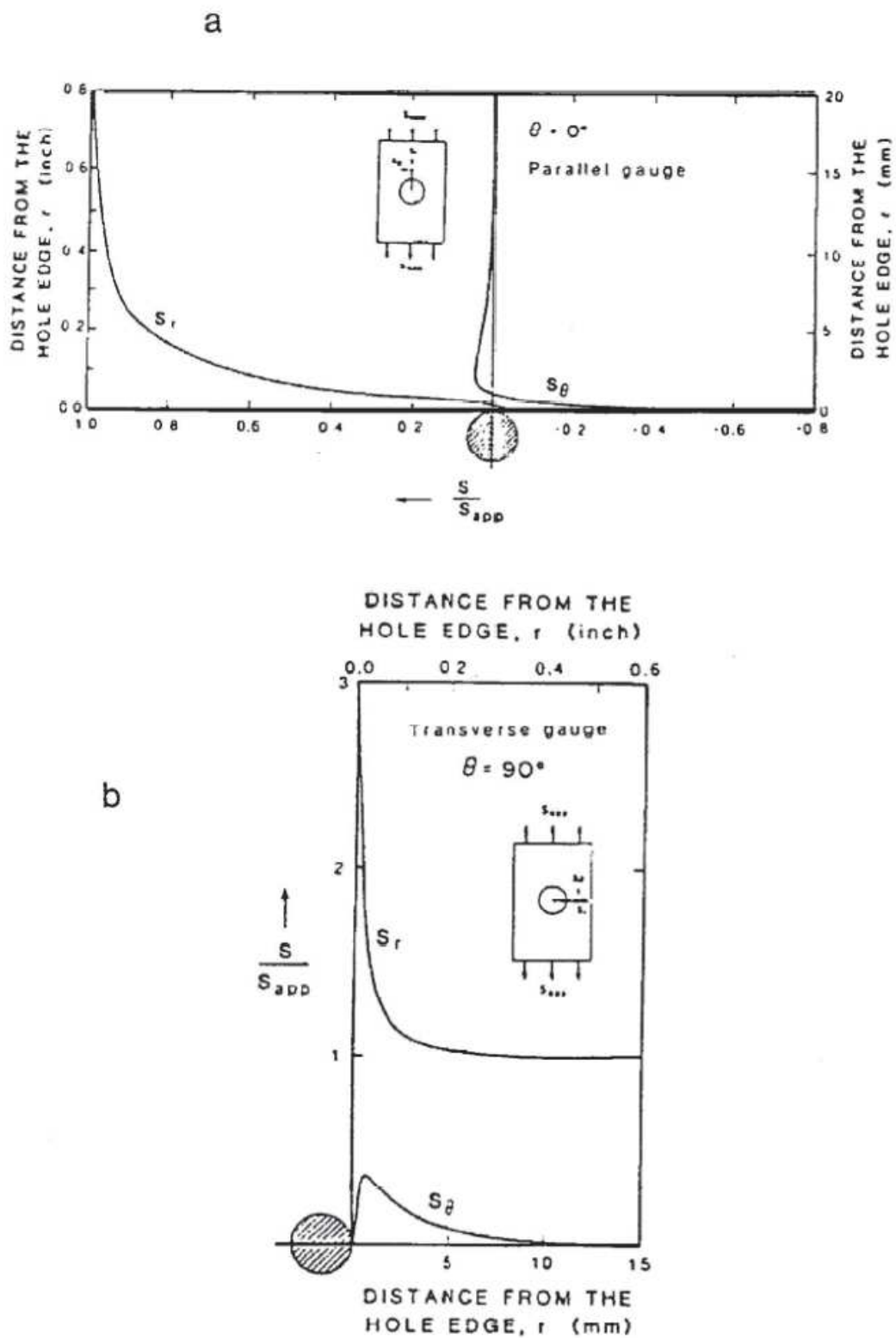


Figure 1. Variation of resolved stresses  $S_r$  and  $S_\theta$  as a function of the distance  $r$ , from the hole edge in a direction (a) parallel to the applied stress  $S_{app}$ ,  $\theta = 0^\circ$  and (b) at right angles to the applied stress,  $\theta = 90^\circ$ .

#### 2.4. Residual Stresses in Butt Welds

The theoretical study of the development of residual stresses when two plates are butt welded dates back to the 1930's and today there exists an excellent correlation between the theory and experimental results. <sup>25-29</sup> It is well known that weld shrinkage in butt weldments results in large tensile longitudinal residual stresses adjacent to the welds, balanced by compression elsewhere in the section (Figure 2). Typically, the longitudinal residual stresses close to the weld approach yield point of the base metal, and the stress distribution is symmetrical across the weld center line.

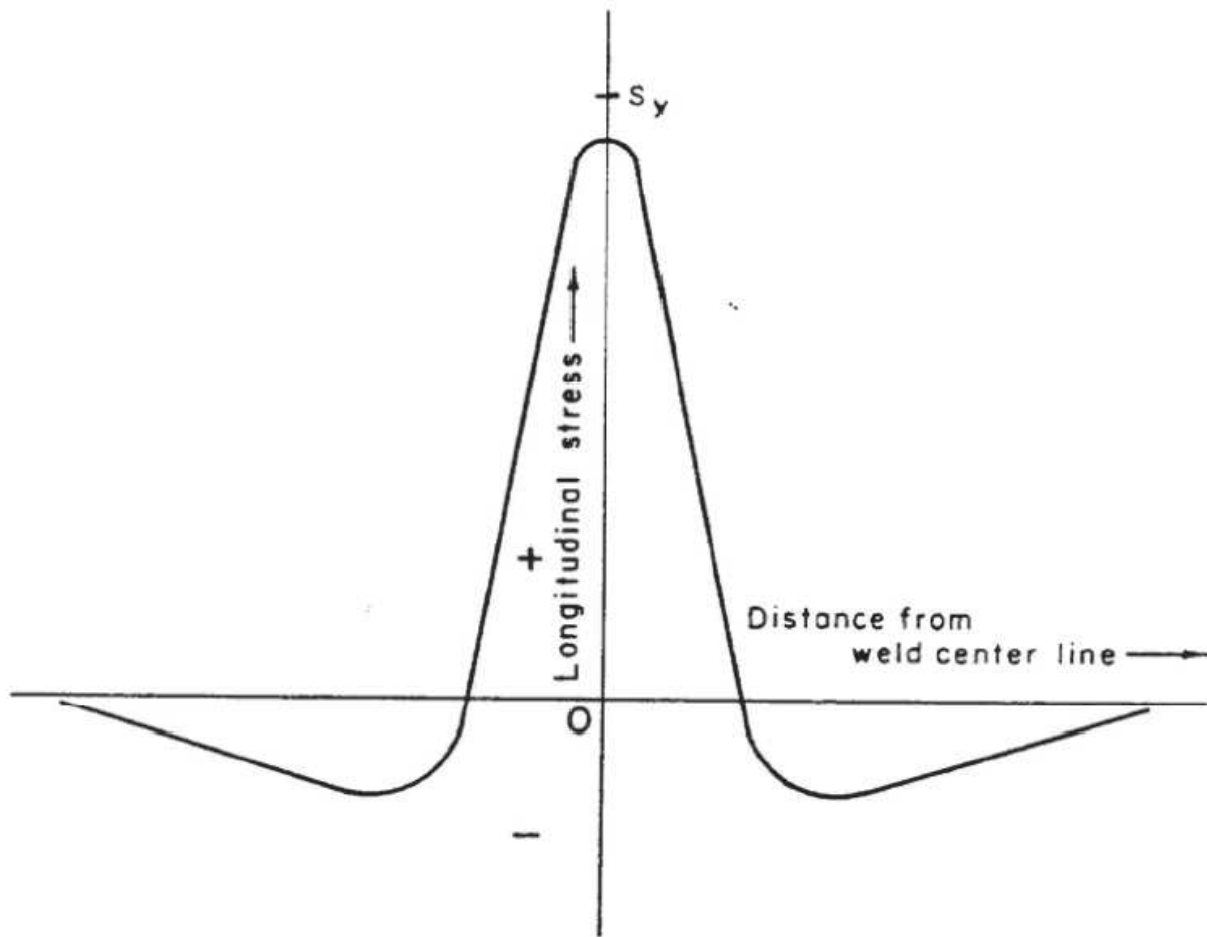


Figure 2. A schematic plot of longitudinal residual stress vs. distance from the weld center line.  $S_y$  is the yield stress of the base material.

## CHAPTER 3

## EXPERIMENTAL

## 3.1. Material Selection

In this investigation, mill plates of ASTM designation A-36 constructional steel were used. The chemical composition of the as-received steel is given in Table I. All the plates used to make the butt weldments were first annealed to completely relieve the as-received residual stresses. The annealing treatment consisted of heating the plates for one hour at 870°C in an inert atmosphere, furnace cooling to 540°C and then air cooling to the room temperature. The tensile properties of the as-received and the annealed A-36 steel are also shown in Table I. Two SAE 1018 steel plates were also given the previous annealing treatment.

## 3.2. Weldment Preparation

In order to verify and confirm the pattern of longitudinal residual stress distribution in a butt welded sample, the annealed SAE 1018 steel plates, each 305 x 102 x 6.4 mm, were butt welded using 3.2 mm E-7024 electrode. No weld joint preparation was made.

The annealed A-36 steel plates were butt welded using 4 mm E-6013 electrodes. The weld joint preparation is shown in Figure 3. Double-vee bevels were used to minimize the distortion and to ensure

Table I.

CHEMICAL COMPOSITION (IN WT. PCT.) AND MECHANICAL PROPERTIES  
OF A-36 MILD STEEL

Chemical Composition

C	Mn	P	S
0.23	0.44	0.008	0.029

Mechanical Properties

	As Received	Fully Annealed
Yield Strength (MPa)	309	280
Tensile Strength (MPa)	470	431
Elongation %	28.0	38.0



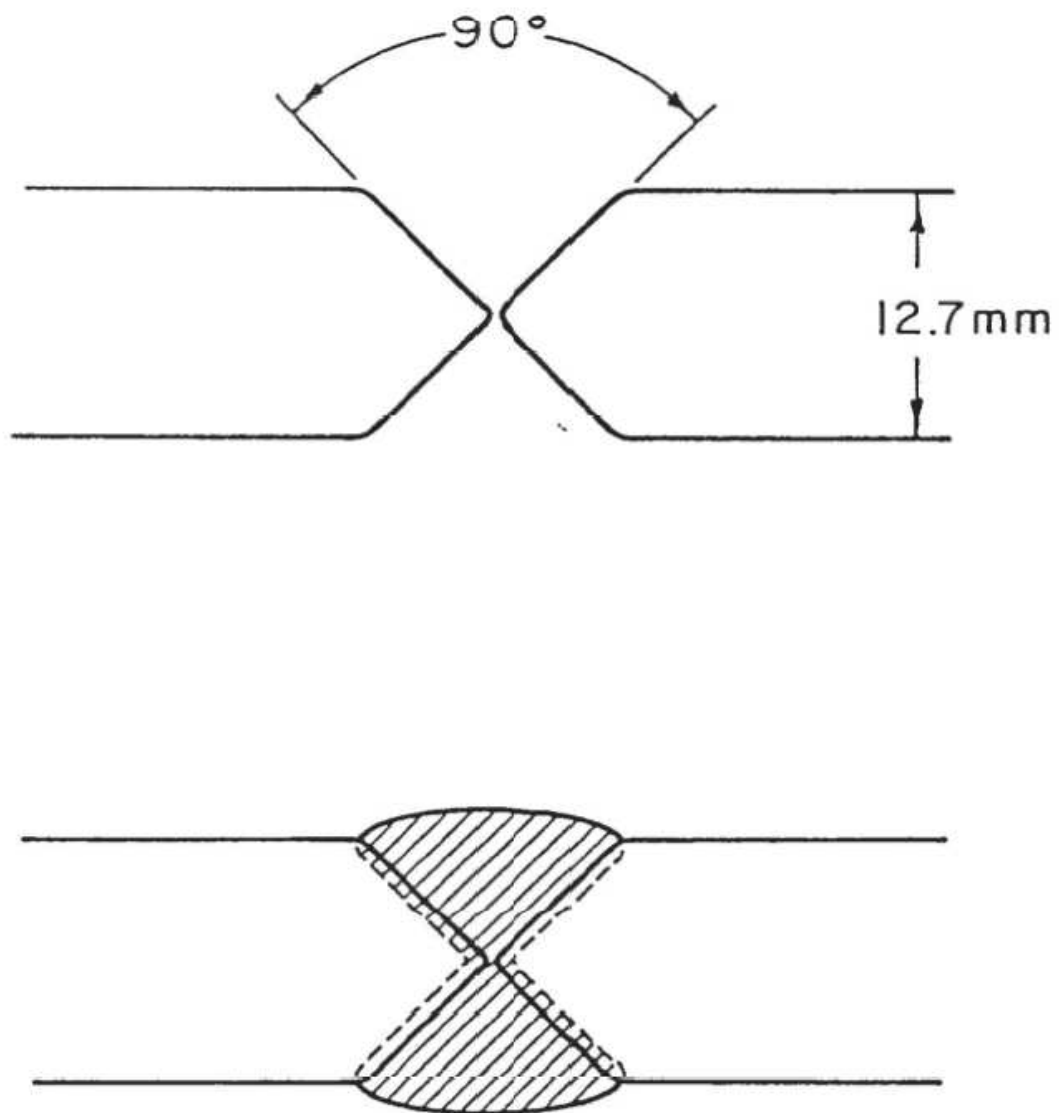


Figure 3. Schematic of weld-joint preparation.

uniform through thickness stress distribution in the weldment.<sup>30</sup> Distortion was further reduced by clamping the plates by the edge. The clamping was such that the lateral motion of the plates was unhindered during welding which would result in low values of transverse stresses. A total of six butt welds were made of which three were 914 x 406 x 12.7 mm and the other three were 305 x 508 x 12.7 mm in size.

In order to study the vibratory stress relief of a heavy structure without using the vibration table, the following tension weldment was prepared (Figure 4). An annealed A-36 mild steel plate 762 x 457 x 19 mm was first welded along weld 1 to a strongback with about 12.5 mm clearance between the two. The plate was then heated to about 143°C and while still hot, was welded along weld 2 to the strongback. The plate, on cooling, contracts and develops uniform, yield point magnitude tensile stresses sufficiently removed from the welded ends.

### 3.3. Vibration Table Analysis

The vibratory treatments were carried out using a vibration table (Figure 5). The table top was 1830 x 1219 x 25.4 mm aluminum alloy plate, braced rigidly by several steel I beams. It was mounted on four inflatable rubber pads which helped to isolate the table from the ground during vibrating. The vibrations were produced by a bottom center bolted DC motor containing eccentric weights mounted on each end of its shaft.

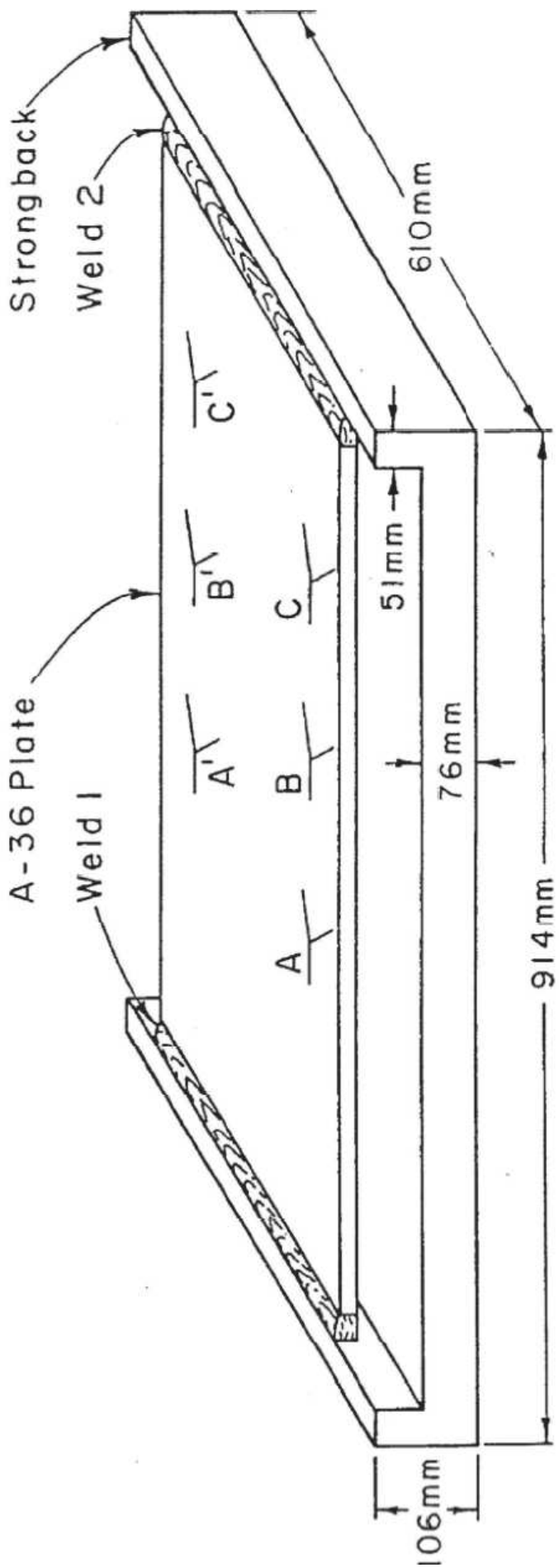


Figure 4. Schematic of the tension plate weldment.

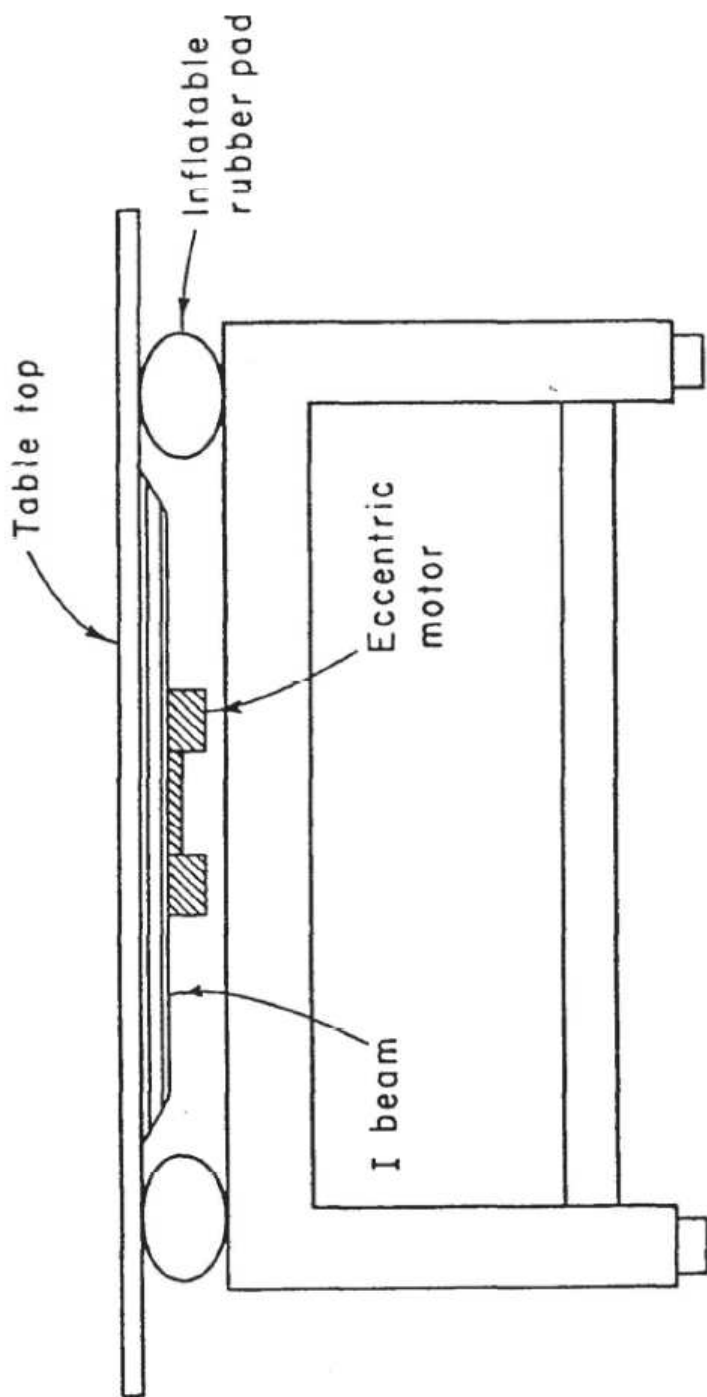


Figure 5. Schematic showing the end view of the vibration table.

Grid lines 254 mm apart crisscrossed the surface of the table. The motor was energized to selected frequencies up to 40 Hz, and at each frequency the amplitude of vibration and the phase difference of the amplitudes were measured at the intersecting points of grid lines.

A schematic of the setup used to monitor the vibrations is shown in Figure 6. Two sensitive piezoelectric transducers, one fixed and the other movable, were used to monitor the amplitudes and phase differences. Filters were used to obtain a clear sinusoidal signal free from higher harmonics and interfering waves from the boundaries of the table.

#### 3.4. VSR Treatment of Welded Specimens

The weldments were subjected to vibratory stress relief treatment by bolting rigidly to the vibration table. A good mechanical contact was necessary to efficiently transfer vibrations from the table to the weldment. The duration of the vibratory treatment was a fixed time of 20 minutes, and the resonant frequency was maintained manually.

The effect of weldment location on the vibration table was studied using the three 305 x 508 x 12.7 mm weldments. Of the three weldments, one was vibrated by clamping to the center of the table and the other two at two corners of the table. The frequency of vibration in all the three cases was 40 Hz.

Additionally, the effect of frequency of vibration treatment was studied using the three 914 x 406 x 12.7 mm weldments. One

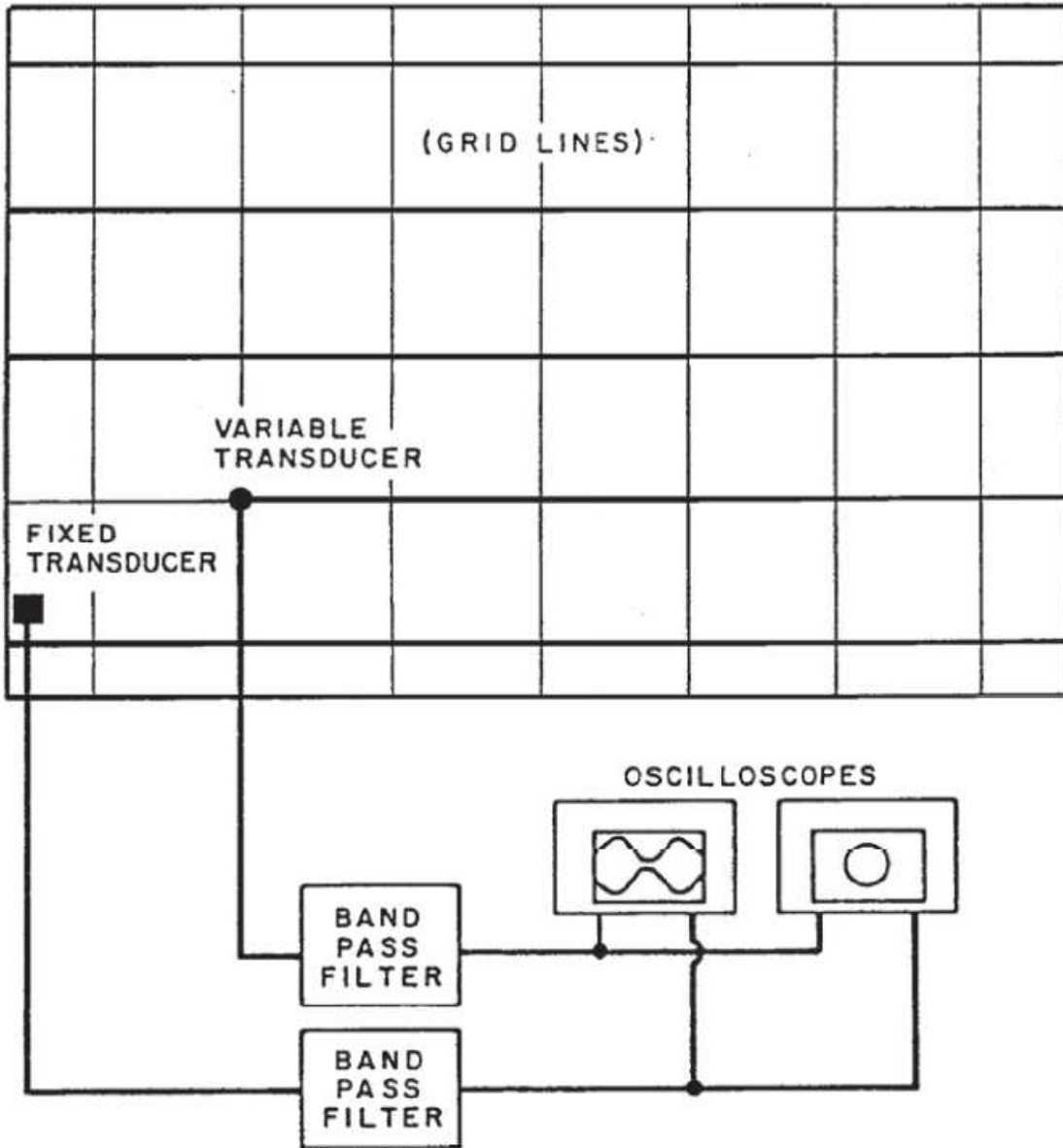


Figure 6. Schematic of the setup used for the vibrational analysis of table top.

weldment was vibrated at 40 Hz, the second at 30 Hz and the third was not vibrated and was used as a control.

The 400 kg weldment shown in Figure 4 was vibrated by clamping the vibrator directly to it. The frequency of vibration was 37 Hz, a fundamental vibrational frequency of the assembly. The weldment and the vibrator assembly were placed on heavy duty rubber pads to isolate the workpiece. The duration of treatment was 20 minutes.

### 3.5. Residual Stress Measurement

Residual stresses in weldments were determined by sectioning, x-ray, and blind-hole-drilling techniques.

#### 3.5.1. Sectioning

This technique of residual stress measurement was used in all the weldments. The surface of the SAE 1018 butt welded specimen was cleaned and a total of seven resistance strain gauges (type EA-06-125 AD-120 supplied by Micro Measurements Co.) were then bonded to the sample as shown in Figure 7. The initial readings from the strain gauges were zeroed using a Vishay Portable Strain Indicator. Next, two slices, each 32 mm wide, were cut from the welded plates, along the dotted line as shown in Figure 7. The sectioning was done on a Micromech wet cut-off saw. Strain readings were once again taken after the sectioning.

In the 914 x 406 x 12.7 mm weldments, strain gauges (CEA-06-125 VT-120) were bonded on a 127 mm square area in the middle of each

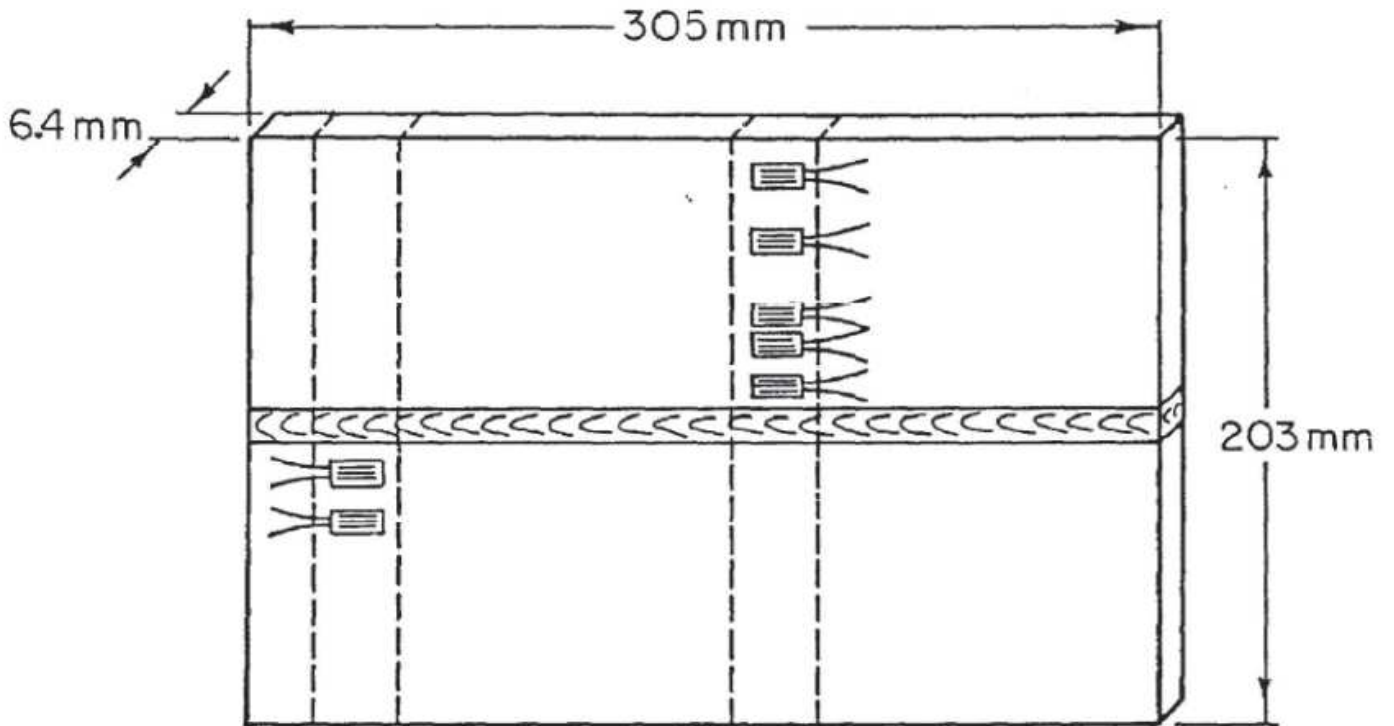


Figure 7. Schematic of strain gauge layout in a SAE 1018 butt welded specimen used to verify the pattern of longitudinal residual stress distribution. Sectioning was done along the dotted lines.



weldment (Figure 8). This square region was then sectioned off using a saw mill operating at a slow speed. Care was taken not to heat the area by directing a jet of coolant at the cutting edge of the saw blade. Strain, as well as resistance, measurements were made from these strain gauges before and after sectioning. A Vishay 1011 portable strain indicator together with a Vishay 1012 portable switch and balance unit were used for strain measurements. Resistances from the strain gauges were measured using a standard potentiometer.

In the 305 x 508 x 12.7 mm samples used for the blind-hole-drilling experiments, sectioning technique was employed as a check for the residual stresses measured after vibration. In these samples a strip 25.4 mm wide was cut across the weld.

### 3.5.2. X-Ray

Further measurements of residual stresses, using an x-ray method, were made in the 127 mm square pieces obtained from the sectioning technique. The  $\sin^2\psi$  technique<sup>13</sup> employed for residual stress measurement used six  $\psi$  angles at equal values of  $\sin^2\psi$  from  $\psi = 0$  to  $\psi = 45$  degrees.

### 3.5.3. Blind-Hole-Drilling

Residual stresses in the 305 x 508 x 12.7 mm weldments were determined by the blind-hole-drilling technique. Strain gauge rosettes (type EA-06-125 RE-120 supplied by Micro Measurements Co.) were bonded at predetermined locations on either side of the weld. Before

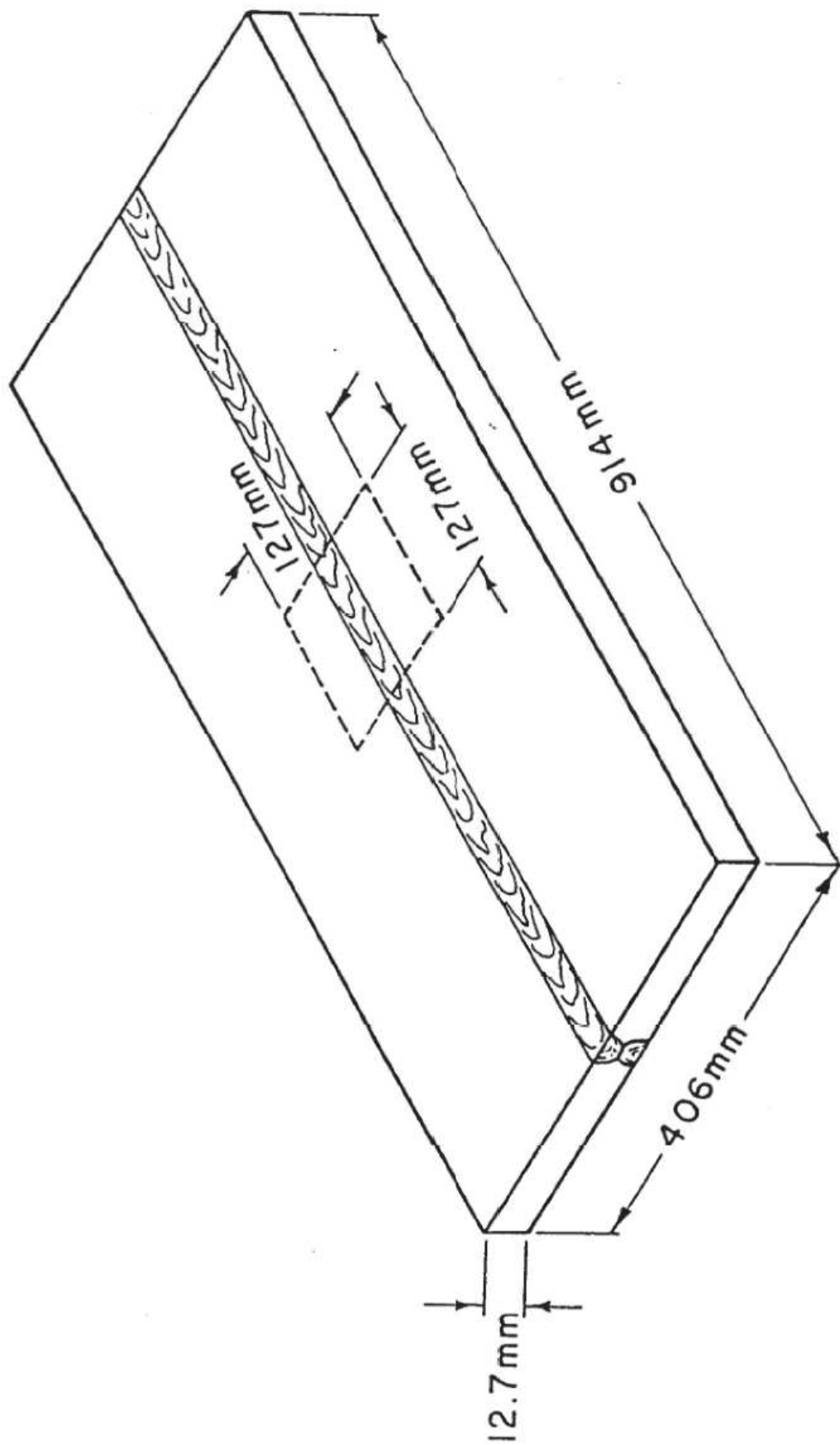


Figure 8. Schematic of the weldment used for sectioning.

vibrating each weldment, holes approximately 3 mm in diameter and depth were drilled at the center of rosettes mounted on one side of the weld to determine the residual stresses in the as-welded condition. The weldments were then individually vibrated at 40 Hz for 20 minutes by clamping them at several locations on the vibration table. Holes were again drilled in the rosettes on the other side of the weld to obtain the residual stress distribution after vibration. A Photolastic model RS-200 milling guide was used to align the drill bit exactly at the center of the rosette and also to rigidly guide the drill bit to produce consistently straight, true, and clean holes.

The blind-hole-drilling technique was also employed to determine the effect of vibratory treatment on the residual stresses in the tension plate of Figure 4. Residual stresses before vibration were determined using the strain gauge rosettes at A, B and C. After the vibratory treatment the residual stresses were again measured using rosettes A', B' and C'.

### 3.6. Electron Microscopy

In order to detect the evidence of plastic deformation, 1 mm thick coupons were sectioned off from the 19 mm A-36 tension plate. These coupons were cut from areas 13 mm around the rosettes. They were then ground on abrasive wheels to a thickness of 0.25 mm. Further thinning to about 75 microns was done by electrolytic polishing. Disks of about 3 mm in diameter were punched out carefully for

jet polishing. Both the electrolytic and the jet polishing were done at about 5°C in a solution of 135 cc of glacial acetic acid, 25 g of chromium trioxide and 7 cc of distilled water. The samples were studied in a Hitachi HU-11B3 electron microscope at an operating voltage of 125 kV.

### 3.7. Mechanical Testing

Tensile and fatigue experiments were carried out using the samples machined out of the three 914 x 406 x 12.7 mm weldments. A 10,000 kg Instron Lawrence dynamic test system was used for all testing. The samples were sectioned off of regions 12.7 mm from either side of the weld center line. A total of 4 tensile and 16 fatigue samples from each of the three weldments were tested.

#### 3.7.1. Tensile Testing

Tensile bars of 6.35 mm diameter were machined according to the ASTM specification A370-77. Testing was carried out at a crosshead speed of 1 mm/minute. Strain was measured with a strain gauge extensometer.

#### 3.7.2. Fatigue Testing

Constant amplitude axial fatigue tests were conducted using 5.08 mm diameter fatigue samples satisfying the ASTM specification E466-76 (Figure 9). The surface of all the samples was finely polished using a 600 grit emery cloth. The tests were performed in

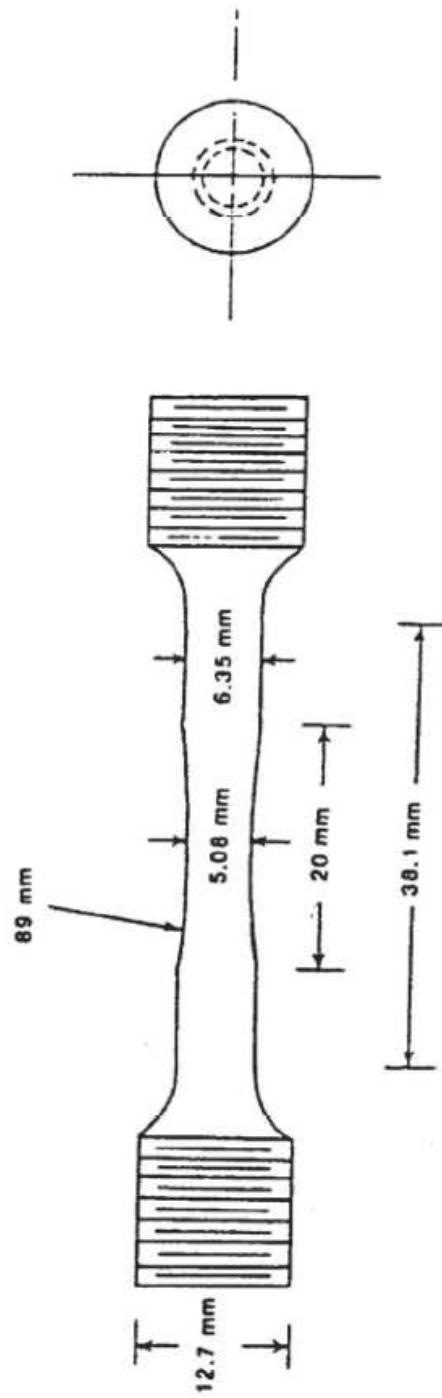


Figure 9. Geometry of constant amplitude axial fatigue test specimen.

air at room temperature at a frequency of 30 Hz and with an R ratio of 0.1. Samples that did not fail after  $10^7$  cycles were reused again at higher stress levels. This method of testing is known as the staircase fatigue testing.

CHAPTER 4  
RESULTS AND DISCUSSION

4.1. Vibration Analysis

The vibration table was vibrated, with the vibrator clamped at three different locations on the table, viz., the edge, the corner and the center of the table. At each position, the table was vibrated at 10 Hz, 20 Hz, 30 Hz and at the resonant frequency of 40 Hz. Beyond 40 Hz, the motion of the table was extremely complex. At each frequency a plot of isoamplitude lines together with their phase difference as measured on the table was prepared. These plots were helpful in characterizing the motion of the table. Figures 10, 11 and 12 show the schematics for various positions and frequencies of the vibrator. In all these figures the phase difference between the solid and the dashed line is  $180^\circ$ .

First, the vibrator was clamped to a side of the table as shown in Figure 10a. At 10 Hz, the motion of the table was an oscillatory type, as though hinged along a nodal line roughly a third of the table length away, Figure 10b. The nodal line moved away as the frequency of the vibrator was increased. At a frequency of 30 Hz it was approximately two-thirds of the table length away (Figure 10c). Beyond 30 Hz, there was excessive noise coupled with violent motion of the table, which did not permit making measurements.

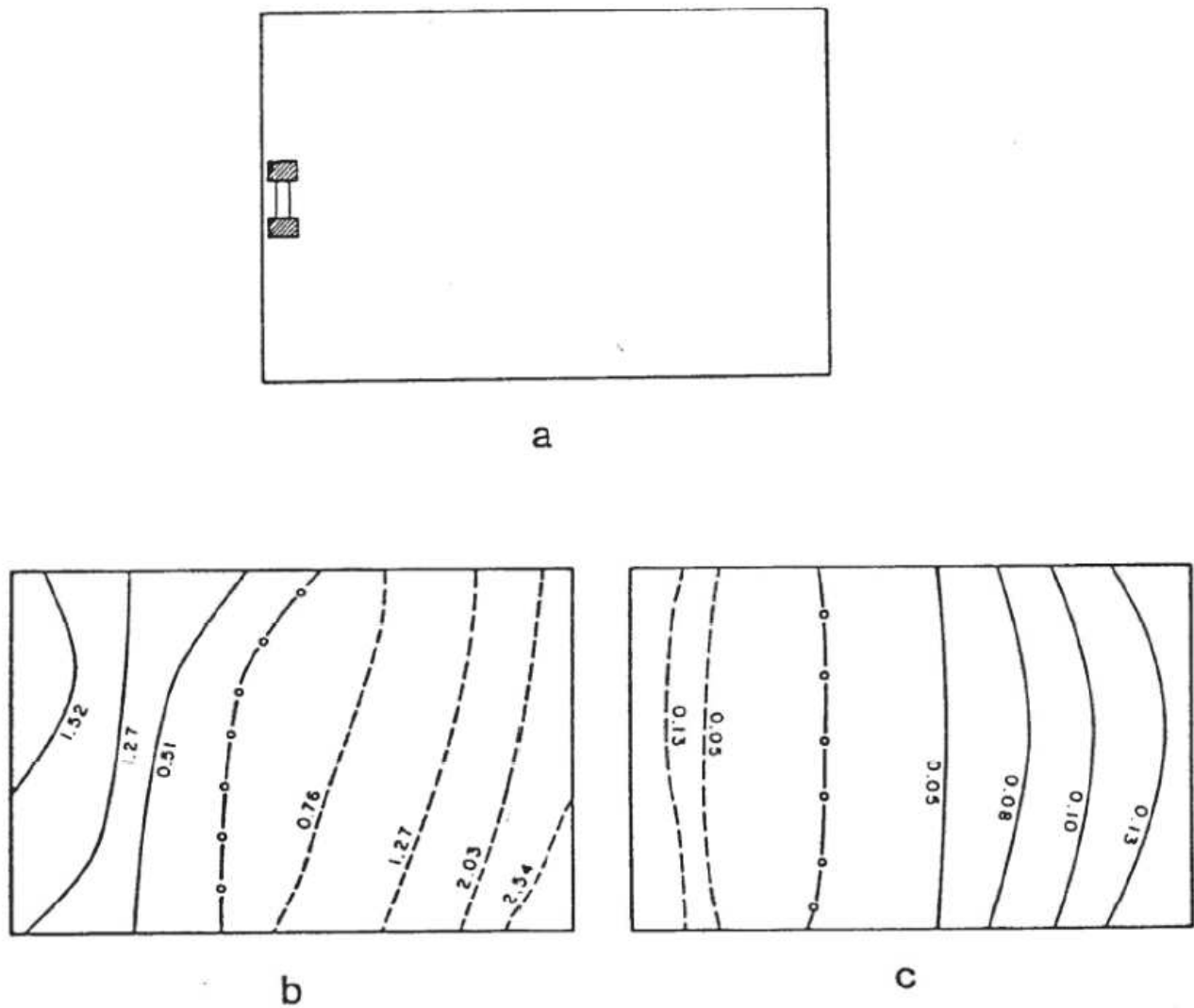


Figure 10. Schematics showing , (a) the position of vibrator on the table, (b) iso-amplitude lines at 10 Hz, and (c) iso-amplitude lines at 30 Hz. The numbers are amplitudes of vibration in millimeters.



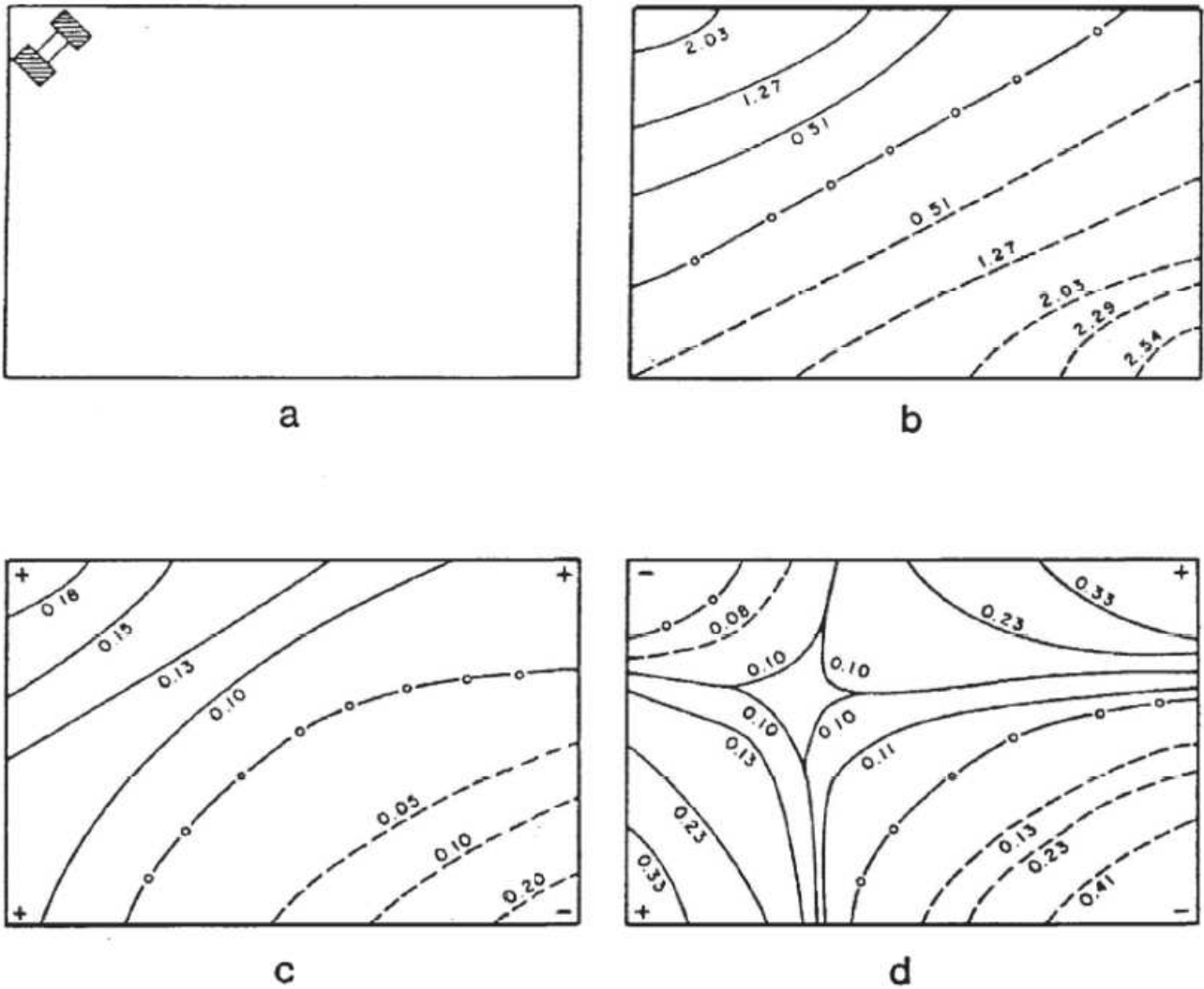


Figure 11. Iso-amplitude lines at (b) 10 Hz, (c) 20 Hz, and (d) 30 Hz, when (a) the vibrator is clamped to a corner of the table.

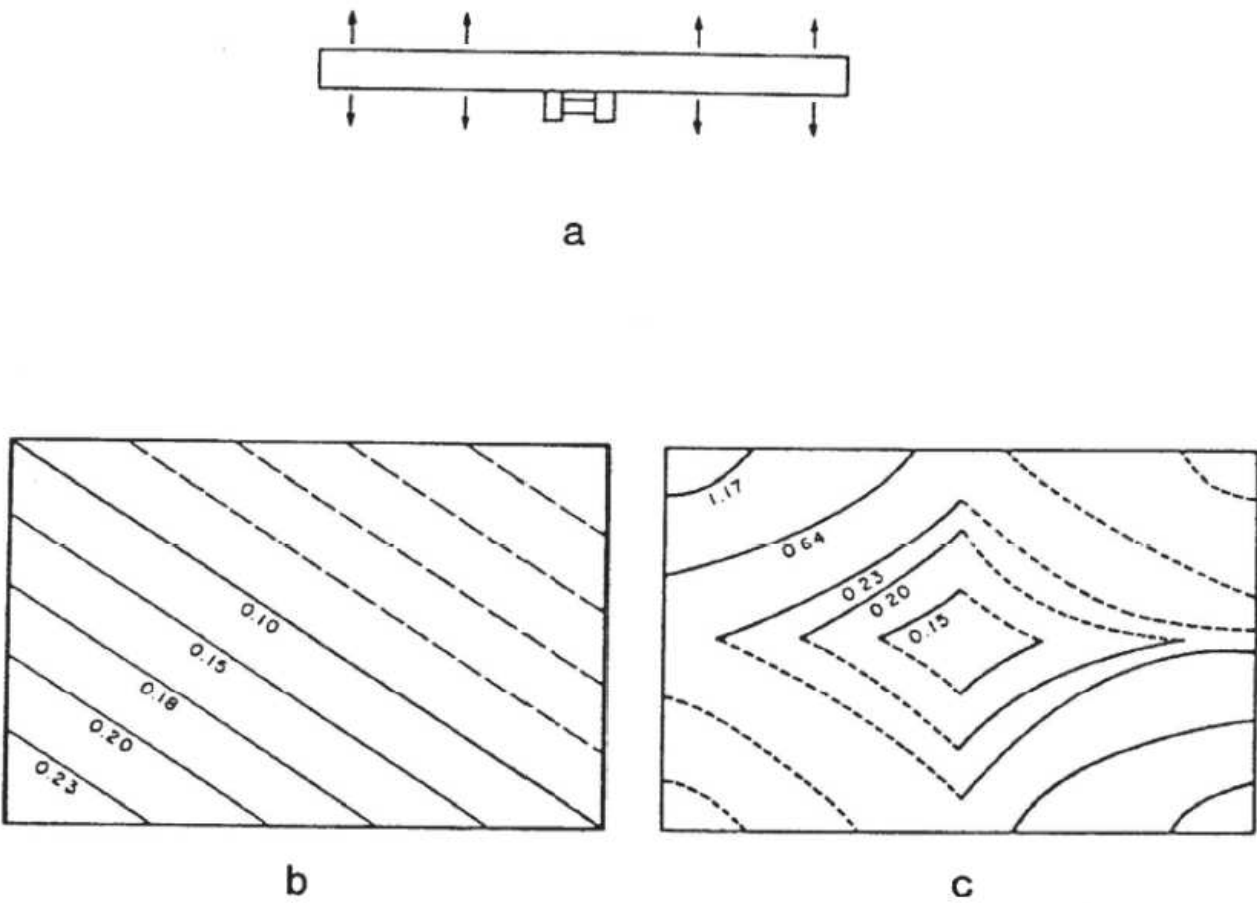


Figure 12. Motions of the table when vibrator was clamped to the center of the table and vibrated at (a) 10 Hz, (b) 30 Hz, and (c) 40 Hz.

The table showed similar oscillatory types of motion when the vibrator was clamped to a corner (Figure 11a). The nodal line moved away from the corner to which the motor was clamped, Figures 11b and 11c, as the frequency was increased. However, at 30 Hz, the motion was complex and contained two nodal lines, one close to the motor, the other closer to the opposite corner (Figure 11d). Once again, increasing the frequency beyond 30 Hz resulted in excessive vibration amplitude of the table and hence, no measurements could be taken.

The motion of the table, when the motor was clamped at the center, was quite interesting. As shown in Figure 12a, at 10 Hz, the entire table moved up and down about its unvibrated position, with a constant peak-to-peak amplitude. At 20 and 30 Hz, the motions of the table were identical, a rocking type about the diagonal. Figure 12b shows such a type of motion, when the table was vibrated at 30 Hz. It was possible, now, with the motor at the center, to increase the frequency to 40 Hz. The fact that this was a fundamental resonant frequency of the table was confirmed by a large increase in the acceleration. Figure 12c shows a flexing, buckling type of motion of the table at 40 Hz. With the exception of this particular case, the motion of the table was a rigid body motion, where the whole table vibrated as a body. On the other hand, the flexible body motion shown in Figure 12c produced waves of tension-compression necessary to affect a change in the state of residual stress. A rigid body motion, from the point of view of stress relieving by actual plastic deformation, seems useless. Indeed in section 4.2.3., the effectiveness of

flexural motion upon stress relieving has been clearly demonstrated. Also, recently one of the manufacturers of the commercial vibratory stress relief equipment has advised the use of a "motion sensing transducer" which reports only the flexural motion in a workpiece.

#### 4.2. Residual Stress Analysis

A detailed description of the calculation of residual stresses by the blind-hole-drilling method is given in Reference 41. The measured values of relaxed strains from the three gauges in the rosette (Figure 13) and the diameter of the drilled hole are used to calculate the principal stresses using the following equations:

$$S_1 = \frac{\epsilon_3 + \epsilon_1}{4A} + \frac{\epsilon_3 - \epsilon_1}{4B \cos 2\beta} \quad (1)$$

$$S_2 = \frac{\epsilon_3 + \epsilon_1}{4A} - \frac{\epsilon_3 - \epsilon_1}{4B \cos 2\beta} \quad (2)$$

$$\tan 2\beta = \frac{\epsilon_3 + \epsilon_1 - \epsilon_2}{\epsilon_3 - \epsilon_1} \quad (3)$$

$$A = \frac{-(1 + \nu)}{2E} \left( \frac{R_o}{R} \right)^2 \quad (4)$$

$$B = -\frac{1}{E} \left[ 2 \left( \frac{R_o}{R} \right)^2 - \frac{3(1 + \nu)}{2} \left( \frac{R_o}{R} \right)^4 \right] \quad (5)$$

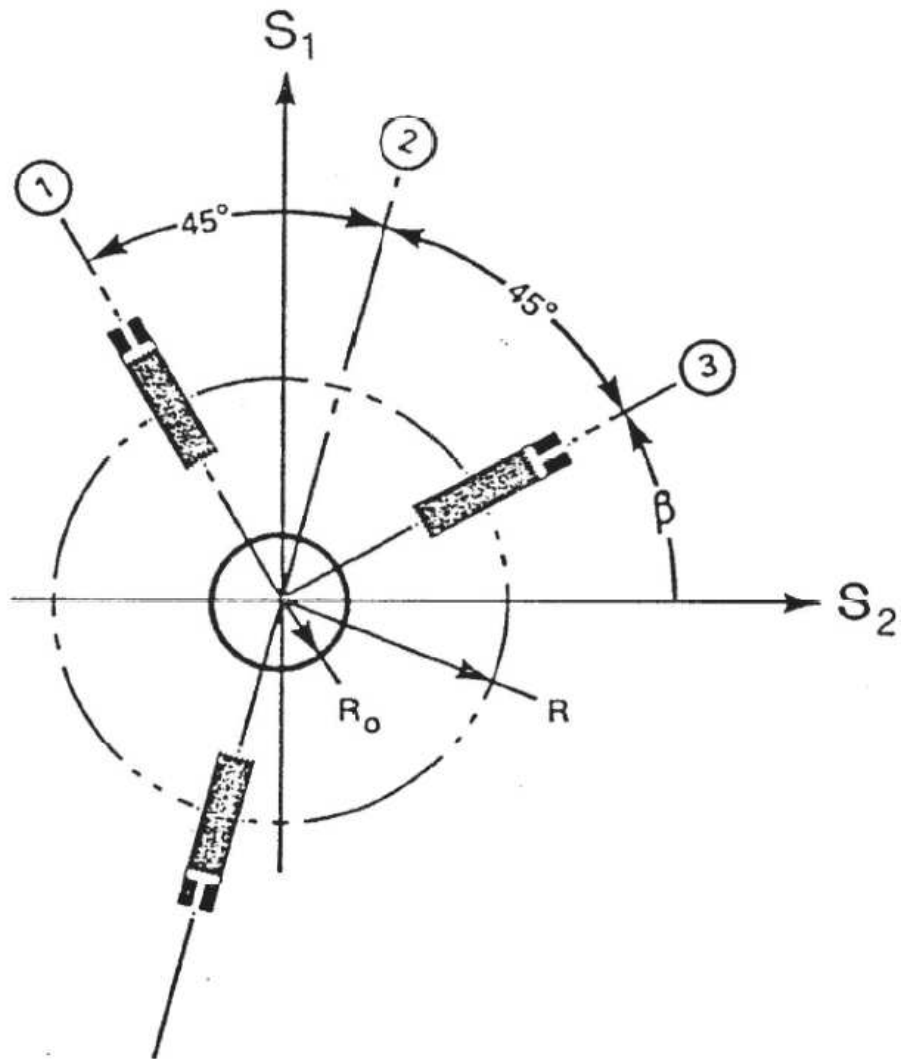


Figure 13. Strain gauge rosette arrangement and the blind-hole geometry for determining residual stresses.

where:

$S_1, S_2$  = principal stresses

$\epsilon_1, \epsilon_2, \epsilon_3$  = relaxed strains from gauges 1, 2 and 3

$\beta$  = angle between  $S_1$  and gauge 3

$\nu$  = Poisson's ratio

$E$  = Young's modulus

$R_o$  = radius of the drilled hole

$R$  = radius of the gauge circle.

Once the maximum and the minimum principal stresses and  $\beta$  are known, the longitudinal,  $S_L$ , transverse,  $S_T$ , and the shear stress,  $S_{LT}$ , at the surface of the weldment can be calculated using the equations:

$$S_{\max} = \frac{S_L + S_T}{2} + \left[ \left( \frac{S_L - S_T}{2} \right)^2 + S_{LT}^2 \right]^{1/2} \quad (6)$$

$$S_{\min} = \frac{S_L + S_T}{2} - \left[ \left( \frac{S_L - S_T}{2} \right)^2 + S_{LT}^2 \right]^{1/2} \quad (7)$$

$$\tan 2\theta = \frac{2 S_{LT}}{S_L - S_T} \quad (8)$$

where  $\theta$  is the positive angle measured counterclockwise from the direction of  $S_L$  to that of  $S_{\min}$ . The angle  $\theta$  can be determined using the value  $\beta$ . Since a large amount of data was gathered from experiments, the PRIME computer was utilized to perform the calculations.

In the sectioning technique, longitudinal stresses were calculated directly from the elastic strains relieved due to the action of cutting.

Stresses were also calculated from the strains obtained by measuring the resistance change. Strain, then, was calculated using the equation,

$$\epsilon = \frac{\Delta R}{(R) \times (G.F.)}$$

where:

$\Delta R$  = change in resistance due to sectioning

$R$  = resistance of unloaded strain gauge

G.F. = gauge factor of the strain gauge.

#### 4.2.1. Verification of Longitudinal Residual Stress Pattern

Developed in a Butt Weldment

The longitudinal residual stresses relieved by sectioning the 1018 mild steel weldment were calculated using the relation,

$$\sigma = \frac{\epsilon}{E}$$

where:

$\sigma$  is the longitudinal residual stress

$\epsilon$  is the strain recorded after sectioning

$E$  is the Young's modulus.

Figure 14 shows the distribution of longitudinal residual stress at several distances from the weld center line. Due to the symmetrical nature of the distribution, only half the curve on one side of the weld is shown. The stress distribution closely resembles

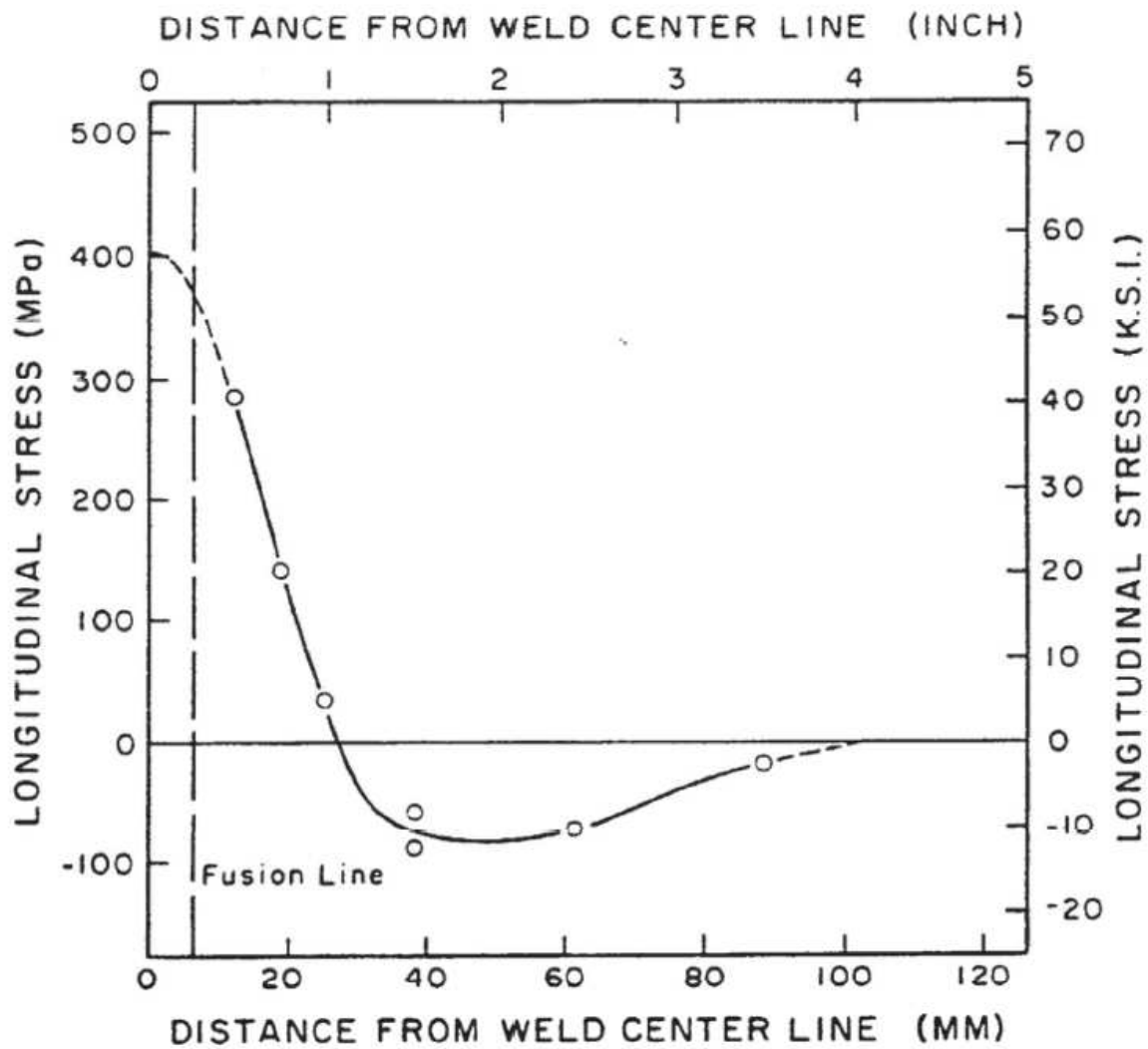


Figure 14. Longitudinal residual stress distribution in a SAE 1018 butt weldment.  
Note the similarity of the stress distribution to that in figure 2.



the general pattern of Figure 2. Also, it can be seen that the magnitude of peak stresses approaches the yield point.

#### 4.2.2. The Effect of Resonant Vibratory Treatment on the Longitudinal Residual Stress Distribution

The measured relaxed strains and the calculated longitudinal residual stresses for the three 305 x 508 x 12.7 mm weldments clamped at different locations on the vibration table, before and after the vibratory treatment at 40 Hz, are given in Tables II and III, respectively. These strains were determined by the blind-hole-drilling method. The average longitudinal stress distribution from the three weldments, as a function of the distance from weld center line, is shown graphically in Figure 15. The limitations of the blind-hole-drilling technique when measuring stresses of the yield point magnitude near a weld are clearly evident from this figure. If the local yielding effect due to the stress concentration in the vicinity of the hole is ignored, the measured stresses can be greatly overestimated.<sup>42</sup> Measured stresses, in the base plate close to the weld, exceeded the ultimate tensile strength indicating gross overestimation. Longitudinal residual stresses after vibration were also measured by the sectioning technique and are given in Table IV. A comparison of the longitudinal stresses from Tables III and IV also clearly indicates the exaggerated stresses obtained by the blind-hole-drilling technique when corrections for local plasticity effects are not made.

TABLE II.

BLIND-HOLE-DRILLING STRESS ANALYSIS OF AS WELDED, UNVIBRATED WELDMENTS  
(WITHOUT CORRECTION FACTORS)

II (a)

Weldment #1

Rosette #	Distance From Weld Center Line mm (inch)	Relaxed Strain, $\mu$ strain			Principal Stress MPa (ksi)		Longitudinal Stress, $S_L$ MPa (ksi)	Transverse Stress, $S_T$ MPa (ksi)
		$\epsilon_1$	$\epsilon_2$	$\epsilon_3$	$S_1$	$S_2$		
1	14 (0.55)	-218	40	-190	169 (24.50)	423 (61.39)	423 (61.36)	169 (24.53)
2	23 (0.90)	-105	-114	-15	124 (17.94)	50 (7.33)	153 (22.26)	63 (9.09)
3	33 (1.30)	-48	-118	-98	133 (19.25)	79 (11.48)	55 (8.02)	129 (18.76)
4	48 (1.90)	-125	-146	80	-51 (-7.38)	114 (16.59)	-32 (-4.62)	95 (13.81)
5	74 (2.90)	10	-130	-24	79 (11.49)	-58 (-8.39)	-57 (-8.28)	79 (11.40)
6	114 (4.50)	-12	-62	26	-50 (-7.28)	29 (4.17)	-28 (-4.05)	55 (8.03)

TABLE II.  
(cont.)  
BLIND-HOLE-DRILLING STRESS ANALYSIS OF AS WELDED, UNVIBRATED WELDMENTS  
(WITHOUT CORRECTION FACTORS)

II (b) Weldment #2

Rosette #	Distance From Weld Center Line mm (inch)	Relaxed Strain, $\mu$ strain			Principal Stress MPa (ksi)		Longitudinal Stress, $S_L$ MPa (ksi)	Transverse Stress, $S_T$ MPa (ksi)
		$\epsilon_1$	$\epsilon_2$	$\epsilon_3$	$S_1$	$S_2$		
13	13 (0.51)	-186	46	-200	163 (23.62)	442 (64.09)	440 (63.89)	165 (23.96)
14	21 (0.83)	- 81	- 96	-122	189 (27.49)	143 (20.71)	177 (25.63)	157 (22.80)
15	32 (1.26)	- 52	-118	-103	73 (10.57)	101 (14.63)	66 ( 9.75)	108 (15.64)
16	48 (1.90)	- 64	-128	112	- 34 (-4.89)	101 (14.67)	- 21 (-3.00)	95 (13.76)
17	74 (2.90)	- 20	-110	14	87 (12.68)	- 32 (-4.72)	- 29 (-4.24)	83 (12.09)
18	114 (4.50)	- 14	- 63	24	- 53 (-7.74)	29 ( 4.25)	- 31 (-4.52)	59 ( 8.62)

TABLE II.  
(cont.)  
BLIND-HOLE-DRILLING STRESS ANALYSIS OF AS WELDED, UNVIBRATED WELDMENTS  
(WITHOUT CORRECTION FACTORS)

II (c) Weldment #3

Rosette #	Distance From Weld Center Line mm (inch)	Relaxed Strain, $\mu$ strain			Principal Stress MPa (ksi)		Longitudinal Stress, $S_L$ MPa (ksi)	Transverse Stress, $S_T$ MPa (ksi)
		$\epsilon_1$	$\epsilon_2$	$\epsilon_3$	$S_1$	$S_2$		
25	15 (0.59)	-207	51	-163	150 (21.75)	409 (59.25)	419 (60.70)	140 (20.30)
26	23 (0.90)	-126	- 84	- 97	129 (18.74)	168 (24.43)	139 (20.15)	159 (23.02)
27	34 (1.34)	- 74	- 92	-119	119 (17.28)	45 ( 6.48)	43 ( 6.25)	121 (17.51)
28	48 (1.90)	18	-108	- 30	86 (12.49)	- 44 (-6.32)	- 43 (-6.19)	85 (12.36)
29	75 (2.95)	12	-129	- 22	78 (11.27)	- 58 (-8.39)	- 56 (-8.14)	76 (11.02)
30	114 (4.50)	4	- 73	- 7	28 ( 4.07)	- 54 (-7.78)	- 53 (-7.70)	28 ( 3.99)

TABLE III.

BLIND-HOLE-DRILLING STRESS ANALYSIS OF THE VIBRATED WELLEMENTS  
(WITHOUT CORRECTION FACTORS)

III (a) Weldment #1 Center

Rosette #	Distance From Weld Center Line mm (inch)	Relaxed Strain, $\mu$ strain			Principal Stress MPa (ksi)		Longitudinal Stress, $S_L$ MPa (ksi)	Transverse Stress, $S_T$ MPa (ksi)
		$\epsilon_1$	$\epsilon_2$	$\epsilon_3$	$S_1$	$S_2$		
7	14 (0.55)	-170	56	-250	485 (70.41)	176 (25.58)	484 (70.17)	178 (25.83)
8	23 (0.90)	- 90	- 80	-232	316 (45.78)	192 (27.82)	300 (43.55)	207 (30.05)
9	33 (1.30)	-148	- 78	-136	143 (20.78)	188 (27.30)	153 (22.25)	178 (25.85)
10	48 (1.90)	32	-193	-104	149 (21.69)	- 39 (-5.69)	- 31 (-4.56)	142 (20.56)
11	74 (2.90)	-150	49	131	- 65 (-9.42)	92 (13.30)	- 59 (-8.55)	86 (12.42)
12	114 (4.50)	- 80	- 4	74	- 36 (5.19)	44 (6.44)	- 36 (-5.17)	44 ( 6.44)

TABLE III.

BLIND-HOLE-DRILLING STRESS ANALYSIS OF THE VIBRATED WELDMENTS  
(WITHOUT CORRECTION FACTORS)

Rosette #	Distance From Weld Center Line mm (inch)	Relaxed Strain, $\mu$ strain			Principal Stress MPa (ksi)		Longitudinal Stress, $S_L$ MPa (ksi)	Transverse Stress, $S_T$ MPa (ksi)
		$\epsilon_1$	$\epsilon_2$	$\epsilon_3$	Edge			
					$S_1$	$S_2$		
19	13 (0.51)	-174	68	-238	468 (67.85)	163 (23.71)	465 (67.46)	166 (24.10)
20	21 (0.83)	-108	-322	-140	288 (41.84)	75 (10.92)	288 (41.79)	75 (10.97)
21	32 (1.26)	-136	-156	-40	89 (12.90)	181 (26.22)	162 (23.47)	108 (15.64)
22	48 (1.90)	38	-174	-119	134 (19.46)	-47 (-6.83)	-29 (-4.25)	116 (16.88)
23	74 (2.90)	-132	53	157	98 (14.29)	-73 (-10.06)	-55 (-8.49)	88 (12.71)
24	114 (4.50)	-84	-9	72	-37 (-5.44)	46 (6.75)	-34 (-4.87)	43 (6.19)

TABLE III.  
(cont.)  
BLIND-HOLE-DRILLING STRESS ANALYSIS OF THE VIBRATED WELLEMENTS  
(WITHOUT CORRECTION FACTORS)

Rosette #	Distance From Weld Center Line mm (inch)	Relaxed Strain, $\mu$ strain			Principal Stress MPa (ksi)		Longitudinal Stress, $S_L$ MPa (ksi)	Transverse Stress, $S_T$ MPa (ksi)
		$\epsilon_1$	$\epsilon_2$	$\epsilon_3$	MPa (ksi)			
					$S_1$	$S_2$		
31	15 (0.59)	-178	62	-261	492 (71.38)	156 (22.65)	490 (71.01)	159 (23.02)
32	23 (0.90)	-212	- 60	- 88	170 (24.59)	290 (42.08)	300 (43.48)	160 (23.18)
33	34 (1.34)	-115	13	-105	123 (17.89)	155 (22.48)	146 (21.25)	132 (19.13)
34	48 (1.90)	41	-129	-109	103 (14.87)	- 34 (-4.93)	- 35 (-5.15)	104 (15.09)
35	75 (2.95)	-153	37	120	-57 (-8.21)	86 (12.48)	- 56 (-8.08)	85 (12.35)
36	114 (4.50)	32	-116	- 74	56 ( 8.11)	- 34 (-4.91)	- 35 (-5.08)	57 ( 8.28)

III (c)

Weldment #3

Corner

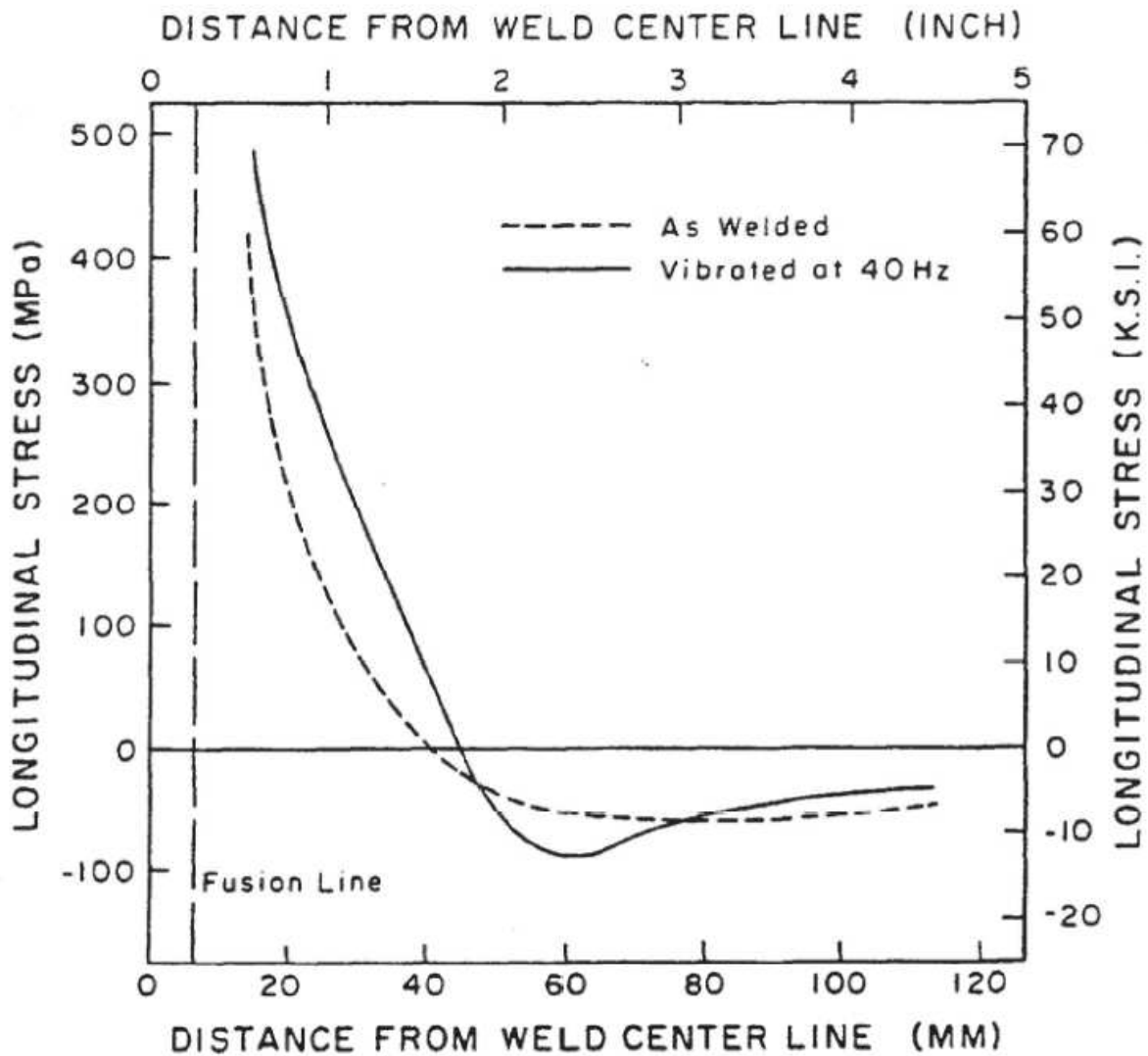


Figure 15. Longitudinal residual stress distributions as determined by the uncorrected hole-drilling method.



TABLE IV.

LONGITUDINAL RESIDUAL STRESSES IN VIBRATED SAMPLES  
AS DETERMINED BY THE SECTIONING TECHNIQUE

Distance From Weld Center Line mm (inch)	Resistance (Ohms)		Change in Resistance (Ohms)	Longitudinal Stress, $S_L$ MPa (ksi)
	Weldment #1			
	Before Cutting	After Cutting		
15 (0.60)	119.9925	119.6850	-0.3075	240 ( 34.75)
22 (0.85)	120.3200	120.0275	-0.2925	228 ( 33.05)
32 (1.25)	120.1325	119.8775	-0.2550	199 ( 28.81)
48 (1.90)	120.3650	120.3525	-0.0125	10 ( 1.41)
74 (2.90)	120.0800	120.2125	+0.1325	-103 (-14.97)
114 (4.50)	119.9875	120.0625	+0.0750	- 58 (- 8.47)
Young's Modulus - $19.3 \times 10^4$ MPa				
Gauge Factor = 2.065 (2.8 x 10 <sup>7</sup> psi)				

TABLE IV.  
(cont.)  
LONGITUDINAL RESIDUAL STRESSES IN VIBRATED SAMPLES  
AS DETERMINED BY THE SECTIONING TECHNIQUE

Distance From Weld Center Line mm (inch)	Resistance (Ohms)		Change in Resistance (Ohms)	Longitudinal Stress, $S_L$ MPa (ksi)
	Before Cutting	After Cutting		
15 (0.59)	120.2225	119.9075	-0.3150	245 ( 35.59)
22 (0.87)	120.1575	119.8725	-0.2850	222 ( 32.20)
32 (1.26)	119.9925	119.7350	-0.2575	201 ( 29.10)
48 (1.89)	119.8850	119.8675	-0.0175	14 ( 1.98)
74 (2.90)	120.1325	120.2700	+0.1375	<sup>-107</sup> (-15.54)
114 (4.50)	120.4025	120.4725	+0.0750	<sup>- 54</sup> (- 7.91)
Young's Modulus - $19.3 \times 10^4$ MPa Gauge Factor = 2.065      ( $2.8 \times 10^7$ psi)				

IV (b)      Weldment #2      Edge

TABLE IV.  
(cont.)  
LONGITUDINAL RESIDUAL STRESSES IN VIBRATED SAMPLES  
AS DETERMINED BY THE SECTIONING TECHNIQUE

Distance From Weld Center Line mm (inch)	Resistance (Ohms)		Change in Resistance (Ohms)	Longitudinal Stress, $S_L$ MPa (ksi)
	Before Cutting	After Cutting		
15 (0.50)	119.9775	119.6650	-0.3125	243 ( 35.31)
22 (0.85)	120.2425	119.9600	-0.2825	220 ( 31.92)
32 (1.25)	120.0575	119.8075	-0.2500	195 ( 28.25)
48 (1.90)	120.0525	120.0450	-0.0075	6 ( 0.85)
74 (2.90)	120.1750	120.3000	+0.1250	- 97 (-14.12)
114 (4.50)	119.9925	120.0400	+0.0475	- 37 (- 5.37)
Young's Modulus - $19.3 \times 10^4$ MPa Gauge Factor = 2.065      ( $2.8 \times 10^7$ psi)				

IV (c)

Weldment #3

Corner

Also, errors due to machining stresses caused by the drilling of the hole using end mills have been reported by other investigators.<sup>21-23</sup> This machining stress, coupled with errors due to local yielding, could vastly change the measured stresses.

Thus, additional experiments were conducted to estimate the effect of both the machining stresses and the local yielding due to stress concentration. The details of the experiments and the corrections employed are given in the Appendix. Corrections were made for all the relaxed strains obtained by the blind-hole-drilling method and the corrected values are shown in Tables V and VI. Figure 16 shows a good agreement between the corrected values from blind-hole-drilling method and the values from the sectioning technique for weldments vibrated at the resonant frequency of 40 Hz. Similar agreement also in the case of as-welded weldments is shown in section 4.2.4. Blind-hole-drilling technique can thus be successfully employed to measure yield point magnitude stresses, such as those near welds, when suitable corrections for the machining and the local yielding errors are made. Figure 17 is a composite of residual stress distributions before and after the vibratory treatment, where the stresses are the average values from the three weldments. Several points are evident from this figure. First, the peak stress was reduced from about 359 MPa to about 276 MPa, a drop of about 30%. Similar reductions in peak stresses were obtained by Zubchenko, et al., in two separate investigations;<sup>39, 43</sup> by Grudz, et al.,<sup>38</sup> in mild steel,

TABLE V.  
 BLIND-HOLE-DRILLING STRESS ANALYSIS OF AS WELDED, UNVIBRATED WELDMENTS  
 (WITH CORRECTION FACTORS)

V (a) Weldment #1

Rosette #	Distance From Weld Center Line mm (inch)	Relaxed Strain, $\mu$ strain			Principal Stress MPa (ksi)		Longitudinal Stress, $S_L$ MPa (ksi)	Transverse Stress, $S_T$ MPa (ksi)
		$\epsilon_1$	$\epsilon_2$	$\epsilon_3$	$S_1$	$S_2$		
1	14 (0.55)	-148	75	-120	85 (12.40)	303 (44.02)	311 (45.18)	77 (11.24)
2	23 (0.90)	- 70	- 79	20	182 (26.46)	86 (12.50)	230 (33.36)	109 (15.76)
3	33 (1.30)	- 13	- 83	- 63	75 (10.90)	127 (18.45)	137 (19.84)	68 ( 9.90)
4	48 (1.90)	- 90	-111	55	- 32 (-4.69)	84 (12.24)	- 15 (-2.25)	70 (10.20)
5	74 (2.90)	35	- 95	- 5	91 (13.27)	- 45 (-6.60)	- 45 (-6.53)	91 (13.16)
6	114 (4.50)	23	- 27	61	29 (4.25)	- 34 (-4.98)	- 33 (- 4.84)	28 ( 4.04)

TABLE V.  
(cont.)  
BLIND-HOLE-DRILLING STRESS ANALYSIS OF AS WELDED, UNVIBRATED WELDMENTS  
(WITH CORRECTION FACTORS)

V (b) Weldment #2

Rosette #	Distance From Weld Center Line mm (inch)	Relaxed Strain, $\mu$ strain			Principal Stress MPa (ksi)		Longitudinal Stress, $S_L$ MPa (ksi)	Transverse Stress, $S_T$ MPa (ksi)
		$\epsilon_1$	$\epsilon_2$	$\epsilon_3$	$S_1$	$S_2$		
13	13 (0.51)	-122	81	-136	120 (17.48)	298 (43.28)	298 (43.16)	122 (17.64)
14	21 (0.83)	- 46	- 61	- 87	99 (14.38)	172 (24.98)	219 (31.76)	77 (11.20)
15	32 (1.26)	- 20	- 83	- 52	79 (11.45)	142 (20.64)	145 (21.10)	72 (10.41)
16	48 (1.90)	- 29	- 93	132	- 17 (-2.42)	85 (12.39)	- 10 (-1.49)	79 (11.46)
17	74 (2.90)	20	- 75	49	- 51 (-7.42)	25 ( 3.58)	- 44 (-6.42)	18 ( 2.59)
18	114 (4.50)	15	- 28	69	- 46 (-6.75)	36 ( 5.22)	- 34 (-5.01)	48 ( 6.92)

TABLE V.  
(cont.)  
BLIND-HOLE-DRILLING STRESS ANALYSIS OF AS WELDED, UNVIBRATED WELDMENTS  
(WITH CORRECTION FACTORS)

Rosette #	Distance From Weld Center Line mm (inch)	Relaxed Strain, $\mu$ strain			Principal Stress MPa (ksi)		Longitudinal Stress, $S_L$ MPa (ksi)	Transverse Stress, $S_T$ MPa (ksi)
		$\epsilon_1$	$\epsilon_2$	$\epsilon_3$	$S_1$	$S_2$		
		V (c) Weldment #3						
25	15 (0.59)	-132	80	-108	101 (14.63)	267 (38.70)	272 (39.47)	96 (13.86)
26	23 (0.90)	- 91	- 49	- 62	121 (17.51)	185 (26.84)	228 (33.13)	77 (11.23)
27	34 (1.34)	- 39	- 57	- 84	133 (19.25)	57 ( 8.20)	135 (19.55)	54 ( 7.90)
28	48 (1.90)	53	- 73	5	102 (14.83)	- 13 (-1.94)	- 13 (-1.94)	102 (14.83)
29	75 (2.95)	47	- 94	13	65 ( 9.44)	- 37 (-5.42)	- 38 (-5.58)	66 ( 9.60)
30	114 (4.50)	39	- 38	28	27 ( 3.82)	- 35 (-5.09)	- 35 (-5.15)	27 ( 3.90)

TABLE VI.

BLIND-HOLE-DRILLING STRESS ANALYSIS OF THE UNVIBRATED WELDMENTS  
(WITH CORRECTION FACTORS)

Rosette #	Distance From Weld Center Line mm (inch)	Relaxed Strain, $\mu$ strain			Principal Stress MPa (ksi)		Longitudinal Stress, $S_L$ MPa (ksi)	Transverse Stress, $S_T$ MPa (ksi)
		$\epsilon_1$	$\epsilon_2$	$\epsilon_3$	$S_1$	$S_2$		
7	14 (0.55)	-100	16	-160	259 (37.49)	107 (15.49)	260 (37.70)	106 (15.36)
8	23 (0.90)	- 50	- 40	-170	226 (32.83)	120 (17.46)	215 (31.23)	130 (18.86)
9	33 (1.30)	-103	- 43	-101	166 (24.02)	169 (24.55)	177 (25.72)	157 (22.85)
10	48 (1.90)	67	-113	- 69	130 (18.84)	- 45 (-6.50)	- 36 (-5.22)	123 (17.86)
11	74 (2.90)	-115	89	105	- 93 (-13.49)	88 (12.78)	- 84 (-12.24)	82 (11.94)
12	114 (4.50)	- 45	30	105	- 46 (-6.70)	43 (6.26)	- 43 (-6.25)	46 ( 6.71)



TABLE VI.  
(cont.)  
BLIND-HOLE-DRILLING STRESS ANALYSIS OF THE UNVIBRATED WELDMENTS  
(WITH CORRECTION FACTORS)

Rosette #	Distance From Weld Center Line mm (inch)	Relaxed Strain, $\mu$ strain			Principal Stress MPa (ksi)		Longitudinal Stress, $S_L$ MPa (ksi)	Transverse Stress, $S_T$ MPa (ksi)
		$\epsilon_1$	$\epsilon_2$	$\epsilon_3$	$S_1$	$S_2$		
19	13 (0.51)	-104	33	-148	247 (35.89)	103 (14.97)	253 (36.74)	97 (14.12)
20	21 (0.83)	-73	-232	-100	217 (31.48)	128 (18.59)	207 (30.05)	138 (20.02)
21	32 (1.26)	-96	-111	-56	72 (10.43)	189 (27.42)	184 (26.70)	77 (11.15)
22	48 (1.90)	73	-129	-89	65 (9.44)	-57 (-8.22)	-50 (-7.21)	58 (8.43)
23	74 (2.90)	-97	88	-112	101 (14.71)	-81 (-11.75)	-82 (-11.75)	102 (14.82)
24	114 (4.50)	-49	26	107	-43 (6.24)	85 (12.24)	-40 (-5.78)	82 (11.88)

TABLE VI.  
(cont.)  
BLIND-HOLE-DRILLING STRESS ANALYSIS OF THE UNVIBRATED WELDMENTS  
(WITH CORRECTION FACTORS)

Rosette #	Distance From Weld Center Line mm (inch)	Relaxed Strain, $\mu$ strain			Principal Stress MPa (ksi)		Longitudinal Stress, $S_L$ MPa (ksi)	Transverse Stress, $S_T$ MPa (ksi)
		$\epsilon_1$	$\epsilon_2$	$\epsilon_3$	$S_1$	$S_2$		
31	15 (0.59)	-103	27	-166	252 (36.48)	112 (16.31)	255 (36.93)	109 (15.87)
32	23 (0.90)	-137	-25	-53	102 (14.79)	203 (29.48)	204 (29.62)	101 (14.65)
33	34 (1.34)	-80	48	-70	47 (6.82)	183 (26.51)	178 (25.80)	52 (7.53)
34	48 (1.90)	56	-94	-74	73 (10.56)	-45 (-6.56)	-28 (-4.12)	56 (8.12)
35	75 (2.95)	-98	72	115	-81 (-11.81)	55 (8.03)	-82 (-11.96)	56 (8.19)
36	114 (4.50)	67	-71	-39	46 (6.63)	-29 (-4.19)	-32 (-4.57)	48 (7.01)

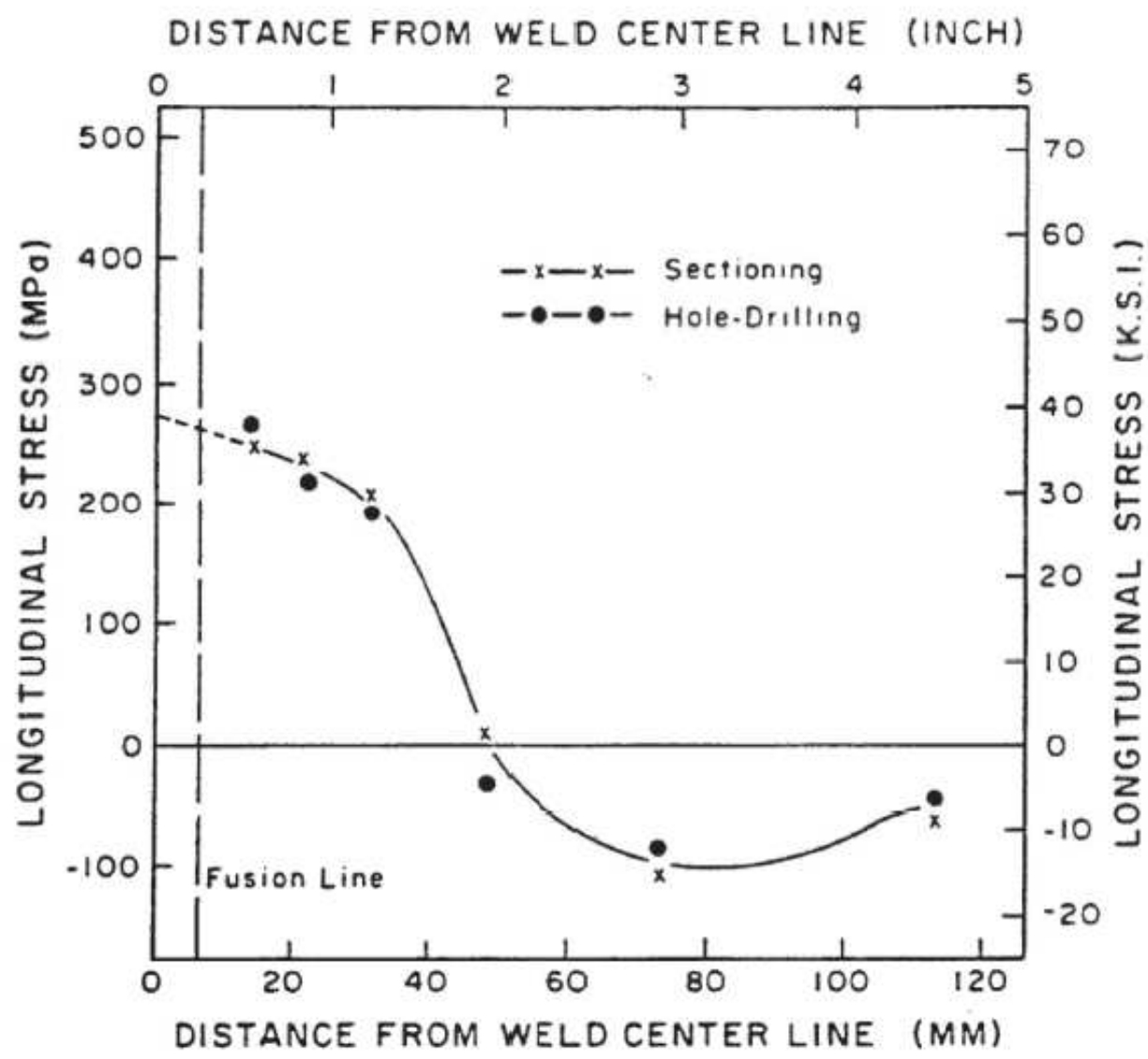


Figure 16. Residual stress distribution in a weldment vibrated at 40 Hz. The stresses determined by the corrected hole-drilling technique agree well with those obtained from the sectioning method.

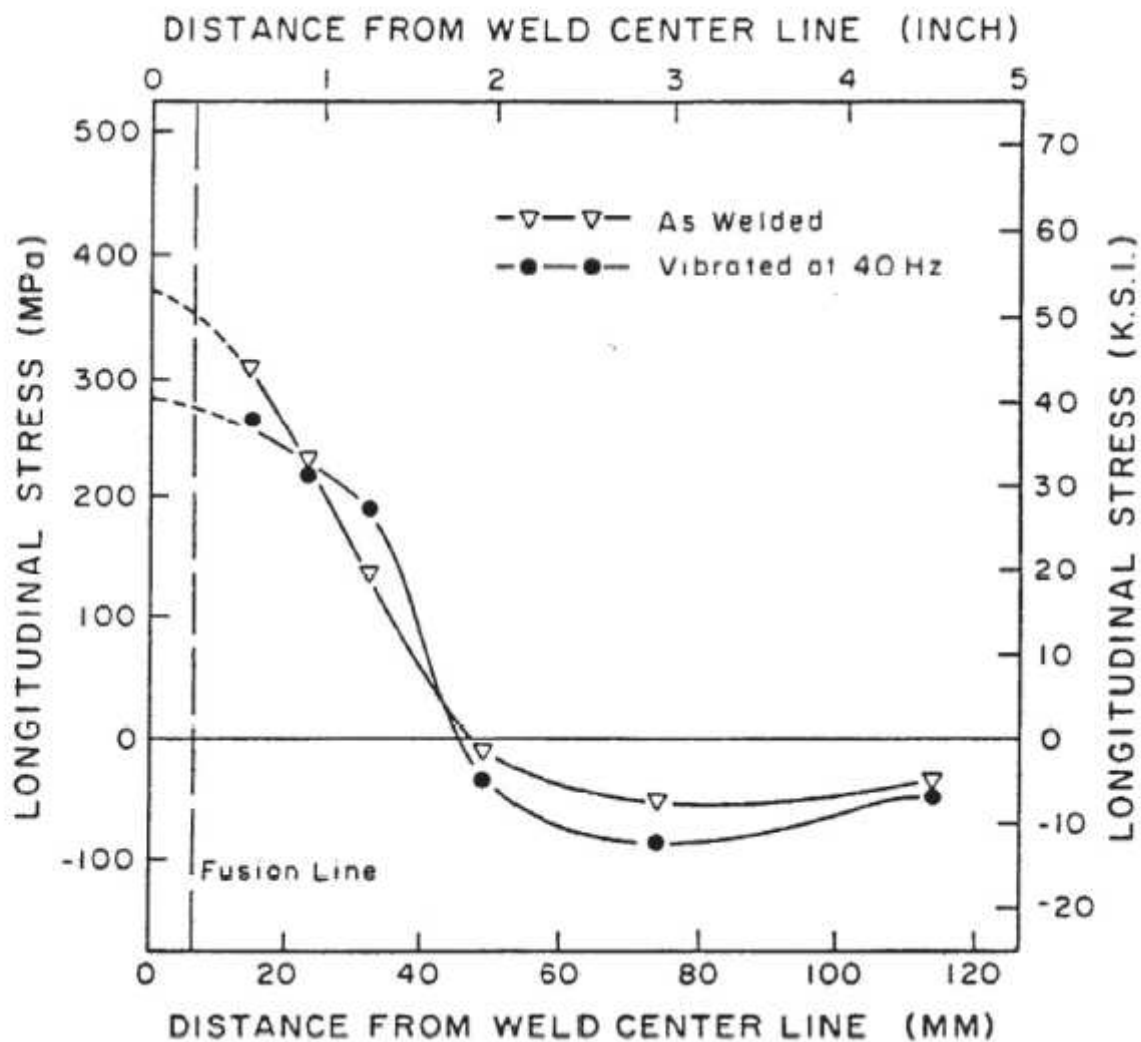


Figure 17. The redistribution of longitudinal residual stresses as a result of the resonant vibratory treatment at 40 Hz. Stress analysis done by the corrected hole-drilling method.

aluminum and titanium alloy weldments; and by Weiss, et al.,<sup>40</sup> in a plain carbon steel weldment.

Second, the residual stresses were not completely eliminated by the vibratory treatment, although several Russian authors have noticed up to 90% reduction in residual stresses.<sup>44</sup> On the other hand, there seemed to be a redistribution of residual stresses across the weld. A similar stress redistribution has been noticed by other investigators.<sup>38,39</sup>

Thus, resonant vibratory treatment when applied to mild steel weldments resulted in a definite redistribution of longitudinal stresses, and reduction in the peak residual stresses very close to the weld. The actual mechanism by which the stress reduction occurred will be discussed in section 4.3.

#### 4.2.3. Effectiveness of the Vibratory Treatment on the Location of Weldments

An examination of the longitudinal residual stress values from Table VI shows that due to the resonant vibratory treatment, all the three weldments have achieved about the same residual stress distribution, regardless of their position on the table during vibration. The considerable bending moments and torques noticed on the table at resonant frequency seem to act along a passing wave rather than a stationary wave. This would naturally expose any location on the table to the same amount of bending moment and thus make all the locations on the vibration table equally effective for the treatment.

The effectiveness of the treatment, within the length of each weldment, too, seems uniform. In a 305 mm long weld, the longitudinal stresses would remain constant in a region at the center and begin to decrease toward the ends. Conservatively, the middle 150 mm long portion of the weld can be assumed to have uniform stresses, with stresses decreasing in 75 mm regions on either end. In the residual stress measurement, holes were randomly drilled in a 100 mm long region at the center of each weldment. For example, in one weldment holes closest to the weld were drilled in the middle of the weldment, while in the other two, the holes were drilled 50 mm on either side of the center of the weld. Similarly, other holes were drilled on a random basis. Despite the randomness in the location of the holes, there was uniformity of stress redistribution in all three weldments, at least in the central 100 mm region.

#### 4.2.4. The Effect of Frequency of Vibration on the Longitudinal Residual Stress Distribution

The three 914 x 406 x 12.7 mm butt weldments were used in the study of the role of frequency of vibration on the residual stress distribution in the weldments. One weldment was given the standard resonance treatment at 40 Hz; the second, a sub-resonance treatment at 30 Hz; and the third was not vibrated and was used as a control. It was decided to monitor the stresses in the weldments using x-ray and sectioning techniques of stress measurement. For the purpose of x-ray studies, it was necessary to cut out a 127 mm square piece from

the middle of each weldment. Stresses relieved due to this sectioning were monitored and are given in Table VII for the three weldments studied. It was assumed that sectioning the 127 mm square pieces would not significantly relieve the stresses and that most of the residual stresses would be still locked up in those pieces. However, as seen in Table VII, and from the residual stress distributions plotted in Figure 18, it appeared that sectioning has relieved the majority of the locked-in stresses and that insignificant amounts of stress would be left in the 127 mm square pieces. Even though the x-ray analysis showed stresses of the order of 7 to 55 MPa in some locations, these stress values were not added onto those obtained from the sectioning method because of the inherently low accuracy of stress measurement (about 35 MPa) by this method due to the large grain size involved in the samples. Further, the stress readings were so randomly distributed without any trend of the classic stress distribution of Figure 2, it was assumed that sectioning had practically relieved all the residual stresses.

Referring to Figure 18, once again there was substantial reduction in peak stresses (from about 380 MPa to about 250 MPa) due to the resonance treatment at 40 Hz, coupled with stress redistribution similar in nature to that shown in Figure 17. For the 305 x 508 x 12.7 mm weldments, though there was a general stress reduction due to the sub-resonance treatment at 30 Hz, vibrating at resonant frequency apparently was more effective than that at a sub-resonant frequency.

TABLE VII.

RESIDUAL STRESS ANALYSIS BY THE SECTIONING TECHNIQUE  
(GAUGE FACTOR = 2.04 FOR ALL THE STRAIN GAUGES)

(a) As welded, control weldment

Gauge N <sup>o</sup>	Distance From Weld Center Line mm (inch)	Strain (microstrain)			Resistance (ohm)			Longitudinal Residual Stress, MPa (ksi)	
		After Cutting	Before Cutting	Change	After Cutting	Before Cutting	Change	From Resistance	From Strain
1	13 (0.50)	3530	5000	-1470	119.9200	120.2850	-0.3650	288 (41.75)	284 (41.16)
2	25 (1.00)	4023	5000	- 977	120.0025	120.2450	-0.2425	191 (27.74)	189 (27.36)
3	47 (1.85)	4943	5000	- 57	120.3450	120.3625	-0.0175	14 ( 2.00)	11 ( 1.60)
4	48 (1.90)	4989	5000	- 11	120.3025	120.3050	-0.0025	2 ( 0.29)	2 ( 0.31)
5	48 (1.90)	Gauge came off	5000	----	Gauge came off	120.2475	----	----	----
6	48 (1.90)	Gauge came off	5000	----	Gauge came off	120.1825	----	----	----



TABLE VII.  
(cont.)  
RESIDUAL STRESS ANALYSIS BY THE SECTIONING TECHNIQUE  
(GAUGE FACTOR = 2.04 FOR ALL THE STRAIN GAUGES)

(b) Weldment vibrated at 30 Hz

Gauge N <sup>o</sup>	Distance From Weld Center Line mm (inch)	Strain (microstrain)			Resistance (ohm)			Longitudinal Residual Stress, MPa (ksi)	
		After Cutting	Before Cutting	Change	After Cutting	Before Cutting	Change	From Resistance	From Strain
1	13 (0.50)	3608	5000	-1392	120.0200	120.3575	-0.3375	266 (38.60)	269 (38.98)
2	30 (1.20)	4085	5000	- 915	120.0650	120.2975	-0.2325	183 (26.59)	177 (26.62)
3	47 (1.85)	4864	5000	- 136	120.1225	120.1575	-0.0350	28 ( 4.00)	26 ( 3.81)
4	48 (1.90)	4910	5000	- 90	120.2025	120.2225	-0.0200	16 ( 2.29)	17 ( 2.52)
5	47 (1.85)	4852	5000	- 142	120.0900	120.1225	-0.0325	26 ( 3.72)	27 ( 3.98)
6	48 (1.90)	4935	5000	- 65	120.2800	120.2950	-0.0150	12 ( 1.72)	12 ( 1.82)

TABLE VII.  
(cont.)  
RESIDUAL STRESS ANALYSIS BY THE SECTIONING TECHNIQUE  
(GAUGE FACTOR = 2.04 FOR ALL THE STRAIN GAUGES)

(c) Weldment vibrated at 40 Hz

Gauge No	Distance From Weld Center Line mm (inch)	Strain (microstrain)			Resistance (ohm)			Longitudinal Residual Stress, MPa (ksi)	
		After Cutting	Before Cutting	Change	After Cutting	Before Cutting	Change	From Resistance	From Strain
1	13 (0.50)	3754	5000	-1246	120.2250	120.5275	-0.3025	238 (34.60)	240 (34.89)
2	25 (1.00)	3848	5000	-1152	120.1275	120.4100	-0.2825	223 (32.31)	222 (32.26)
3	47 (1.85)	4830	5000	- 170	120.2875	120.3325	-0.0450	35 ( 5.15)	33 ( 4.76)
4	48 (1.90)	4858	5000	- 142	120.2350	120.2750	-0.0400	31 ( 4.56)	27 ( 3.98)
5	47 (1.85)	4776	5000	- 224	120.1775	120.2250	-0.0475	37 ( 5.43)	43 ( 6.27)
6	48 (1.90)	Gauge broke	5000	----	Gauge broke	120.2075	----	----	----

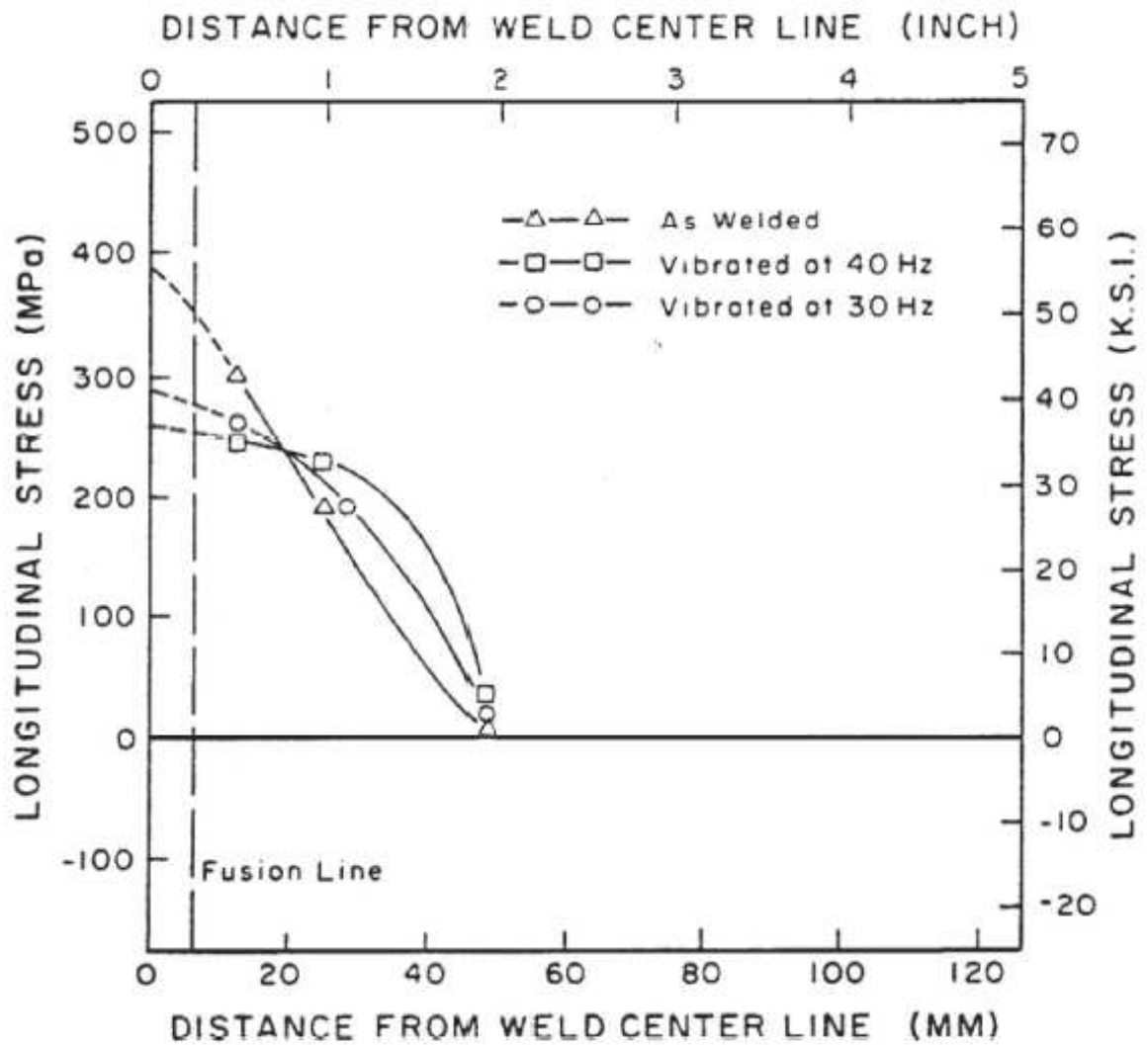


Figure 18. The effect of frequency of vibration on the longitudinal residual stress distribution. Stress analysis done by the sectioning technique.

As shown in Figure 19, in the case of an as-welded unvibrated weldment, the agreement between the corrected hole-drilling stress values obtained from the three 305 x 508 x 12.7 mm weldments and from the 914 x 406 x 12.7 mm control weldment was excellent. Once again, this proved that the corrected hole-drilling technique was comparable in accuracy to that of the sectioning method. Figure 20 shows the residual stress distribution for the four weldments vibrated at 40 Hz, indicating definite overall stress redistribution due to the vibratory treatment, whether the stress was measured by the sectioning or by the blind-hole-drilling technique.

#### 4.2.5. Effect on Macrostress

It has been shown in a number of investigations<sup>36-40</sup> that actual stress reduction occurs during vibrational treatments only in those locations where the combined residual vibratory stresses exceeded the yield point of the material. Usually these locations were where high stress concentration occurs, like the region adjacent to a weld. However, if the entire part being vibrated had a uniform stress level, a level close to the yield point of the material, will the vibratory treatment reduce the stress level? In order to test the action of vibratory treatment on high, uniform macrostresses, the tension weldment shown in Figure 4 was vibrated at its resonance. Table VIII shows the stress values obtained at three locations by the corrected hole drilling method. It can be seen that the plate developed an average residual tensile stress of about 234 MPa in a direction parallel to

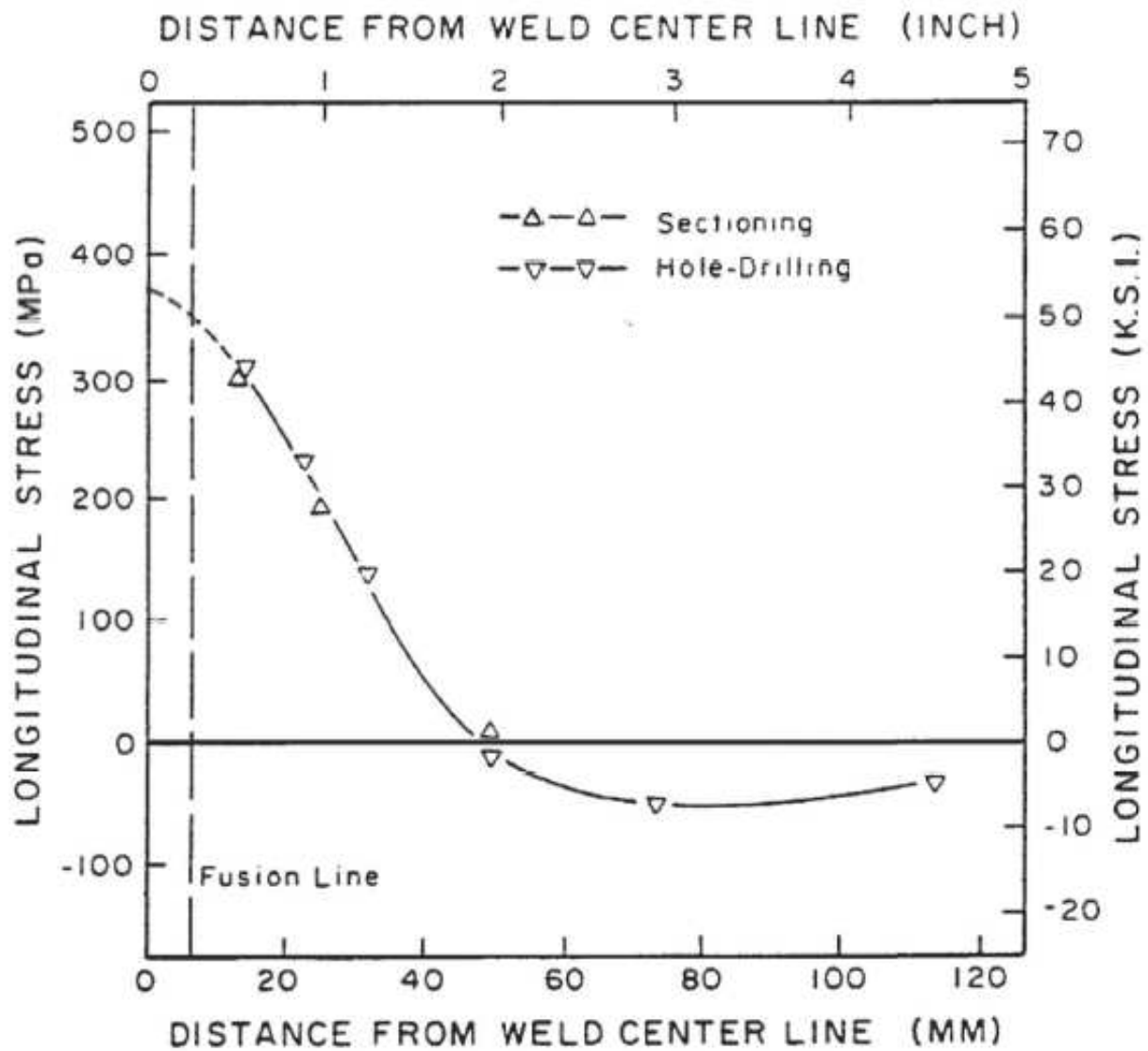


Figure 19. Residual stress distribution in the unvibrated weldments showing excellent agreement between sectioning and corrected hole-drilling techniques.

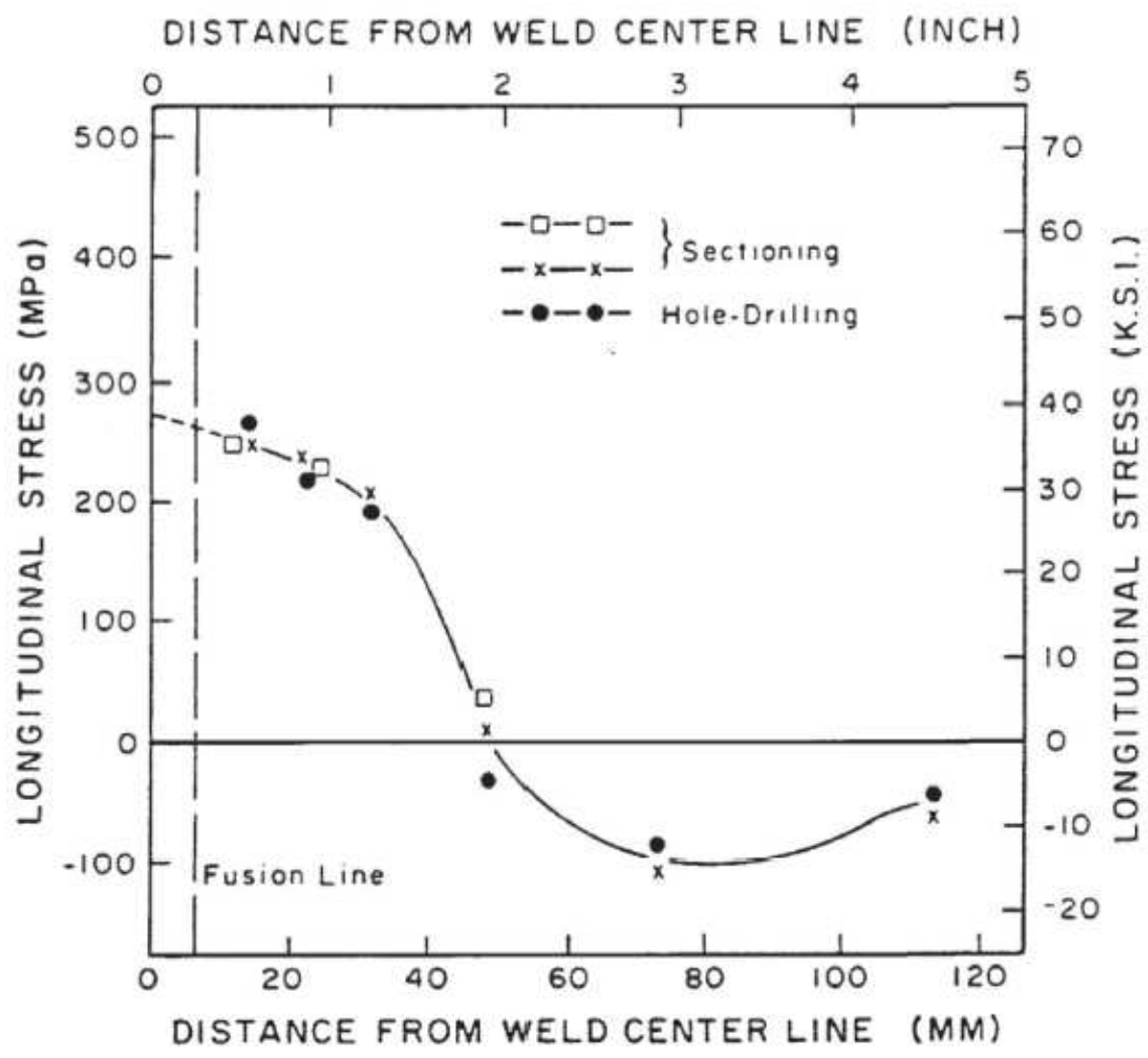


Figure 20. Residual stress distribution in the weldments vibrated at 40 Hz.

TABLE VIII.

RESIDUAL STRESSES IN THE TENSION WELDMENT AS DETERMINED FROM THE CORRECTED HOLE-DRILLING TECHNIQUE

(a) Before Vibration

Rosette #	Relaxed Strain, microstrain			Principal Stress MPa (ksi)		Longitudinal Stress, $S_L$ MPa (ksi)	Transverse Stress, $S_T$ MPa (ksi)
	$\epsilon_1$	$\epsilon_2$	$\epsilon_3$	$S_1$	$S_2$		
A	- 84	-283	-80	12 ( 1.80)	228 (33.09)	235 (34.04)	6 (0.85)
B	-123	-263	-67	48 ( 6.95)	231 (33.47)	240 (34.78)	39 (5.64)
C	- 63	-293	-55	39 ( 5.60)	219 (31.82)	229 (33.25)	29 (4.17)

(b) After Vibration

A'	- 65	-212	-54	10 ( 1.42)	173 (25.03)	180 (26.08)	3 (0.36)
B'	- 55	-220	-71	183 (26.56)	10 ( 1.44)	181 (26.28)	12 (1.72)
C'	- 52	-220	-71	182 (26.37)	7 ( 0.96)	179 (25.92)	10 (1.41)

its length. The stresses measured using a mechanical extensometer also were approximately the same. There was virtually no transverse stress developed in the plate. On vibrating at a resonant frequency of 37 Hz for 20 minutes, the average residual tensile stress dropped to about 179 MPa.

#### 4.3. Microstructural Analysis

Although it has been often proposed by a number of investigators<sup>37~0</sup> that peak residual stresses are reduced when combined residual and vibratory stresses exceed the yield point of the material, there are no direct observations of the evidence of the attendant plastic deformation. This is surprising, considering the interest in the industrial usage of vibratory stress relief techniques. To date, only Prohaszka, et al.,<sup>45</sup> explained their observed stress relief due to vibration by the dislocation theory. However, even they have not reported direct microscopic examination of the dislocation behavior they proposed.

In this investigation transmission electron microscopic analysis was done to observe the dislocation nature in both annealed and in vibrated samples. Due to the complex nature of microstructure next to a weld, the observation and interpretation of dislocation structures were extremely difficult. However, due to the observed reduction of the stresses in the A-36 tension plate weldment, samples for microscopic examination were obtained from the tension plate. Since the plate was in an annealed condition, before introducing tensile



stresses, any change in dislocation substructure could be directly compared with that from an annealed A-36 mild steel sample for qualitative assessment. Quantitative dislocation density measurements were not made.

Figure 21 shows the microstructure of annealed A-36 samples. At low magnifications (Figures 21a and 21b) very few dislocations can be seen within ferrite grains. A high magnification micrograph (Figure 21c) shows a region where dislocations exist in close proximity to one another; they are all relatively straight, showing the absence of long range internal stresses.

Figure 22 shows the typical dislocation structure observed in samples that were vibrationally treated. Figure 22a is a low magnification micrograph showing extensive dislocation network within a ferrite grain. At higher magnifications (Figures 22b,c,d) various dislocation interactions can be seen. The obvious increase in dislocation density is definite proof of the plastic deformation that accompanied the stress reduction by vibratory treatments.

In the absence of quantitative dislocation density measurement studies, attempts were made to estimate the percentage of plastic deformation by comparing the microstructure of vibrated samples to that from tensile samples loaded to 3.2, 6.8 and 23.7% plastic strain. The comparison indicated an approximate plastic strain of 4 to 5%.

Thus, for the first time, direct evidence of plastic deformation as a result of stress reduction by vibration was found by transmission electron microscopy studies.

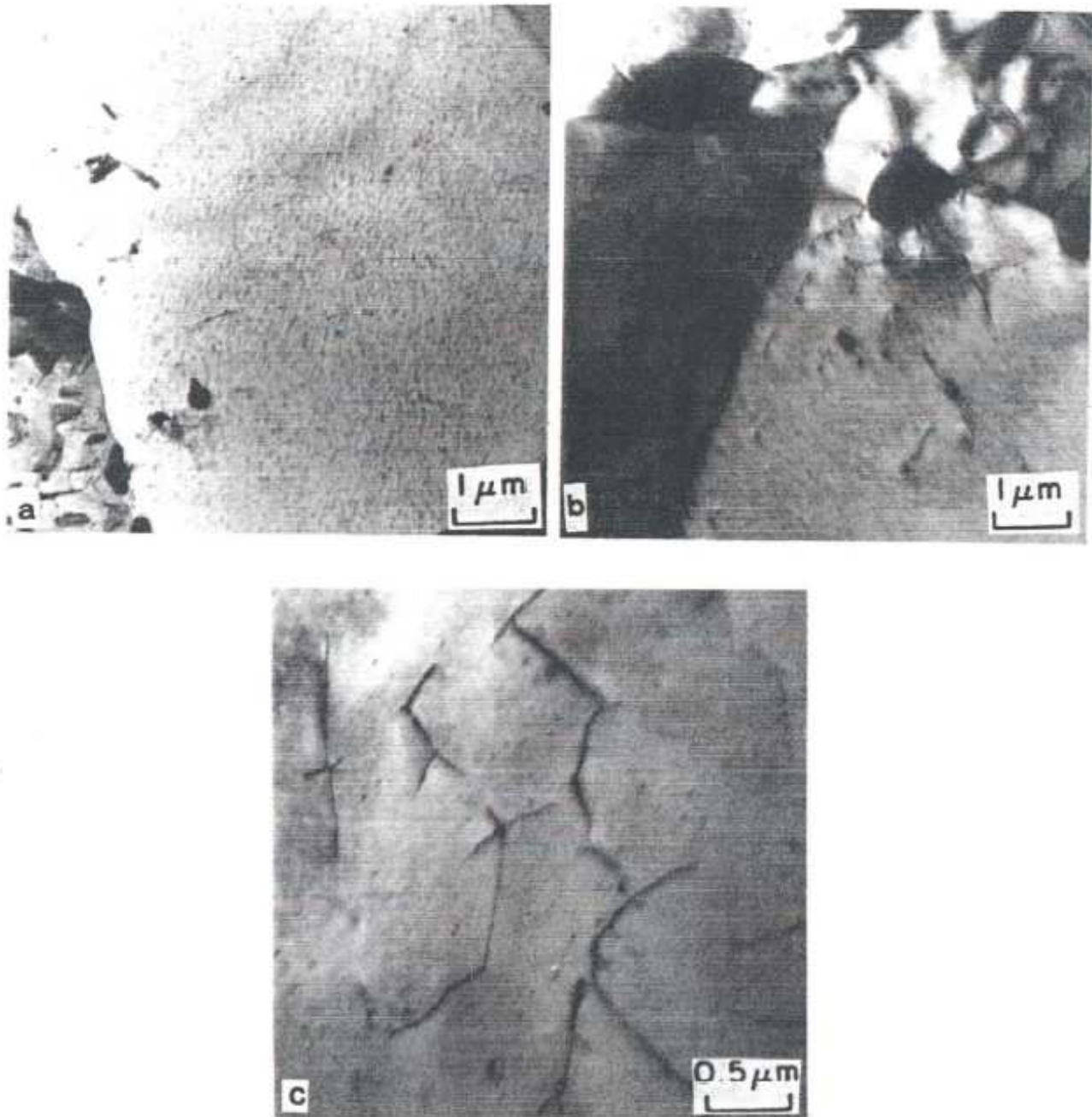


Figure 21. Transmission electron micrographs of the annealed A-36 mild steel samples.

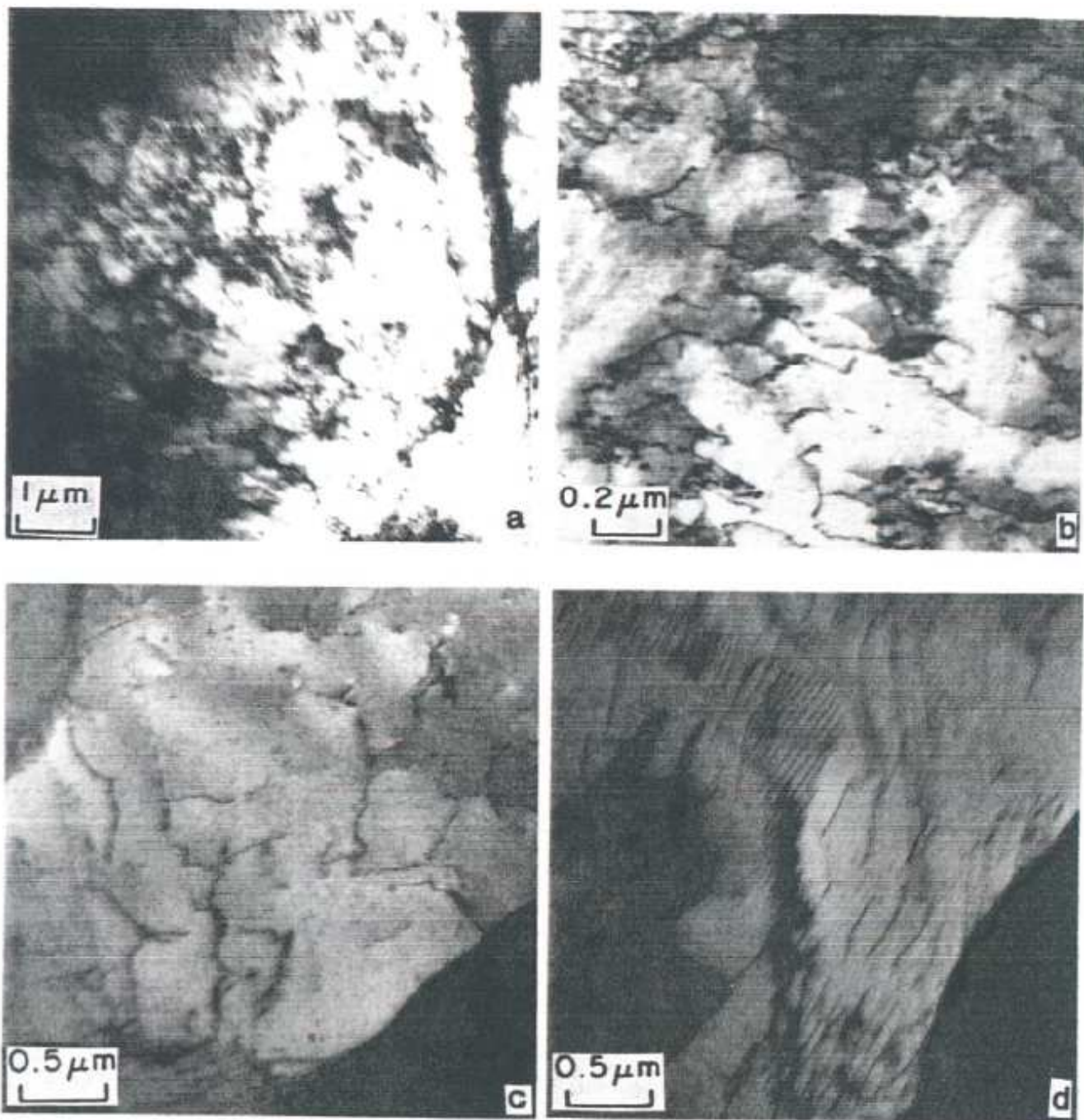


Figure 22. Transmission electron micrographs of samples obtained from the resonance vibration treated A-36 mild steel plate.

#### 4.4 Effect on Mechanical Properties

One of the main concerns of the usage of vibratory techniques of stress relief is potential fatigue damage.<sup>37</sup> In most instances, fatigue failure is due to already-present cracks which open up upon vibrating<sup>32</sup>. In actual practice, there are very few reports of damage of vibrated parts due to fatigue failure.

In order to test the effect of vibration on fatigue properties in the case of welds that showed pronounced stress redistribution, fatigue tests were conducted using samples obtained from the three 914 x 406 x 12.7 mm weldments. Figures 23, 24 and 25 shown the S-N curves for the samples from control weldment, weldment vibrated at 30 Hz and at 40 Hz respectively. Tensile testing was also performed on these weldments and the summary of results is shown in Table 9. The fatigue limit did not change as a result of either the sub-resonance or the resonance treatment. The tensile stress remained the same. However, there was a slight increase in the yield strength of about 38 MPa as a result of the resonance treatment. This result is consistent with the observation of plastic deformation, which could lead to work hardening and hence, an increase in yield strength.

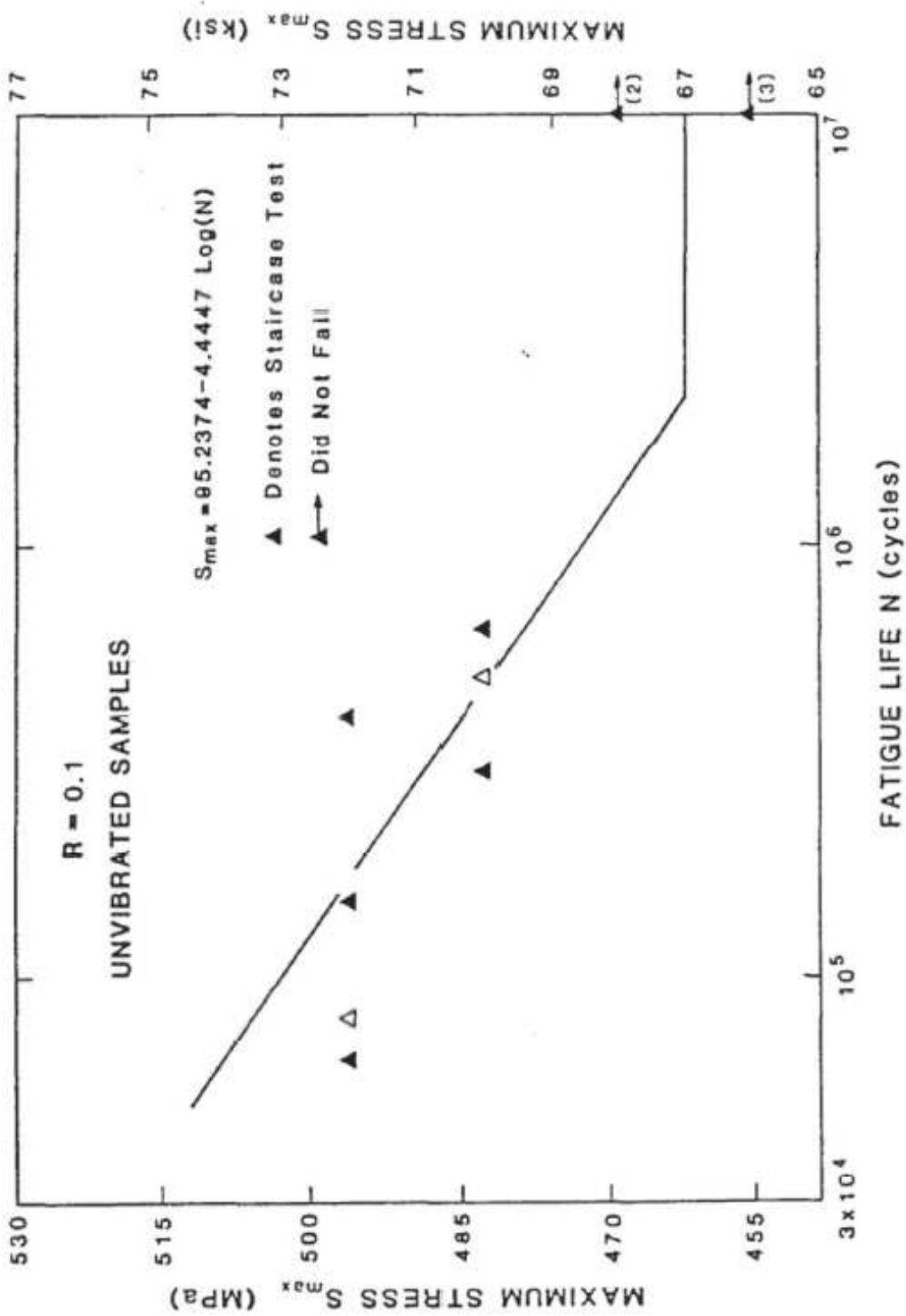


Figure 23. S-N curve of fatigue samples from the unvibrated A-36 steel weldment. R is the ratio of the minimum stress to the maximum stress.

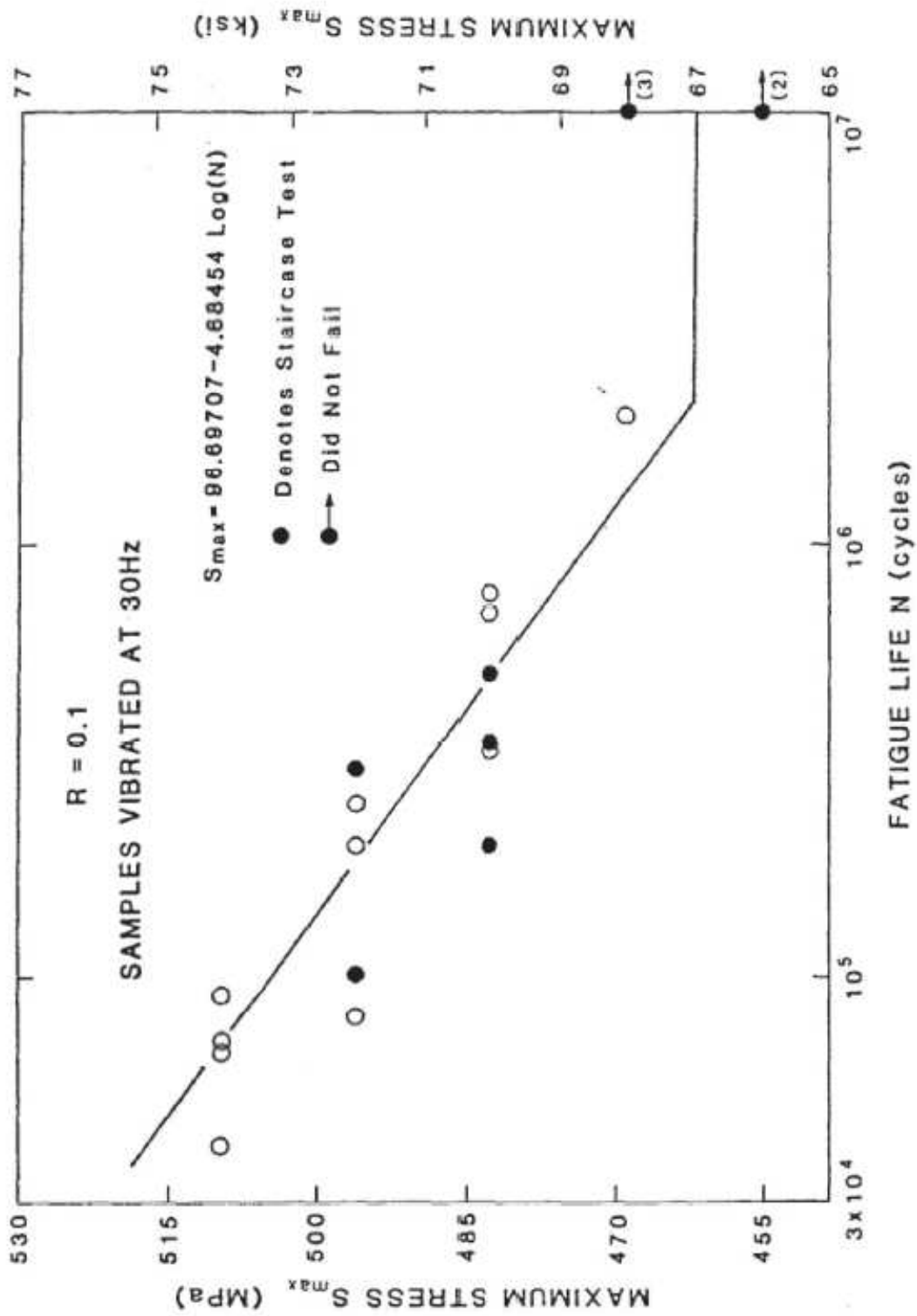


Figure 24. S-N curve obtained from the fatigue samples of weldment treated at 30 Hz.

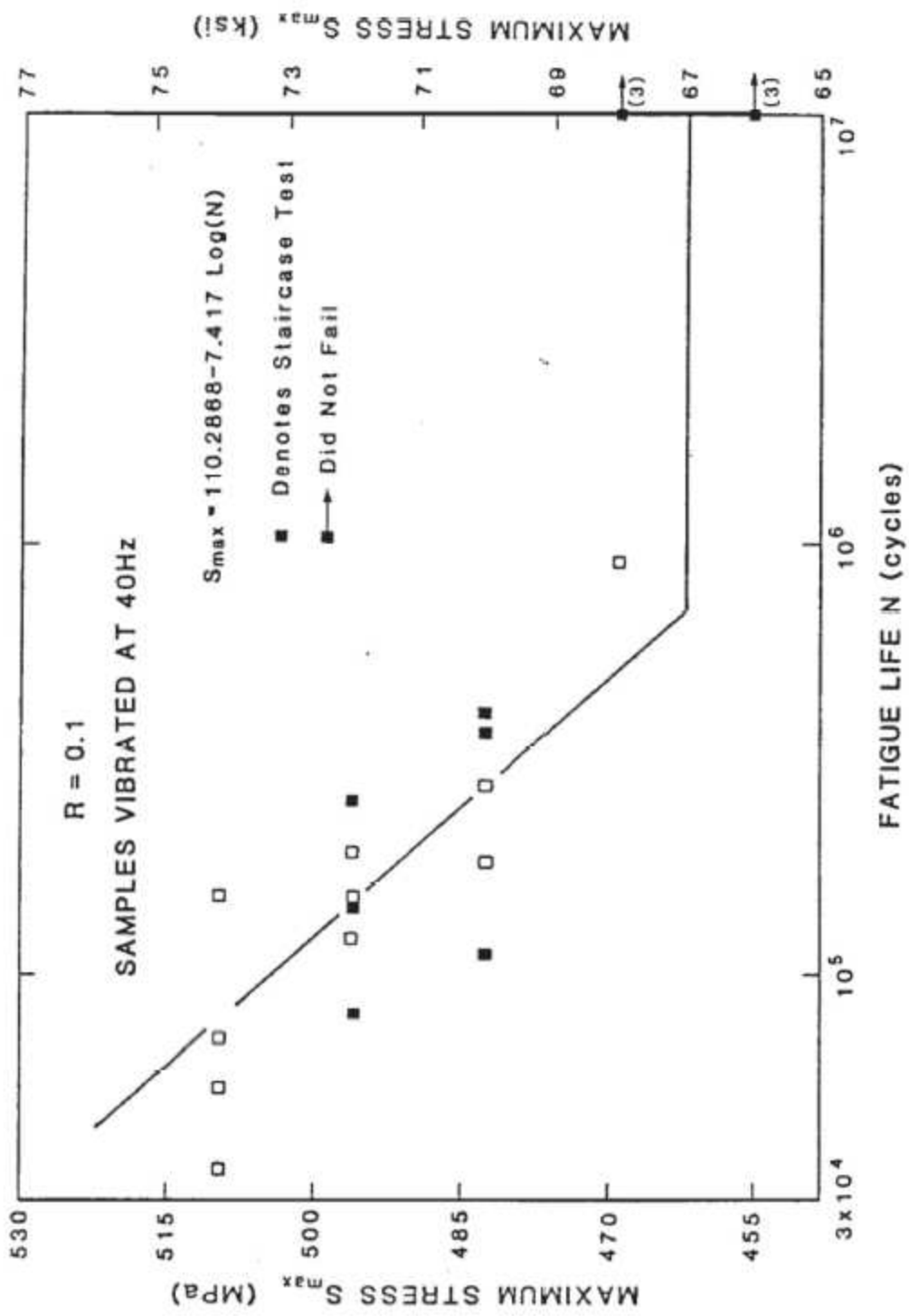


Figure 25. S-N curve obtained from the fatigue samples of resonant vibrated weldment.

Mechanical property		Unvibrated	Vibrated at 30 Hz	Vibrated at 40 Hz
0.2% Yield stress	P.S.I.	51,667	52,000	57,125
	MPa	356	357	394
Tensile stress	P.S.I.	73,250	74,000	74,000
	MPa	505	510	510
Fatigue limit S min/S max = 0.1	P.S.I.	67,000	67,000	67,000
	MPa	462	462	462

Table IX. Effect of the frequency of vibration on the mechanical properties of A-36 steel butt welds



## CHAPTER 5

## CONCLUSIONS

The following conclusions were drawn from this investigation:

1. Vibratory stress relief treatment performed at the resonant frequency effectively redistributed the residual stresses in A-36 butt weldments.
2. The sub-resonance treatment apparently was less effective than the treatment at the resonant frequency.
3. When a vibration table is used to treat smaller samples, the effectiveness of the treatment was the same irrespective of the location of the sample.
4. As a result of the treatments, a reduction of about 30% was noticed in peak longitudinal residual stresses in A-36 butt weldments.
5. Unlike some of the thermal treatments, residual stresses did not vanish as a result of the vibratory treatment.
6. Transmission electron microscopy studies indicated that the mechanism by which peak-stress reduction occurs is one of plastic deformation.
7. There was no fatigue damage as a result of the vibratory treatment.
8. The tensile properties of the weldment did not change as a result of the treatment.

9. Hole-drilling techniques can be effectively used to measure yield point level stresses by taking into account the machining strains and the strains due to local yielding as a result of stress concentration.

10. The accuracy of the corrected hole-drilling technique approached that of a sectioning method.

## REFERENCES

1. "Vibratory Stress Relief", *Weld. Eng.*, 1967, vol. 52, p. 46.
2. "Big Shake Takes the Stress out of Metal", *Chem. Week*, 1967, vol. 101, p. 119.
3. R. A. Claxton: *Heat Treat. Met.*, 1974, vol. 1, p. 131.
4. J. Varga: *FWP J.*, 1974, vol. 14, p. 23.
5. G. G. Saunders and R. A. Claxton: *Proc. Int. Conf. on Residual Stresses in Welded Construction and their Effects*, London, England, vol. 1, p. 173, 1977.
6. K. C. Schofield: *Int. J. Pressure Vessels Piping*, 1976, vol. 4, p. 1.
7. A. A. Denton: *Metall. Rev.*, 1966, vol. 11, p. 1.
8. R. P. Frick, G. A. Gurtman, and H. D. Meriwether: *J. Mater.*, 1967, vol. 2, p. 719.
9. C. S. Barrett: *Proc. Soc. Exp. Stress Anal.*, 1944, vol. 2, p. 147.
10. B. D. Cullity: *Elements of X-Ray Diffraction*, p. 431, Addison-Wesley Publ. Co., Reading, MA, 1956.
11. H. P. Klug and L. E. Alexander: *X-Ray Diffraction Procedures*, p. 755, John Wiley and Sons, Inc., New York, 1974.
12. "Residual Stress Measurement by X-Ray Diffraction---SAE J 784a", 2nd Edition, Society of Automotive Engineers, Inc., 1971.
13. J.B. Cohen, M. R. James and B. A. MacDonald: *Nav. Res. Rev.*, 1978, vol. 31, p. 1.
14. J. Mathar: *Trans. ASME*, 1934, vol. 54, p. 249.
15. W. Soete and R. Vancrombrugge: *Proc. Soc. Exp. Stress Anal.*, 1950, vol. 8, p. 17.
16. E. W. Suppiger, C. Riparbelli and E. R. Ward: *Weld J.*, 1951, vol. 30, p. 91-s.
17. N. J. Rendler and I. Vigness: *Exp. Mech.*, 1966, vol. 6, p. 577.

18. R. A. Kelsey: Proc. Soc. Exp. Stress Anal., 1956, vol. 14, P. 181.
19. S. P. Timoshenko and J. N. Goodier: Theory of Elasticity, 3rd Edition, p. 71, McGraw-Hill, New York, 1970.
20. R. G. Bathgate: Strain, 1968, vol. 4, p. 20.
21. A. J. Bush and F. J. Kromer: ISA Trans., 1973, vol. 12, p. 249.
22. E. M. Beaney and E. Procter: Strain, 1974, vol. 10, p. 7.
23. S. S. Birley and A. Owens: NDT mt., 1980, vol. 13, p. 3.
24. E. N. Beaney: Strain, 1976, vol. 12, p. 99.
25. D. Rosenthal: Weld. J., 1941, vol. 20, p. 220-s.
26. Rodgers and Fetcher: Weld. J., 1938, vol. 17, p. 4-s.
27. K. Masubuchi: Weld. J., 1960, vol. 39, p. 525-s.
28. L. Tall: Weld. J., 1964, vol. 43, p. 10-s.
29. A. G. Kamtekar, J. D. White and J. B. Dwight: J. Strain Anal. Eng. Des., 1977, vol. 12, p. 140.
30. C. J. Merrick and U. A. Schneider: Proc. Int. Conf. on Control of Distortion and Residual Stress in Weldments, sponsored by Am. Soc. Metals, Chicago, Ill., p. 62, 1976.
31. "Stress Relieve Big Weldments in Minutes with Vibration", Machinery, 1968, vol. 74, p. 100.
32. "A Vibration Shakedown", Weld. Des. Fabr., 1969, vol. 42, p. 81.
33. T. D. Kelso: Tool Manuf. Eng., 1968, vol. 3, p. 48.
34. "Vibratory Stress-Relieving", Weld. Met. Fabr., 1968, vol. 36, p. 212.
35. D. S. Keller: "Ultrasonic Stress Relieving", Met. Treat. (Rocky Mount N.C.), 1970, vol. 21, p. 14.
36. S. R. Rich: Weld. Eng., 1969, vol. 54, p. 44.
37. G. P. Wozney and G. R. Crawmer: Weld. J., 1968, vol. 48, p. 411-s.

38. A. A. Grudz, et al.: Autom. Weld. Engl. Transl., 1972, vol. 25, p. 70.
39. O. I. Zubchenko, A. A. Grudz, G. T. Orekhov and A. G. Sostin: Autom. Weld. Engl. Transl., 1974, vol. 27, P. 59.
40. S. Weiss, G. S. Baker and R. D. Das Gupta: Weld. J., 1976, vol. 56, p. 47-s.
41. C. M. Tran: M. S. Dissertation, Portland State University, Portland, OR, 1977.
42. A. M. Nawwar, K. McLachlan and J. Shewchuk: Exp. Mech., 1976, vol. 16, p. 226.
43. O. I. Zubchenko, et al.: Autom. Weld. Engl. Transl., 1976, vol. 29, p. 53.
44. A. Ya. Nedoseka, et al.: Autom. Weld. Engl. Transl., 1974, vol. 27, p. 61.
45. J. Prohaszka, B. Hidasi and L. Varga: Period. Polytech. Mech. Eng., 1975, vol. 19, p. 69.
46. I. G. Polotskii, et al.: Autom. Weld. Engl. Transl., 1974, vol. 27, p. 67.
47. A. Puskar: Acta Met., 1976, vol. 24, p. 861.

APPENDIX

## CORRECTIONS FOR BLIND-HOLE-DRILLING ANALYSIS

Since the hole-drilling technique of residual stress measurement was employed to monitor the stress distribution near a weld, where the stresses (especially longitudinal residual stresses) reach yield point magnitude, an experimental program was carried out to evaluate the extent of local yielding around the hole. The test procedure was also used to measure machining strains, if any, developed during the drilling of the hole. The correction factors determined from this experiment were used to modify the hole-drilling results shown in the main text.

Theoretical Analysis

The theoretical background for the hole-drilling analysis stems from the work of Kirsch.<sup>19</sup> His solution for the stress distribution around a circular through hole in a thin, wide, linear elastic and isotropic plate is used, since a theoretical solution for the strain at any point on the surface for a blind hole is not known. For a plate subjected to uniaxial tension,  $S$ , Kirsch's solution may be written as:

$$\begin{aligned}
 S_r &= \frac{S}{2} \left[ \left( 1 - \frac{\lambda^2}{4} \right) + (1 + \lambda^2 + 3/16 \lambda^4) \cos 2\theta \right], \\
 S_\theta &= \frac{S}{2} \left[ \left( 1 + \frac{\lambda^2}{4} \right) - (1 + 3/16 \lambda^4) \cos 2\theta \right], \\
 S_{r\theta} &= -\frac{S}{2} \left[ \left( 1 + \frac{\lambda^2}{2} - 3/16 \lambda^4 \right) \cos 2\theta \right]
 \end{aligned}
 \tag{1}$$

Where:

$S_r$ ,  $S_\theta$ ,  $S_{r\theta}$  are the radial, tangential and shear-stress components of  $S$ , and  $a$  is the nondimensional hole diameter defined by  $2a_0 / R$  (see Figure A1)

The strain distribution around the hole after drilling is given by

$$\begin{aligned}\epsilon_r &= \frac{1}{E} (S_r - \nu S_\theta) \\ \epsilon_\theta &= \frac{1}{E} (S_\theta - \nu S_r)\end{aligned}\tag{2}$$

while the strain distribution before drilling may be written as

$$\begin{aligned}\epsilon_r^0 &= \frac{S}{E} (\cos^2\theta - \nu \sin^2\theta) \\ \epsilon_\theta^0 &= \frac{S}{E} (\sin^2\theta - \nu \cos^2\theta)\end{aligned}\tag{3}$$

Strain gauges may be used to detect the change in strain resulting from drilling the hole. This change, defined as "relaxation strain," will be denoted by  $\epsilon_{Rr}$  and  $\epsilon_{R\theta}$  in the radial and tangential directions, respectively. It should be noted that  $\epsilon_{Rr}$  and  $\epsilon_{R\theta}$  are the net relaxation strains due to the stress (applied and/or residual). Relaxation strains are defined as

$$\begin{aligned}\epsilon_{Rr} &= \epsilon_r - \epsilon_r^0 \\ \epsilon_{R\theta} &= \epsilon_\theta - \epsilon_\theta^0\end{aligned}\tag{4}$$



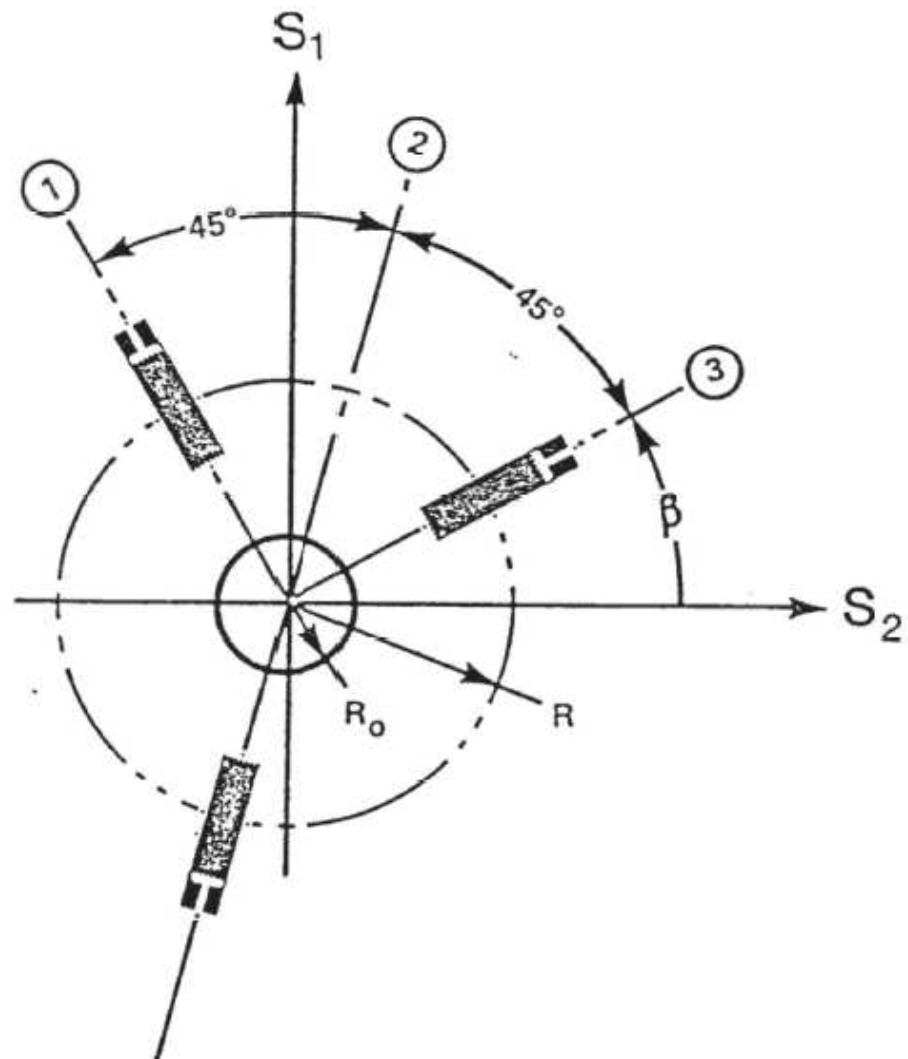


Figure A1. Strain gauge rosette arrangement and the blind-hole geometry for determining residual stresses.

Substitutions of equations (1), (2) and (3) into equation (4) yields

$$\begin{aligned}\epsilon_{Rr} &= K_r \frac{S}{E} \\ \epsilon_{R\theta} &= K_\theta \frac{S}{E}\end{aligned}\tag{5}$$

Where  $K_r$  and  $K_\theta$  are nondimensional quantities called relaxation coefficients and given by

$$\begin{aligned}K_r &= -\frac{(1+\nu)}{8} \lambda^2 - \left[ \frac{1}{2} \lambda^2 - \frac{3(1+\nu)}{32} \lambda^4 \right] \cos^2\theta \\ K_\theta &= -\frac{(1+\nu)}{8} \lambda^2 + \left[ \frac{1}{2} \lambda^2 - \frac{3(1+\nu)}{32} \lambda^4 \right] \cos^2\theta\end{aligned}\tag{6}$$

The equations used in the main text for residual stress measurement can be derived using equations (1) through (4).

Examining equation (5), it can be seen that for a given stress, the value of the relaxed strain is directly related to the relaxation coefficient. In a given experiment, a maximum value of relaxed strain would minimize errors and hence, the points of measurement  $(\lambda, \theta)$  of maximum relaxation coefficient are recommended. A study of equation (6) shows that<sup>42</sup> although a tangential gauge at  $\theta = 90^\circ$  exhibits the maximum value of relaxation coefficient, its use is not advised because the gauge has to lie very close to the edge of the hole. The closer the gauge is to the hole, the larger the errors being caused by machining stresses. This is the primary reason why radial gauges are used in commercial strain gauges rosettes.

### Practical Considerations

For a given strain gauge-hole assembly and material, it has been shown from equation (6) that the relaxation coefficient is fixed and from equation (5), it can be seen that the stress is directly proportional to the relaxation strain. However, the measured strain relaxation is due not only to the applied stress but it also includes (a) relaxation strain due to drilling operation,  $\epsilon_m$  and (b) relaxation strain due to localized plastic flow,  $\epsilon_p$ .

The relaxation strain component  $\epsilon_m$  results from machining residual stresses. Such stresses depend on the drilling conditions and are highly localized in the immediate vicinity of the hole.<sup>23</sup> For steel,  $\epsilon_m$  has been found to be about  $-40 \mu\epsilon$ .<sup>21-23</sup>

The relaxation strain component  $\epsilon_p$  is produced only if the stress field around the hole is disturbed by localized plastic flow. As shown in Figure A2, in uniaxial loading, the stress concentration factor at  $\theta = 90^\circ$  is 3 while for  $\theta = 0$ , it is -1. As the nominal stress exceeds 1/3 of the yield strength, plastic flow will start at the hole edge at  $\theta = 90^\circ$  and the Kirsch's elastic solution is no longer valid.

However, it is always possible to determine the deviation of the elastic estimate from the true value of stress. If the error is acceptable, the elastic solution may be practically used for determining stresses beyond 1/3 of the yield strength.

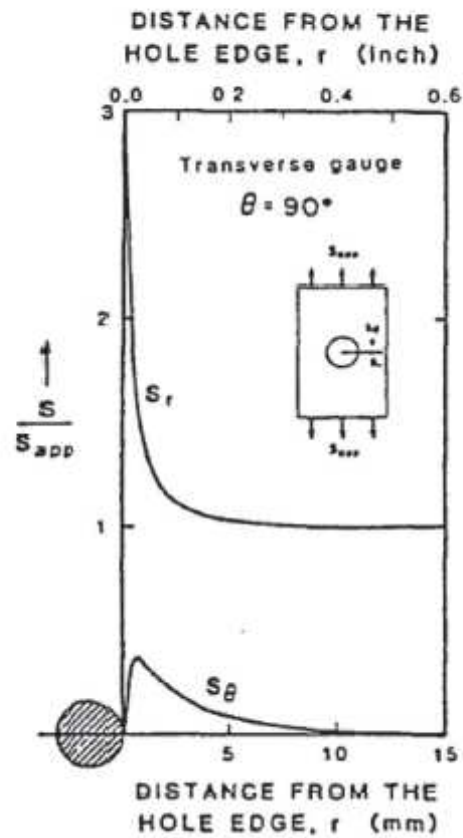
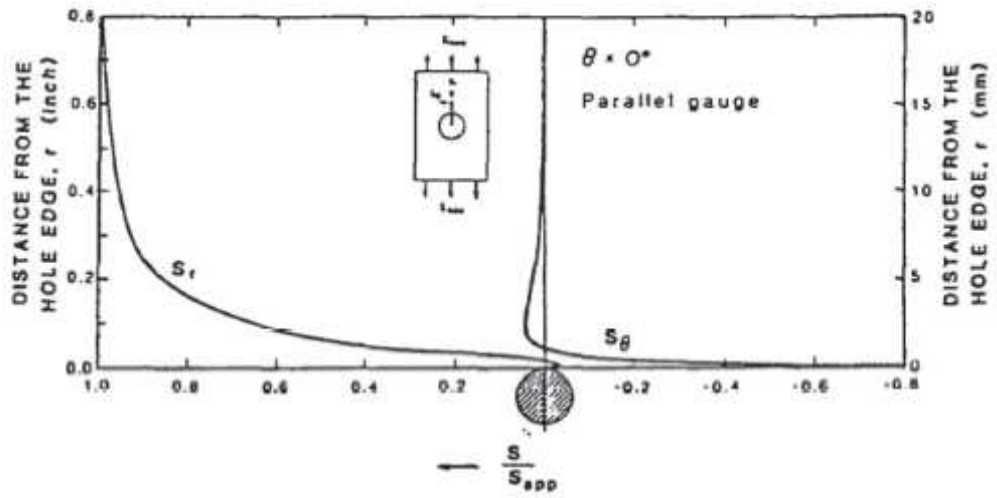


Figure A2: Variation of the resolved stresses as a function of the distance from the hole edge.

It can be seen that  $\epsilon_p$  will always increase the absolute value of the net relaxation strain, regardless of its sign. Thus, if the relaxation strain  $\epsilon_p$  is neglected, the measured stress, being tensile or compressive, will always be overestimated. The presence of  $\epsilon_p$ , being neglected, will lead to unrealistic and misleading results. This may be illustrated with the aid of Figure A3. Assume that a uniform stress  $S_{app} > 1/3 S_y$  is measured by drilling a hole and recording a total relaxation strain  $\overline{ac}$ . If  $\overline{ac}$  is considered entirely due to the existing stress, direct substitution in equation (5) gives a higher stress  $S_{app}' = E/K_r \overline{ac} = E/K_r \overline{a'b'}$ , where line  $cb'$  is drawn parallel to elastic line. However, if  $\epsilon_p = \overline{bc}$  is realized, then the true stress will be  $S_{app} = E/K_r \overline{ab}$  and the error in estimating  $S_{app}$  will be equal to  $\overline{bc} / \overline{ab}$ , i.e.,  $\epsilon_p / \epsilon_{Rr}$ . Similar analysis can be done for a compressive stress. Correction for  $\epsilon_p$  is required for stresses that are in excess of  $1/3 S_y$  or of a limit to be determined from experiments.

### Experimental

To determine the values of relaxation components  $\epsilon_m$  and  $\epsilon_p$ , two 6.35 mm thick annealed A-36 mild steel samples were used. Specimen dimensions and strain gauge layout are shown in Figure A4. A strain gauge rosette (type EA-06-125RE-120) was bonded at the center of the gauge length. The elements of this rosette are shown as 1, 2 and 3 in the figure. Four control gauges a, b, c and d (type EA-06-125AD-120) were also bonded, to measure the magnitude of the uniform

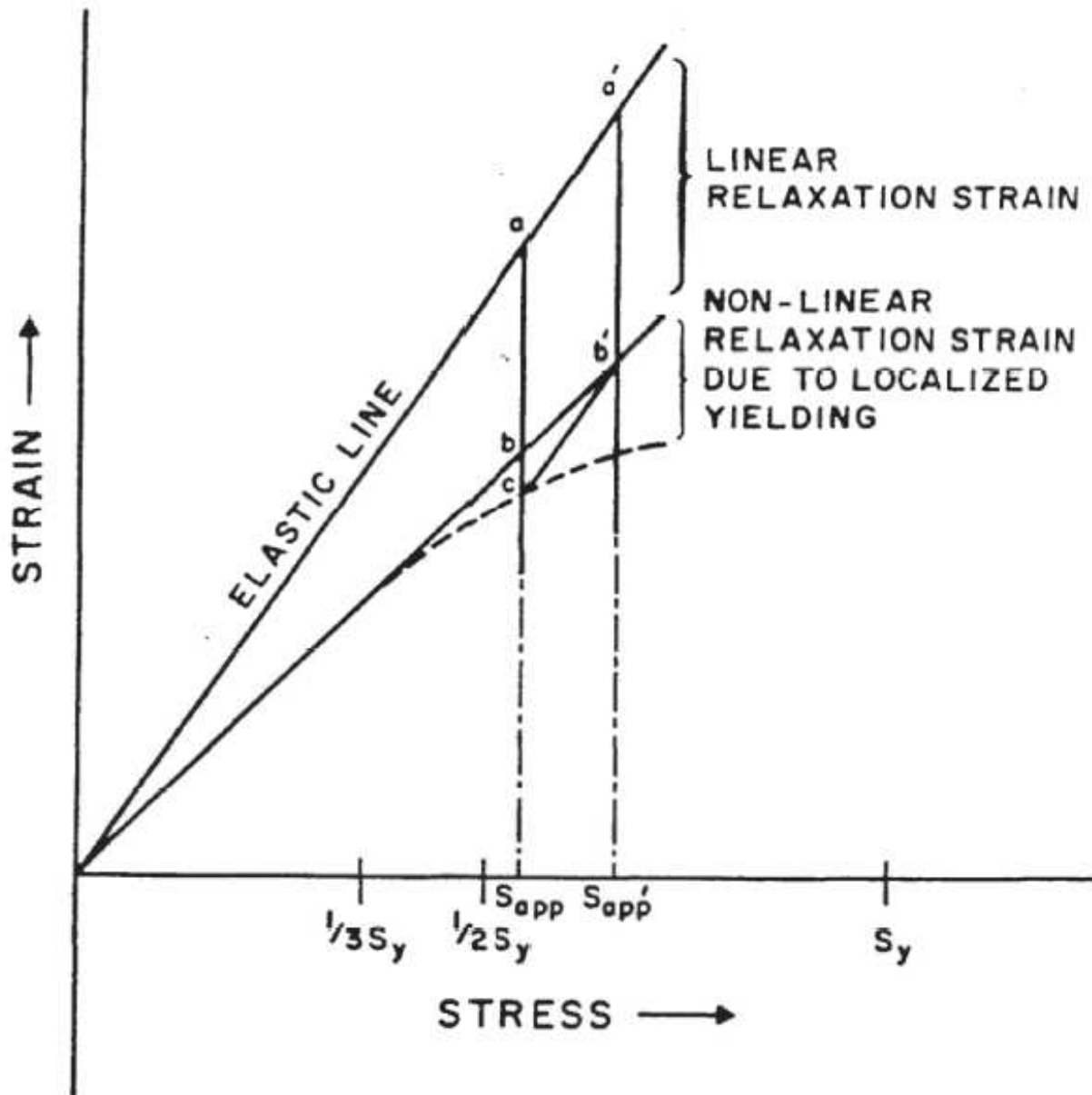


Figure A3. Overestimation of the applied stress  $S_{app}$ , due to localized yielding near the hole.

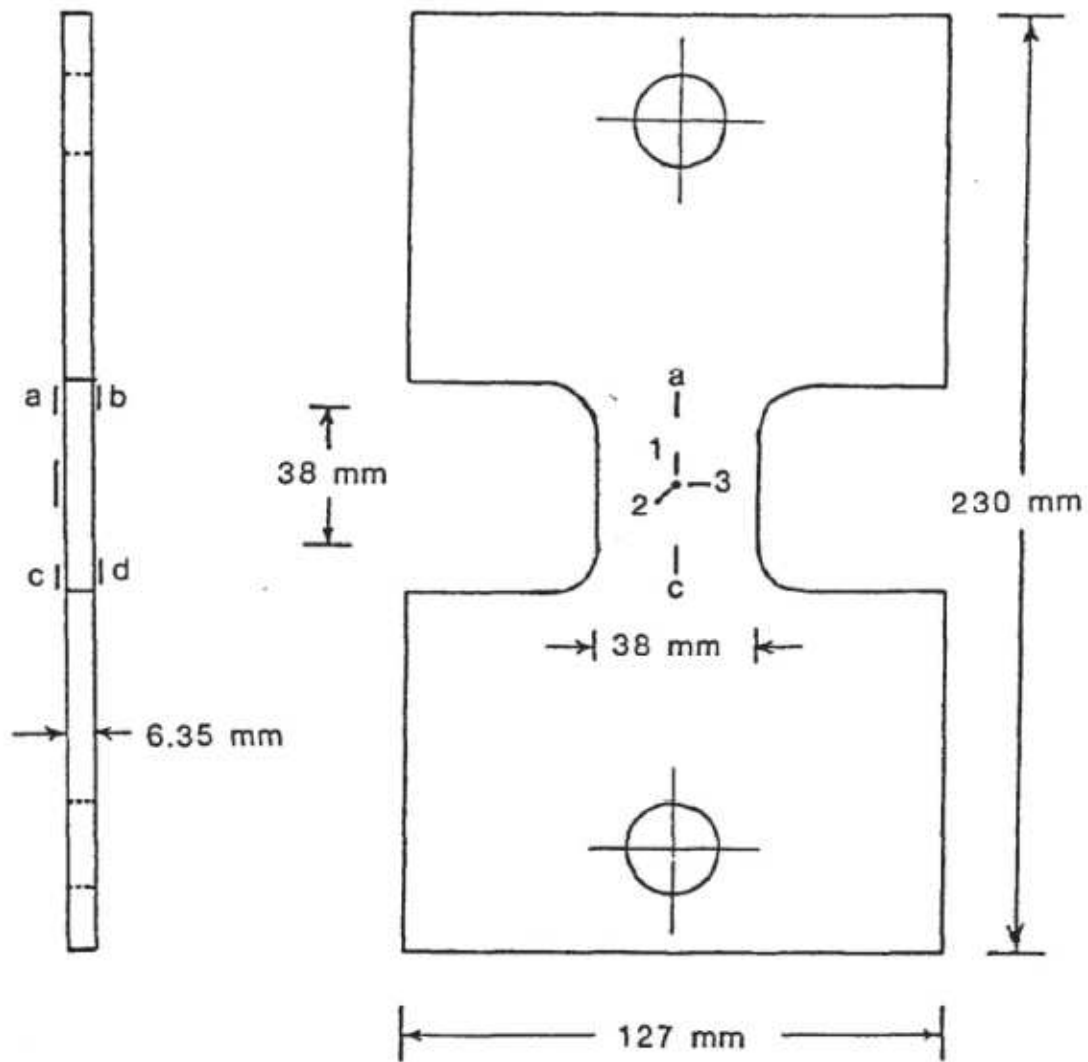


Figure A4. Schematic of the strain gauge layout on the test specimen.

stress field. The sample was gripped by loading pins, to eliminate the bending stresses. Accurate drilling was done using a Photolastic model RS-200 milling guide.

Testing consisted primarily of increasing the hole size by drilling and, at each increment, loading the specimen through a number of applied stress levels and recording the associated strain gauge readings.

In the first experiment conducted to evaluate the machining effect, the hole size was increased from 0.8 mm to 4.4 mm. At each hole size, the sample was loaded a stress value equal to 0.3 times the yield strength. In the second experiment, the second sample was loaded up to 0.7 times the yield strength value. The actual diameter of the drilled hole was accurately measured with a microscope inserted into the tool guide.

## Discussion

### Machining Effect

The results of the first set of experiments are given in Tables A-I and A-II and Figures A5 and A6. The relaxation strain due to machining,  $\epsilon_m$ , was determined by extrapolating the linear strain-stress relations to zero stress level and measuring the intercepts. Figures A7 and A8 determined from Figures A5 and A6, respectively, show the variation of  $\epsilon_m$  with the drilling clearance,  $C_d$ . The drilling clearance is the distance between the hole edge, where maximum machining stresses exist, and the near end of the gauge matrix.



Table A-1

VARIATION OF AVERAGE STRAIN WITH APPLIED STRESS FOR GAUGE #1, WHICH IS PARALLEL TO THE APPLIED STRESS,  $\theta = 0^\circ$ . SPECIMEN #1

Hole Size (mm)	No Hole	Strain (microstrain)												
		0.794	1.590	1.984	2.381	2.778	3.175	3.572	3.969	4.366				
(Before Drilling) 0	0	0	0	0	0	0	0	0	0	0	0	0	0	0
13.79 ( 2)	70	68	54	46	36	28	12	- 24	- 60	- 74				
27.58 ( 4)	142	136	122	110	98	88	64	38	- 12	- 24				
41.37 ( 6)	216	206	192	174	160	144	116	86	32	28				
55.16 ( 8)	284	270	260	244	222	200	172	142	70	78				
68.95 (10)	356	350	324	304	280	258	226	198	138	134				
82.74 (12)	426	420	396	370	346	318	274	248	184	178				
(After Drilling) 0	0	- 4	- 14	- 16	- 24	- 34	- 38	- 78	- 110	- 124				

Stress  
MPa  
(Ksi)

Table A-II

VARIATION OF AVERAGE STRAIN WITH APPLIED STRESS FOR GAUGE #3,  
WHICH IS TRANSVERSE TO THE DIRECTION OF APPLIED STRESS,  $\theta = 90^\circ$   
SPECIMEN #1

Hole Size (mm)		Strain (microstrain)											
		No Hole	0.794	1.590	1.984	2.381	2.778	3.175	3.572	3.969	4.366		
Stress MPa (Ksi.)	(Before Drilling) 0	0	0	0	0	0	0	0	0	0	0	0	0
	13.79 ( 2)	- 21	- 18	- 24	- 20	- 30	- 32	- 40	- 50	- 48	- 30	- 30	
	27.58 ( 4)	- 43	- 38	- 42	- 46	- 46	- 46	- 50	- 60	- 66	- 26	- 26	
	41.37 ( 6)	- 64	- 60	- 62	- 66	- 62	- 62	- 78	- 80	- 80	- 40	- 40	
	55.16 ( 8)	- 86	- 80	- 80	- 74	- 78	- 76	- 94	- 90	- 90	- 44	- 44	
	68.95 (10)	-106	-100	- 98	- 94	- 91	- 90	-108	-100	-100	- 40	- 40	
	82.74 (12)	-128	-122	-116	-110	-108	-104	-124	-114	-114	- 48	- 48	
(After Drilling) 0	0	2	- 6	- 4	- 14	- 18	- 40	- 36	- 36	- 32	- 32		

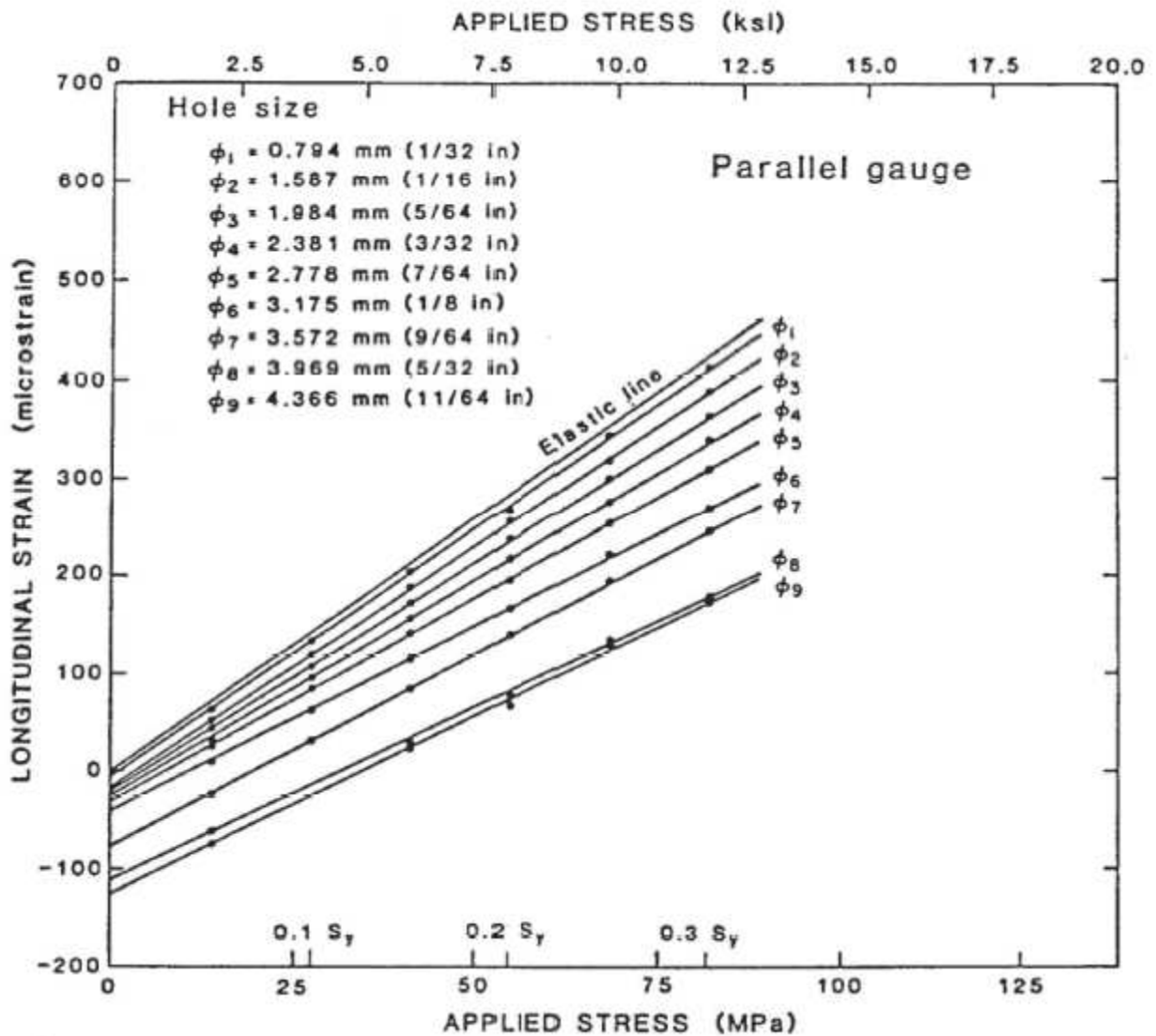


Figure A5. Plot of average strain vs. applied stress for the parallel gauge.  
 $\phi_1$  to  $\phi_9$  are diameters of the holes drilled.

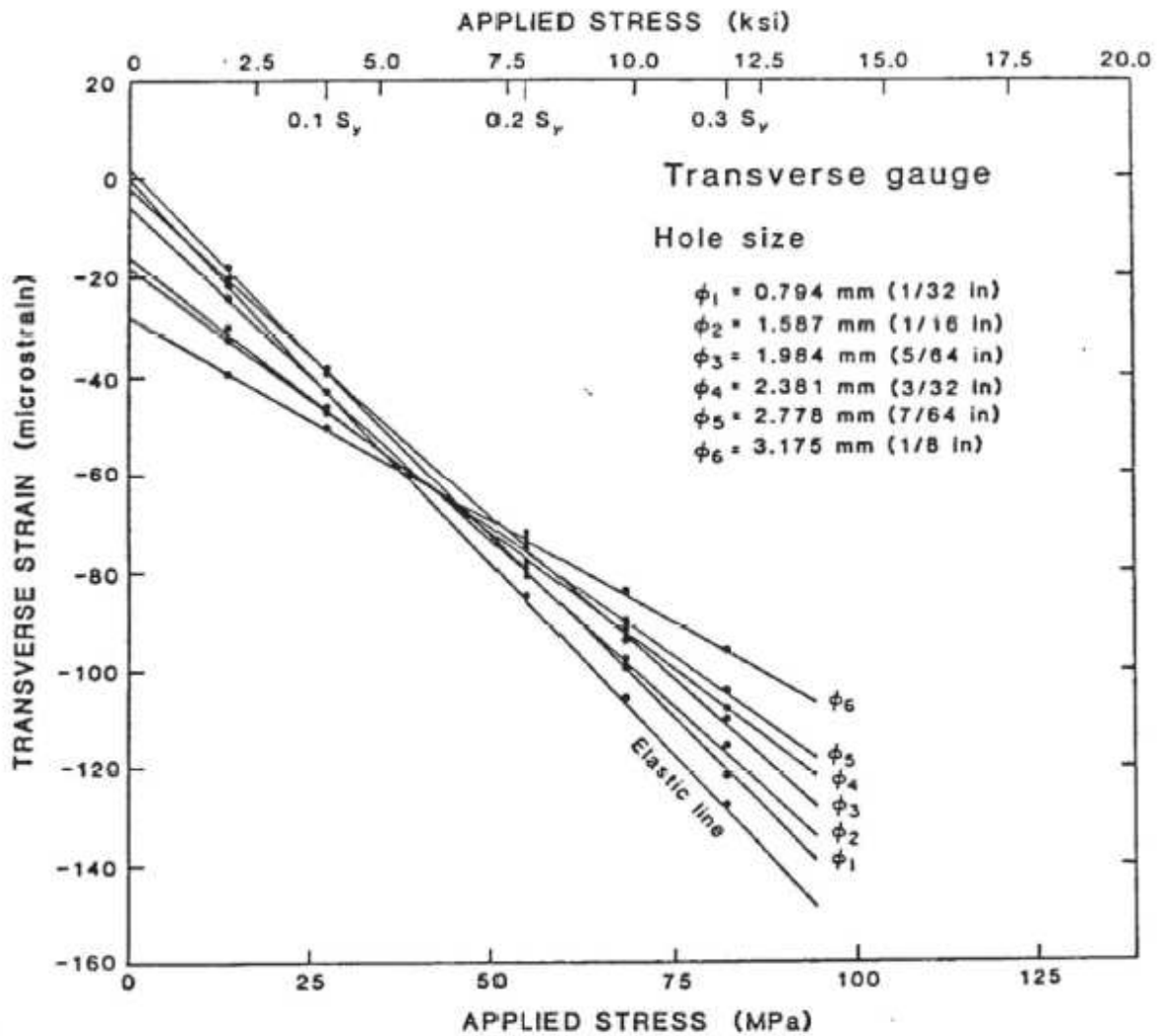


Figure A6. Plot of average strain vs. applied stress for the transverse gauge.

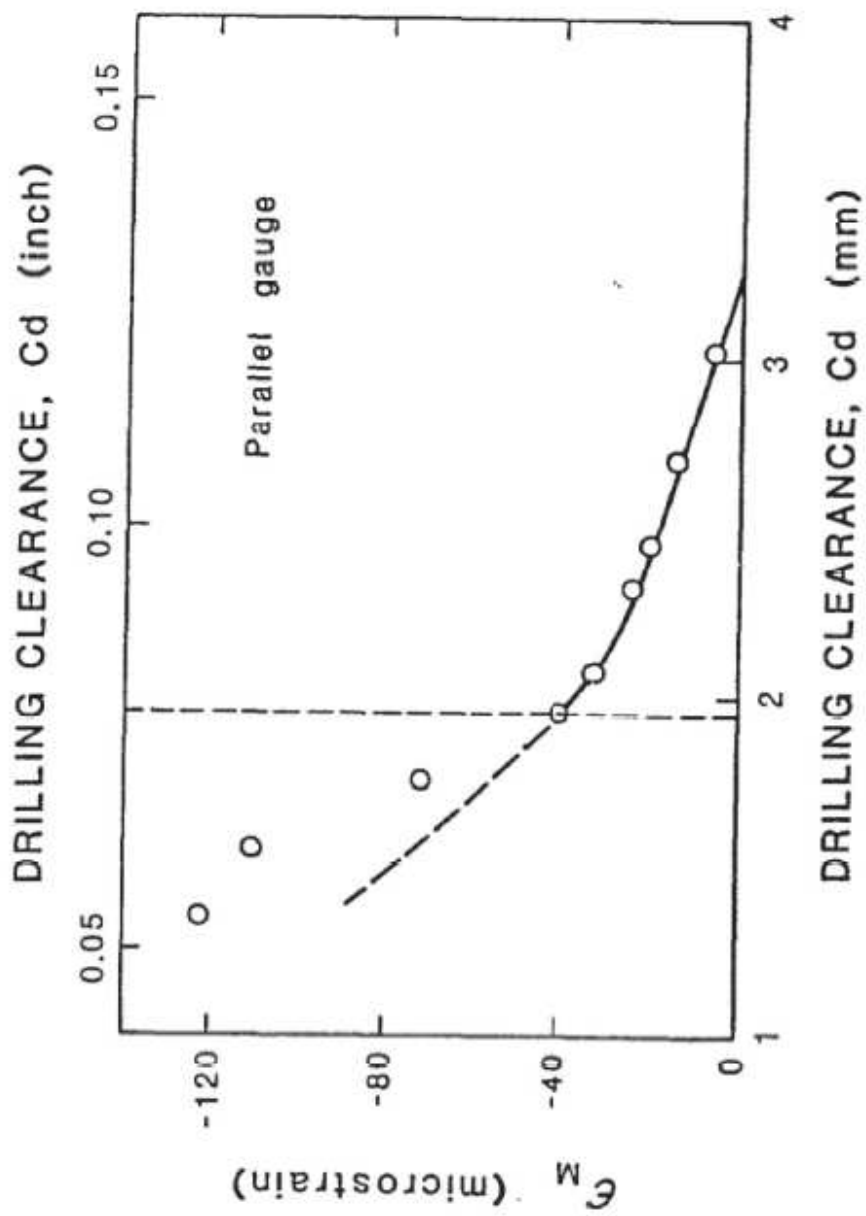


Figure A7. Variation of  $\epsilon_M$  with the drilling clearance for the parallel gauge.

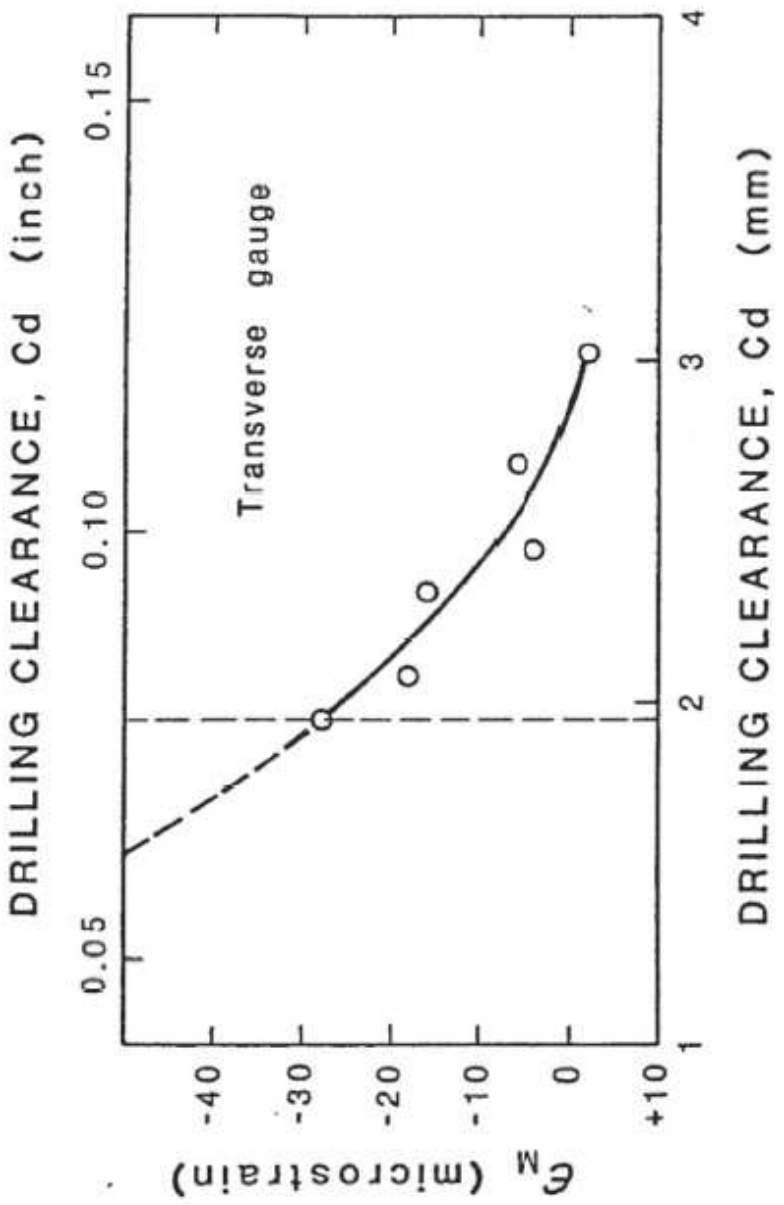


Figure A8. Variation of  $\epsilon_M$  with the drilling clearance for the transverse gauge.

As mentioned before, the highly localized nature of machining stresses is evident. In a situation where preformed strain gauge rosettes cannot be used, precise locations of the strain gauges near the hole are demanded. Hole diameter larger than the suggested 1/8 inch (3.175 mm) diameter, introduced abnormally high machining stresses and hence, in the second set of experiments the maximum hole size was limited to the suggested value of 3.175 mm. For this hole size, the machining strains were  $-40 \mu\epsilon$  and  $-30 \mu\epsilon$  for gauges 1 and respectively. Slightly lower values of  $\epsilon_m$  for gauge 3 could be due to the transverse sensitivity of the gauge. These values of  $\epsilon_m$  for steel agree well with the values obtained by others.<sup>21-23</sup> Also, machining stresses seem to be independent of the stress to be measured, since  $\epsilon_m$  has the same sign regardless of the sign of total relaxation strain.

#### Localized Plastic Flow Effect

The results of the second set of experiments are given in Tables A-III and A-IV, and are plotted in Figures A9 and A10. An examination of the results of Figures A9 and A10 suggests the following:

1. As the stress exceeds a certain value, the strain-stress relations generally deviate from linearity causing the absolute value of relaxation strain to increase. This critical stress is dependent on the hole size and the strain gauge location, or more conveniently,  $C_d$ . The locus of the critical stress that can be measured without error due to localized plastic yielding at the hole edge is shown to

Table A-III

VARIATION OF AVERAGE STRAIN RECORDED FROM GAUGE #1 AS A FUNCTION OF APPLIED STRESS FOR VARIOUS HOLE SIZES. SPECIMEN #2

Hole Size (mm)		Strain (microstrain)							
		No Hole	0.794	1.590	1.984	2.381	2.778	3.175	
Stress MPa (ksi)	0	0	0	0	0	0	0	0	
	28 (4)	144	140	124	120	106	90	72	
	55 (8)	290	278	258	244	230	200	182	
	83 (12)	429	420	390	376	348	330	292	
	110 (20)	572	560	526	500	478	442	400	
	138 (20)	720	700	670	632	606	550	500	
	165 (24)	852	852	806	758	720	664	598	
	193 (28)	1001	990	936	872	834	764	682	



Table A-IV

VARIATION OF AVERAGE STRAIN RECORDED FROM GAUGE #3 AS A FUNCTION OF APPLIED STRESS FOR VARIOUS HOLE SIZES. SPECIMEN #2

Hole Size (mm)	No Hole	Strain (microstrain)							
		0.794	1.590	1.984	2.381	2.778	3.175		
0	0	0	0	0	0	0	0	0	
28 ( 4)	- 44	-42	-40	-46	-48	-52	-58		
55 ( 8)	- 86	-82	-76	-80	-82	-82	-84		
83 (12)	-130	-122	-114	-114	-116	-112	-110		
110 (20)	-172	-160	-150	-148	-148	-142	-138		
138 (20)	-214	-202	-188	-182	-180	-174	-162		
165 (24)	-257	-240	-222	-214	-214	-198	-182		
193 (28)	-300	-280	-256	-242	-232	-214	-190		

Stress  
MPa  
(ksi)

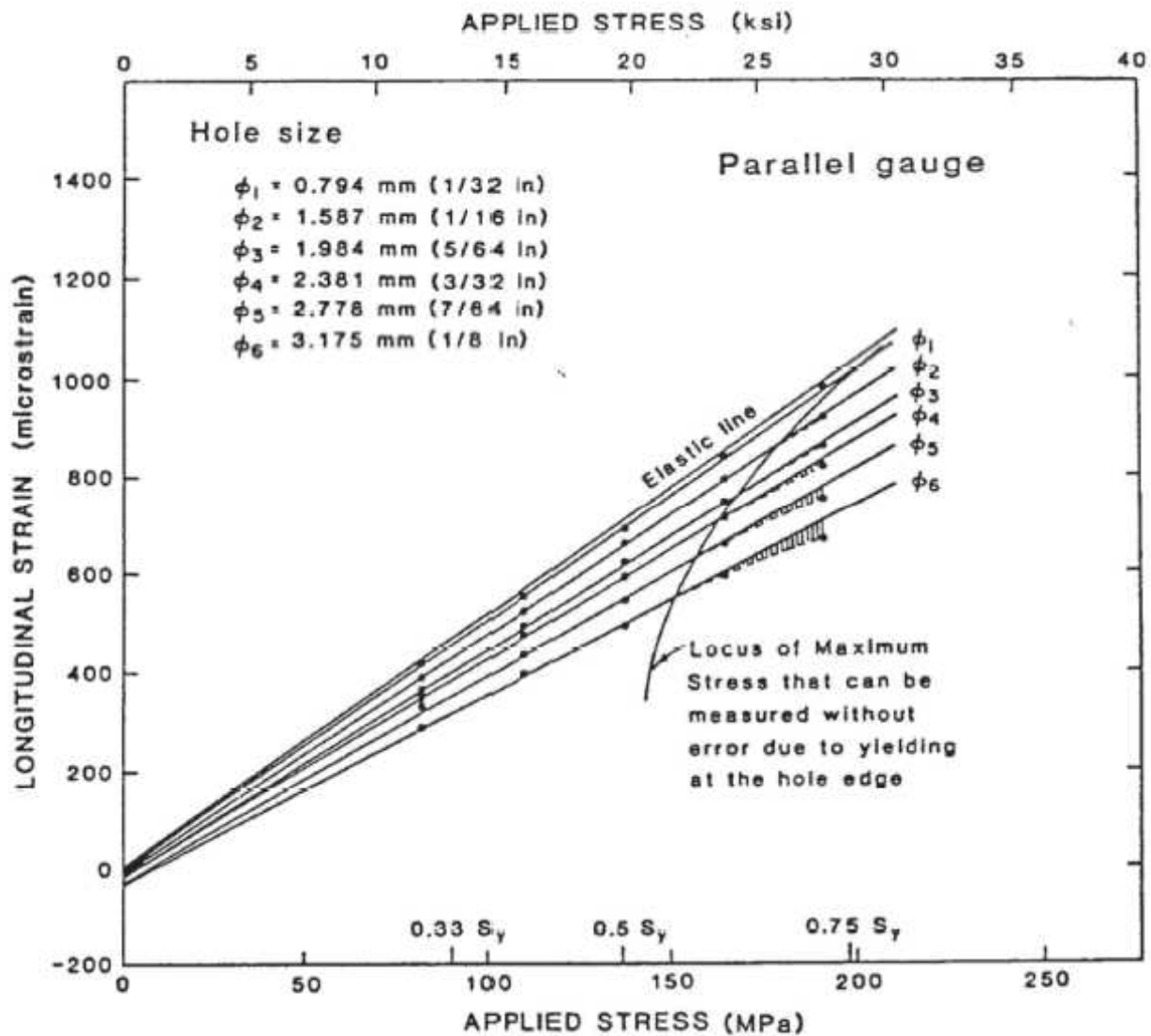


Figure A9. Plot of average strain vs. applied stress for parallel gauge.

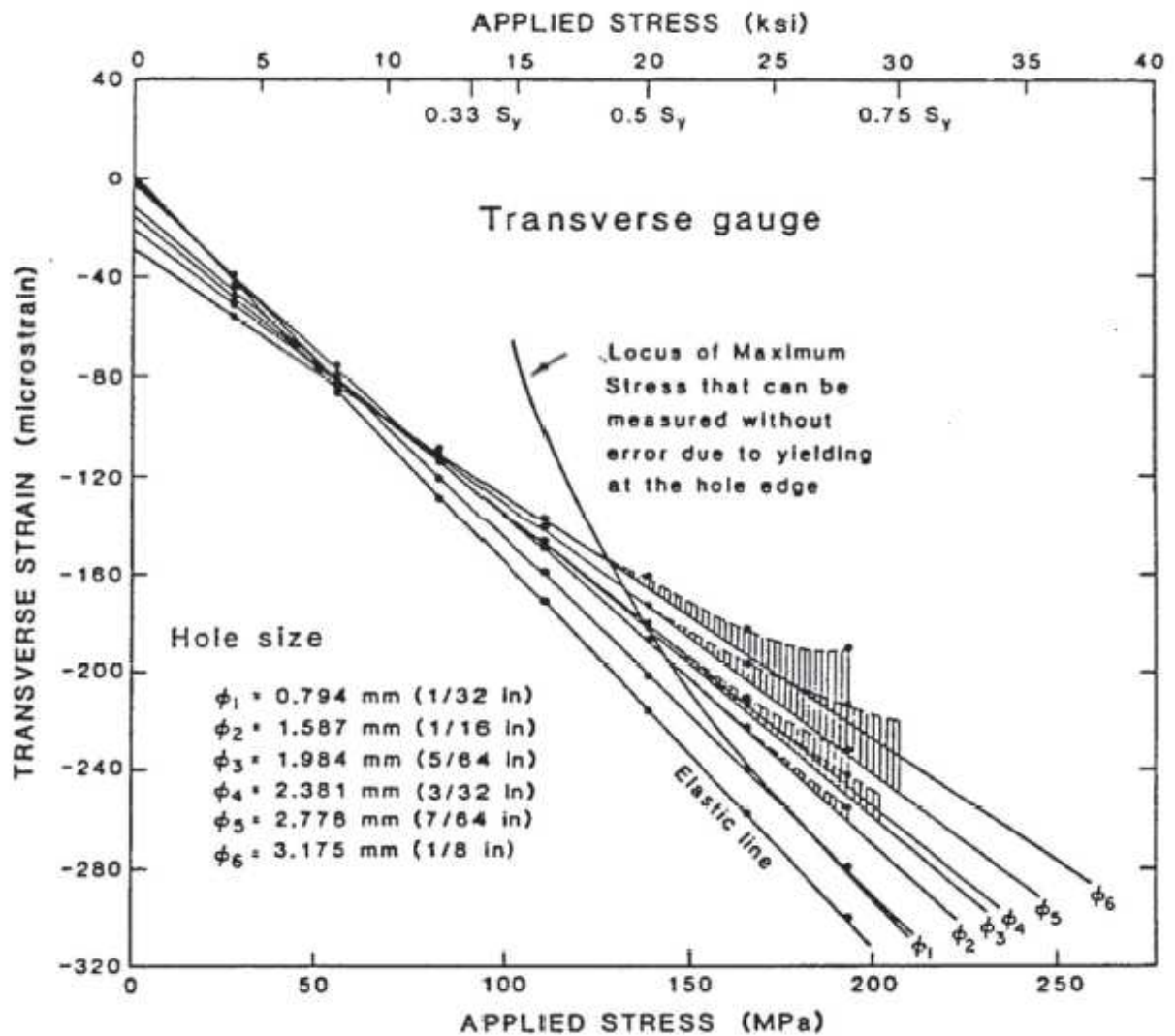


Figure A10. Plot of average strain vs. applied stress for transverse gauge.

be a function of the gauge orientation  $\theta$ . It may be seen that these loci are asymptotic to  $1/2 \sigma_y$  and  $1/3 \sigma_y$  in the parallel and transverse directions, respectively.

2. The interpretations of the experimental results may proceed from the principles enunciated in Figure A3. Figures A11 and A12 are thus constructed from Figures A9 and A10. It may be seen from Figure A12 that a stress of  $0.7 S_y$  may be overestimated by as much as 35% when 3.175 mm drill bits are used. The trend of deviation predicts that the error will drastically increase as the stress approaches the yield strength. Parallel gauges, Figure A11, show a corresponding error of approximately 13%. Therefore, extreme caution must be exercised when using transverse gauges in measurements of stresses higher than  $1/3$  the yield stress of material. However, with the strain gauge rosette-hole size combination used in the main text, stresses of the order of  $0.45 S_y$  can be measured with an overall error of 10%.

#### Recommendations

The machining induced strain for the strain gauge rosette (type EA-06-125RE-120) and the 3.175 mm drill bit combination is on an average  $-35 \mu\epsilon$ . This value must be subtracted from all the net strain relaxation readings recorded in the hole drilling experiments.

The errors due to localized plastic flow effect can be corrected from the results shown in Figures A11 and A12. Thus, if the yield stress,  $S_y$ , of the material is 275.8 MPa, a true residual stress

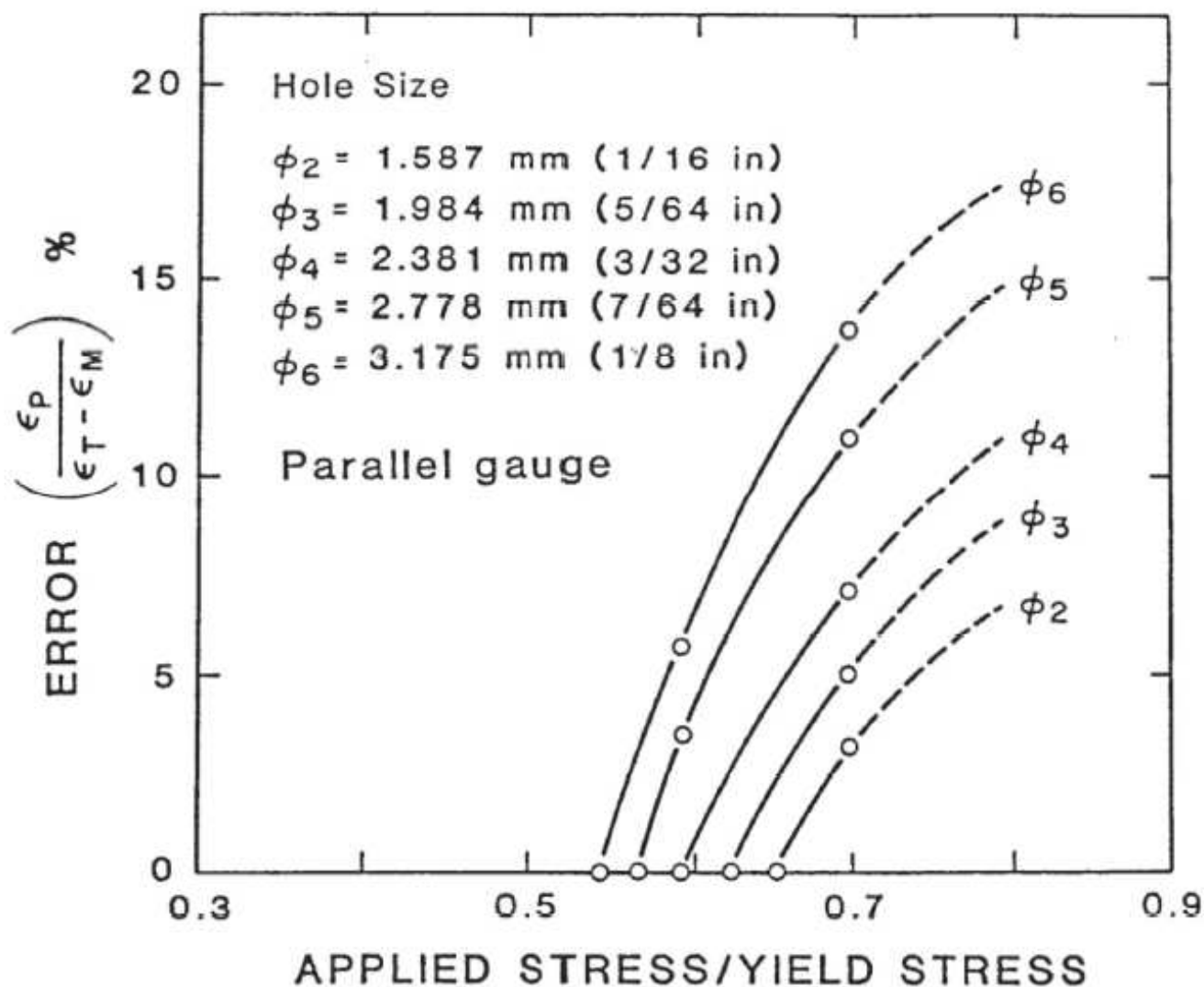


Figure A11. Percentage error in strain as a function of applied stress for a parallel gauge at various hole sizes.

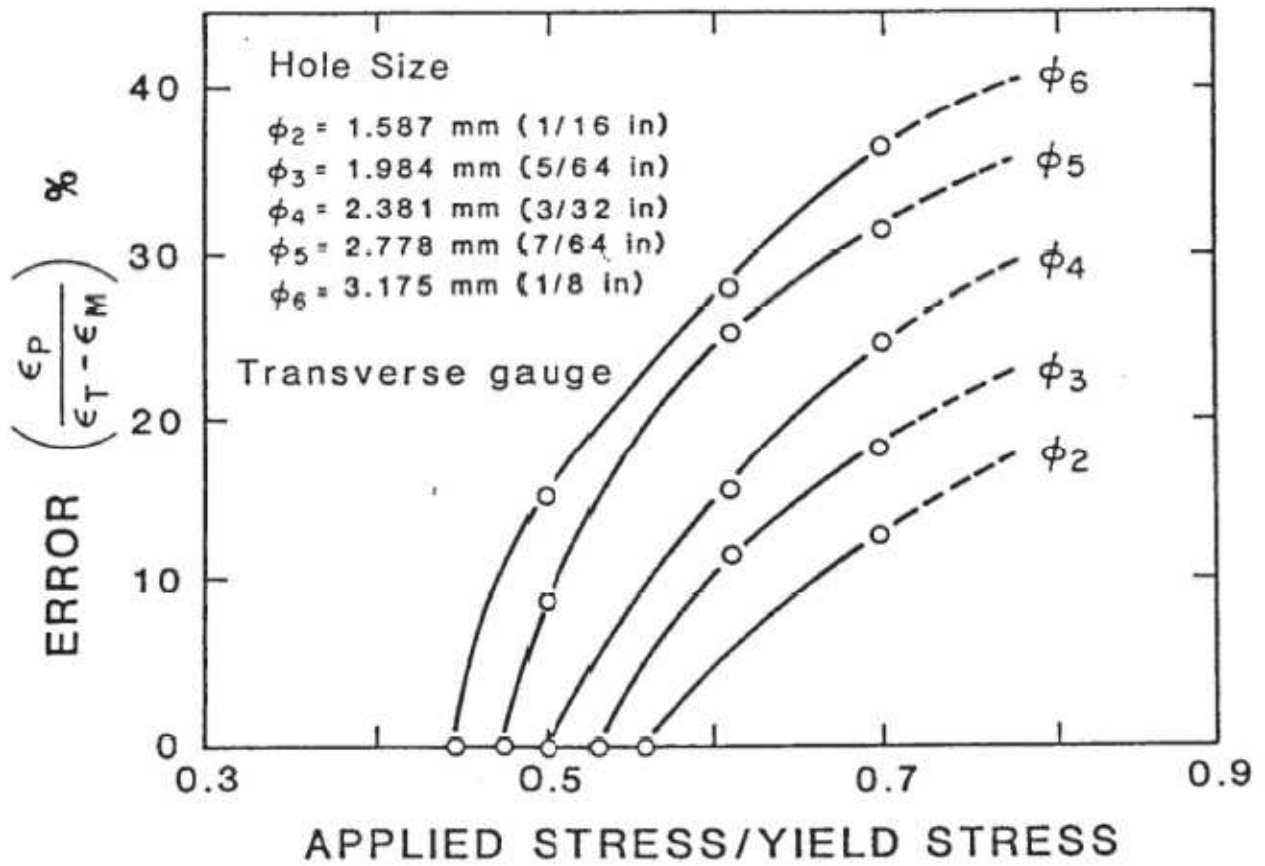


Figure A12. Percentage error in strain as a function of applied stress for a transverse gauge at various hole sizes.

of 193.1 MPa, which is  $0.7 S_y$ , will be exaggerated by about 35% to a value of 262 MPa by a transverse gauge, whereas a parallel gauge will exaggerate it to about 220.6 MPa.

For example, consider the reading from rosette #1 of weldment 1 in the as-welded condition. In the following Table A-V, the successive changes in the stress that occur as a result of modification of the three relaxed strains are shown.

Table A-V

MODIFICATION OF RELAXED STRAINS OF ROSETTE #1, WELDMENT #1, TO ACCOUNT FOR THE DRILLING ERROR AND THE ERROR DUE TO LOCAL YIELDING

	Relaxed Strain, microstrain			Principal Stress (ksi)		Longitudinal Stress, $S_L$ MPa (ksi)	Transverse Stress, $S_T$ MPa (ksi)
	$\epsilon_1$	$\epsilon_2$	$\epsilon_3$	$S_1$	$S_2$		
Before Correction	-218	40	-190	169 (24.50)	423 (61.39)	423 (61.36)	169 (24.53)
Corrected for $\epsilon_m = 35\mu\epsilon$	-183	75	-155	118 (17.11)	372 (54.05)	372 (54.02)	118 (17.13)
Corrected for $\epsilon_p = 35\mu\epsilon$	-148	75	-120	85 (12.40)	303 (44.02)	311 (45.18)	77 (11.24)



## BIOGRAPHICAL NOTE

The author was born in Bangalore, India, on March 8, 1952. He received his B.Sc. degree in 1971 from Bangalore University and his B.E. degree in Metallurgy in 1974 from Indian Institute of Science, Bangalore, India.

In 1975, he began graduate work at the Oregon Graduate Center.

